Evaluation, Transformation, and Extraction of Driving Cycles and Vehicle Operations

Peter Nyberg

Department of Electrical Engineering
Linköping University, SE-581 33 Linköping, Sweden

Linköping 2013

Linköping studies in science and technology
Licentiate Thesis. No. 1596

This is a Swedish Licentiate's Thesis.

Swedish postgraduate education leads to a Doctor's degree and/or a Licentiate's degree.
A Doctor's degree comprises 240 ECTS credits (4 years of full-time studies).
A Licentiate's degree comprises 120 ECTS credits,
of which at least 60 ECTS credits constitute a Licentiate's thesis.

Peter Nyberg
peter.nyberg@liu.se
www.vehicular.isy.liu.se
Division of Vehicular Systems
Department of Electrical Engineering
Linköping University
SE-581 33 Linköping, Sweden

To my family

Abstract

A driving cycle is a representation of how vehicles are driven and is usually represented by a set of data points of vehicle speed versus time. Driving cycles have been used to evaluate vehicles for a long time. A traditional usage of driving cycles have been in certification test procedures where the exhaust gas emissions from the vehicles need to comply with legislation. Driving cycles are now also used in product development for example to size components or to evaluate different technologies. Driving cycles can be just a repetition of measured data, be synthetically designed from engineering standpoints, be a statistically equivalent transformation of either of the two previous, or be obtained as an inverse problem e.g. obtaining driving/operation patterns. New methods that generate driving cycles and extract typical behavior from large amounts of operational data have recently been proposed. Other methods can be used for comparison of driving cycles, or to get realistic operations from measured data.

This work addresses evaluation, transformation and extraction of driving cycles and vehicle operations. To be able to test a vehicle in a controlled environment, a chassis dynamometer is an option. When the vehicle is mounted, the chassis dynamometer simulates the road forces that the vehicle would experience if it would be driven on a real road. A moving base simulator is a well-established technique to evaluate driver perception of e.g. the powertrain in a vehicle, and by connecting these two simulators the fidelity can be enhanced in the moving base simulator and at the same time the mounted vehicle in the chassis dynamometer is experiencing more realistic loads. This is due to the driver's perception in the moving base simulator is close to reality.

If only a driving cycle is considered in the optimization of a controller there is a risk that the controllers of vehicles are tailored to perform well in that specific driving cycle and not during real-world driving. To avoid the sub-optimization issues, the operating regions of the engine need to be excited differently. This can be attained by using a novel algorithm, which is proposed in this thesis, that alters the driving cycle while maintaining that the driving cycle tests vehicles in a similar way. This is achieved by keeping the mean tractive force constant during the process.

From a manufacturers standpoint it is vital to understand how your vehicles are being used by the customers. Knowledge about the usage can be used for design of driving cycles, component sizing and configuration, during the product development process, and in control algorithms. To get a clearer picture of the usage of wheel loaders, a novel algorithm that automatically, using existing sensors only, extracts information of the customers usage, is suggested. The approach is found to be robust when evaluated on measured data from wheel loaders loading gravel and shot rock.

Populärvetenskaplig Sammanfattning

I fordonsindustrin har körcykler bland annat används till att utvärdera olika typer av fordon. Vanligt förekommande är de så kallade certifieringskörcyklerna där det finns lagkrav på tillåtna utsläppsnivåer som fordonstillverkarna måste uppfylla för att få sälja sina fordon inom en viss region. En körcykel i detta sammanhang ska alltså ses som en representation av hur människor kör sina fordon. En körcykel brukar vanligtvis definieras som hastighet som funktion av tid, och följning av en körcykel innebär att fordonet följer denna hastighetsprofil inom vissa gränser i tid och hastighet. Körcykler brukar också användas flitigt i produktutvecklingsprocessen och vid dimensionering av komponenter.

I och med att nya tekniska lösningar på fordonssidan dyker upp ökar behovet av tester. Om till exempel en bil utrustas med ett specifikt förarhjälpsystem så är det viktigt att föraren uppskattar systemet och känner förtroende för det. Ett nytt sätt att utvärdera sådana hjälpsystem på ett realistiskt sätt i en kontrollerad miljö som är säker för föraren och ger möjlighet till upprepade experiment, är att använda sig av en avancerad körsimulator hos VTI som är kopplad till en chassidynamometer med monterad bil i fordonslaboratoriet vid Linköpings universitet. Detta innebär att föraren upplever en riktig drivlina istället för en modell av den. En annan fördel av en sådan uppställning är att fordonet kommer att uppleva realistiska krafter och moment eftersom körupplevelsen i körsimulatorn är nära verklig körning. Detta kan till exempel utnyttjas vid utvärdering av nya styrningsalgoritmer i fordonet.

Om en specifik körcykel används i en allt för stor utsträckning i utvecklingen av styrsystemet finns det en risk att fordonet är mer anpassat för själva körcykeln än till verklig körning. Genom att ändra hastigheten i körcykeln på ett sådant sätt att medeldragkraften bibehålls så ger detta en annan hastighetsprofil samtidigt som fordonen testas på ett liknande sätt. I den här avhandlingen presenteras metoder och algoritmer som gör just detta och dessa kan användas i produktutvecklingen.

I vissa fall är det svårt att få fram en körcykel som är giltig för en stor mängd förare. I sådana fall kan man försöka ta fram flera körcykler där varje körcykel täcker in en viss kund eller kundgrupp. För hjullastare är en körcykel mer än bara hastighet som funktion av tid, och en vanlig situation idag är att bara grova uppskattningar av användningen finns tillgängligt, till exempel medelvärden av diverse signaler. För att få en mer detaljerad bild över hur kunderna använder sig av hjullastarna, föreslås en algoritm som extraherar lastcykler (motsvarigheten till vägfordonens körcykler). En ökad förståelse av kundernas användning av maskinerna kan leda till en bättre matchning mellan maskin och applikation, vilket i sin tur leder till effektivare och billigare maskiner.

Acknowledgments

First of all, I would like to express my gratitude to my supervisors Prof. Lars Nielsen and Dr. Erik Frisk for guiding and supporting me in my PhD studies. Lars is especially acknowledged for his inspiring and motivational skills. Erik is also acknowledged for his sharp eye for details.

I am also grateful to Lars for letting me join the Vehicular Systems group. The administrators Maria Hamnér and her predecessor Maria Hoffstedt have both been a helping hand during my time here. A special thank of mine goes to my colleagues who have created the pleasant atmosphere at work and you never know what kind of topic will pop up during the coffee breaks.

I would like to thank M.Sc. Anders Andersson, M.Sc. Håkan Sehammar, and Dr. Per Öberg for their work in our joint papers and to be honest, at first I was not too keen to be seated on the passenger side of the driverless car when the driven wheels rotates up to a speed of 140 km/h, even if the car was not moving. Per is also acknowledged for his computer support.

My thanks also go to Dr. Mattias Krysander, Dr. Erik Frisk, Lic. Tomas Nilsson, and Lic. Christofer Sundström for our joint work related to the usage of wheel loaders.

Lic. Daniel Eriksson is acknowledged for the help with the LaTeX-template. If you had not paved the road for me, the writing of this thesis would have taken much longer time to finish. Lic. Tomas Nilsson and M.Sc. Andreas Myklebust are acknowledged for proofreading parts of this manuscript.

Thanks to my current roommate M.Sc. Kristoffer Lundahl and my former roommates M.Sc. Andreas Myklebust and Dr. Erik Höckerdal for the company and all the discussions we had. Special thanks to Andreas for all our board games rounds and I especially remember our rough count to estimate the speed of the earth in orbit. To our girlfriends chagrin we where sufficiently close, and the correct answer is 29.8 km/s.

Last but not least, I would like to express my greatest gratitude to Eva for letting me know that there is more to life than work and I appreciate all the times you have dragged me home from my office. I am forever grateful for your love, support, and encouragement and I will always be there for you.

Linköping, April 2013
Peter Nyberg

Contents

Chapter 1

Introduction

Driving cycles have during the years been an important tool for evaluating vehicles. A traditional area where driving cycles have been used is certification test procedures to verify that the vehicle manufacturers comply with legislation. In recent years methods have been proposed that generate driving cycles by using Markov chains (Lee and Filipi, 2011; Gong et al., 2011) that extract typical behavior from large amounts of operational data. Other methods compares different driving cycles in an attempt to sort out different representative driving cycles (Zaccardi and Le Berr, 2012), or extracting driving cycles for other kind of vehicles and regions (Tong et al., 2011) by using proven techniques.

A driving cycle is a representation of how vehicles are driven and is usually represented by a set of data points of vehicle speed versus time. Driving cycles are used on the complete vehicle level to test the performance of vehicles (Karner and Francfort, 2007), and also to estimate the environmental impact, conduct type approval tests, judging different technologies and to estimate the impact on traffic control (André, 1996). Given a vehicle, a driving cycle tests or excites the vehicle in a certain way. This is one of the advantages of driving cycles, that vehicles are tested on the same basis. For example, in certification driving cycles where the exhaust gas emissions and fuel consumption are measured, it is possible to compare important quantities from different vehicles with each other since they have been tested in the same way.

An optimization of the control of the energy management for a certain driving cycle does not necessarily result in a good control for another driving cycle (Schwarzer et al., 2010). Vehicle manufacturers need only to focus on a limited operating regions of the engine (Pelkmans and Debal, 2006) and if another driving cycle excites different regions or even different excitation in the same region, different exhaust gas emissions and fuel consumption characteristics are obtained, and thus if the driving cycle is not representative, the optimization on a single driving cycle, will be a sub-optimal solution for real-world driving (Schwarzer

and Ghorbani, 2013). Instead of having one universal driving cycle that the optimization and sizing of components is based on, the manufacturers uses several different cycles that hopefully will cover and represent real-world driving. Driving cycles are also used in the product development process, for example to size components or to evaluate different technologies, where the driving cycle can be synthetically designed from engineering standpoints. Driving cycles test or excite different vehicle parameters and usually a comparison of driving cycles involve a comparison between different statistical criteria. Examples of such criteria are mean velocity, distribution of acceleration, cruising, deceleration, idling modes, and root mean square of the acceleration, to name a few. Another comparison is based on specific energy (Lee and Filipi, 2011), also called mean tractive force, and can be used for a preliminary estimate of the fuel consumed by the propulsion system (Guzzella and Sciarretta, 2007). The mean tractive force quantity is the required traction energy at the wheels for the driving cycle divided by the distance traveled. In an attempt to reduce the risk for sub-optimization of controllers from a fixed driving cycle, a novel algorithm that alter the driving cycle while maintaining the mean tractive force quantity is presented in Paper C. This alternation results in that the operating regions of the engine are excited differently, and at the same time the driving cycle is similar to the previous one since the specific energy is the same.

A common approach to extract driving cycles is to use data from real-world driving (Lyons et al., 1986; Kenworthy et al., 1992; Tong et al., 1999; André, 2004). Recent studies use Markov process theory to generate driving cycles that are representative to the real-world driving (Lin and Niemeier, 2002; Lee and Filipi, 2011; Gong et al., 2011). A representative driving cycle usually means that some statistical criteria of interest is sufficiently close to data from real-world driving. For off-road vehicles, such as wheel loaders, a correct matching between machine and application yields possibilities for lowering the fuel consumption and purchase cost. In the product development process, a valuable input to the engineers is information about how the vehicles are being used. This gives input for sizing and configuration of components. A common situation for wheel loaders is that only rough estimates of the usage is available. A novel algorithm presented in Paper D extracts information about the usage of wheel loaders in an attempt to get a more detailed view of the customer usage of the machines.

With increasing environmental concern, new vehicle technologies that aims to reduce the environmental impact from automobiles have been proposed. How these technologies are experienced by the drivers are of utmost importance and it is moreover vital to be able to conclude if a certain technology is better in practice and not just in a certain driving scenario. With the development of new experimental equipment, these kinds of questions can be addressed in a more systematic and repeatable way. A moving base simulator is a well-established technique to evaluate driver perception of the powertrain in a vehicle. Paper B presents a connection between the chassis dynamometer in the vehicle propulsion laboratory (presented in Paper A) at Linköping University, LiU, and the moving

base simulator, Sim III, at the Swedish Road and Transportation Research Institute, VTI. The purpose of this is multifold. First, to enhance the fidelity of the moving base simulator by using a real powertrain instead of a model. Second, the vehicle mounted in the chassis dynamometer is experiencing more realistic loads due to that the driver's perception of the simulation being closer to reality.

1.1 CONTRIBUTIONS

The modern development process for vehicles with increased use of simulation and simulators has extended the use of driving cycles from legislative emission cycles to vehicle operations capturing all relevant aspects for vehicle design and operation. Thus, there are many new developments in the wide area of evaluation, transformation and extraction of driving cycles and vehicle operations. The contributions of Papers A - D are summarized below.

PAPER A

Paper A presents the vehicle propulsion laboratory for vehicle research where a chassis dynamometer is used to test light-duty vehicles. The laboratory hardware such as data acquisition, network infrastructure, and the chassis dynamometer, its performance and proposed usage are discussed. The vehicle propulsion laboratory is a requirement for the co-simulation study in Paper B.

PAPER B

Paper B presents a new engineering tool for vehicle testing in a controlled environment by connecting the chassis dynamometer in the vehicle propulsion laboratory to the moving base simulator, Sim III. The purpose of the co-simulation is to improve the experience in Sim III and at the same time the vehicle mounted in the chassis dynamometer is experiencing more realistic loads. This is made possible with the development of a pedal robot that actuates the driver's output in Sim III to the mounted vehicle. Using this new laboratory set-up, new powertrain technologies can be tested in a controlled and realistic setting as a complement to on-road tests.

PAPER C

The main contributions in Paper C are the definition of equivalent driving cycles based on mean tractive force and the development of algorithms and methods for equivalence-modification and equivalence-transformation of driving cycles. For example, an optimization of the energy management strategy for a fixed driving cycle can lead to a controller that would be tailored to details in the driving cycle instead of good performance for real-world driving. The presented

algorithms, that alter driving cycles, can be used to avoid the sub-optimization issue and at the same time the vehicles are tested in a similar way because the mean tractive force is kept constant.

Paper D

In Paper D, a novel on-line algorithm that automatically, using existing sensors only, detect and identify driving patterns for wheel loaders is proposed. The reason for this is a need to get a more detailed view of the customer usage of the machine. The extracted information can be used for design of driving cycles, component sizing and adaption to customers, during the product development process, and could also be used in advanced control algorithms. The algorithm is robust against usage disturbances and is based on automata theory techniques.

1.2   Publications

The following papers are included in the thesis.

Journals

- Per Öberg, Peter Nyberg, and Lars Nielsen. A New Chassis Dynamometer Laboratory for Vehicle Research. *SAE International Journal of Passenger Cars* (Accepted for publication). **(Paper A)**

- Anders Andersson, Peter Nyberg, Håkan Sehammar, and Per Öberg. Vehicle Powertrain Test Bench Co-Simulation with a Moving Base Simulator Using a Pedal Robot. *SAE International Journal of Passenger Cars* (Accepted for publication). **(Paper B)**

Conference papers

- Peter Nyberg, Erik Frisk, and Lars Nielsen. Driving Cycle Adaption and Design Based on Mean Tractive Force. Accepted for publication in *7th IFAC Symposium on Advances in Automotive Control*. Tokyo, Japan, 2013. **(Paper C)**

Submitted

- Tomas Nilsson, Peter Nyberg, Christofer Sundström, Erik Frisk, and Mattias Krysander. Robust Driving Pattern Detection and Identification with a Wheel Loader Application. Submitted for journal publication. **(Paper D)**

References

M. André. Driving cycles development: Characterization of the methods. In *SAE Technical Paper 961112*, 1996. doi:10.4271/961112.

M. André. The ARTEMIS European driving cycles for measuring car pollutant emissions. *Science of The Total Environment*, 334-335(0):73 – 84, 2004. ISSN 0048-9697. doi:10.1016/j.scitotenv.2004.04.070.

Q. Gong, S. Midlam-Mohler, V. Marano, and G. Rizzoni. An iterative markov chain approach for generating vehicle driving cycles. *SAE Int. J. Engines*, 4(1): 1035 –1045, 2011. doi:10.4271/2011-01-0880.

L. Guzzella and A. Sciarretta. *Vehicle Propulsion System: Introduction to Modeling and Optimization*. Springer, 2007.

D. Karner and J Francfort. Hybrid and plug-in hybrid electric vehicle performance testing by the US department of energy advanced vehicle testing activity. *Journal of Power Sources*, 174(1):69 – 75, 2007. ISSN 0378-7753. doi:10.1016/j.jpowsour.2007.06.069.

J.R. Kenworthy, P.W.G. Newman, and T.J. Lyons. The ecology of urban driving I -methodology. *Transportation Research Part A: Policy and Practice*, 26(3):263 – 272, 1992. ISSN 0965-8564. doi:10.1016/0965-8564(92)90036-7.

T-K. Lee and Z.S. Filipi. Synthesis of real-world driving cycles using stochastic process and statistical methodology. *International Journal of Vehicle Design*, 57(1):17 – 36, 2011. doi:10.1504/IJVD.2011.043590.

J. Lin and D.A. Niemeier. An exploratory analysis comparing a stochastic driving cycle to California's regulatory cycle. *Atmospheric Environment*, 36 (38):5759–5770, 2002. doi:10.1016/S1352-2310(02)00695-7.

T.J. Lyons, J.R. Kenworthy, P.I. Austin, and P.W.G. Newman. The development of a driving cycle for fuel consumption and emissions evaluation. *Transportation Research Part A: General*, 20(6):447 – 462, 1986. ISSN 0191-2607. doi:10.1016/0191-2607(86)90081-6.

L. Pelkmans and P. Debal. Comparison of on-road emissions with emissions measured on chassis dynamometer test cycles. *Transportation Research Part D: Transport and Environment*, 11(4):233 – 241, 2006. ISSN 1361-9209. doi:10.1016/j.trd.2006.04.001.

V. Schwarzer and R. Ghorbani. Drive cycle generation for design optimization of electric vehicles. *IEEE Transactions on Vehicular Technology*, 62(1):89 –97, 2013. ISSN 0018-9545. doi:10.1109/TVT.2012.2219889.

V. Schwarzer, R. Ghorbani, and R. Rocheleau. Drive cycle generation for stochastic optimization of energy management controller for hybrid vehicles. In *Proceedings of the 2010 IEEE International Conference on Control Applications (CCA)*, pages 536–540, 2010. doi:10.1109/CCA.2010.5611150.

H.Y. Tong, W.T. Hung, and C.S. Cheung. Development of a driving cycle for Hong Kong. *Atmospheric Environment*, 33(15):2323 – 2335, 1999. ISSN 1352-2310. doi:10.1016/S1352-2310(99)00074-6.

H.Y. Tong, H.D. Tung, W.T. Hung, and H.V. Nguyen. Development of driving cycles for motorcycles and light-duty vehicles in Vietnam. *Atmospheric Environment*, 45(29):5191 – 5199, 2011. ISSN 1352-2310. doi:10.1016/j.atmosenv.2011.06.023.

J-M. Zaccardi and F. Le Berr. Analysis and choice of representative drive cycles for light duty vehicles - case study for electric vehicles. *Proceedings of the Institution of Mechanical Engineers, Part D: Journal of Automobile Engineering*, 2012. doi:10.1177/0954407012454964.

Publications

Paper A

A New Chassis Dynamometer Laboratory for Vehicle Research*

A

A New Chassis Dynamometer Laboratory for Vehicle Research

Per Öberg, Peter Nyberg, and Lars Nielsen

Vehicular Systems, Department of Electrical Engineering,
Linköping University, SE-581 83 Linköping, Sweden.

Abstract

In recent years the need for testing, calibration and certification of automotive components and powertrains have increased, partly due to the development of new hybrid concepts. At the same time, the development within electrical drives enables more versatile chassis dynamometer setups with better accuracy at a reduced cost. We are developing a new chassis dynamometer laboratory for vehicle research, aiming at extending a recently commercially available dynamometer, building a new laboratory around it, and applying the resulting facility to some new challenging vehicle research problems. The projects are enabled on one hand by collaboration with the dynamometer manufacturer, and on the other hand on collaboration with automotive industry allowing access to relevant internal information and equipment. The test modes of the chassis dynamometer are under development in a joint collaboration with the manufacturer. The laboratory has been operational since September 2011 and has already been used for NVH-analysis for a tire pressure indication application, chassis dynamometer road force co-simulation with a moving base simulator, co-surge modeling and control for a 6-cylinder bi-turbo engine, and traditional engine mapping. We are also looking at projects with focus on look-ahead control, as well as clutch and transmission modeling and control, and driving cycle related research.

1   INTRODUCTION

Testing, calibration and certification are vital parts for the development of new automotive technologies. With the development of new hybrid concepts the need for it have also increased. To be able to perform large scale vehicle experiments a chassis dynamometer is an option to use.

This paper presents our new chassis dynamometer laboratory, the design choices that are made and the unique opportunities that are made possible by the implementation. The test modes of the equipment, some of which are newly developed, and some of the projects that have already been performed are discussed together with future projects that we foresee possible having access to our new laboratory. The basis for the laboratory is the development within electrical drives, power electronics and precision motion control of electrical machines also for high torques and powers. This progress has enabled a reduced cost and a versatile setup. In our case the basis for the system is ABB technology, applied by Rototest for vehicle applications. A first glance of the laboratory is seen in Figure 1.

The development of our new facility is exciting since it utilizes, combines and enhances new state-of-the-art commercial technology made possible by tech-

Figure 1: A glance of the new chassis dynamometer lab. A Golf V with a 1.4l multifuel engine has been mounted to the dynamometer units in a 4WD configuration.

nological development with several timely automotive research and development projects. On one hand it is curiosity driven, and on the other hand there is substantial interest from our automotive collaborators since they are facing more and more complex development tasks, and are with interest looking at new possibilities.

2 BACKGROUND

Chassis dynamometer experiments are good alternatives to road tests since they give a higher repeatability, lower cost, and better experimental control and supervision. Another benefit is that the body of the vehicle does not need to be mounted, which yields, a possibility to test different configurations of the powertrain before a complete vehicle is constructed. Using a chassis dynamometer it is possible to test the whole powertrain of a vehicle as opposed to engine tests benches. In the past chassis dynamometers usually meant rolls of different dimensions where the surface of the rolls was in direct contact with the tire of the tested vehicle. They were expensive and required complex facilities, and the time to change vehicles is often long. With the use of absorption, and possibly a drive unit, the rolls can be controlled to brake and propel the vehicle while measuring e.g. the speed of the roll and the transferred torque from the tire to the roll.

There are many examples of work where chassis dynamometers have been used. For example, to get an estimate of the pollutant emissions from light-duty trucks, test or driving cycles have frequently been used while measuring the emissions (André, 2004). These driving cycles, which are speed profiles, are mainly performed at a chassis dynamometer. The legislative certification driving cycle in Europe is the NEDC driving cycle, and in Pelkmans and Debal (2006) on-road emissions and emissions for chassis dynamometer driving NEDC are compared. Another work used transportable chassis dynamometers to compare alternative fuel and diesel fuel heavy-duty vehicles emissions (Wang et al., 1997). The chassis dynamometer used in that study used rolls for the driven wheels, but the power was extracted directly from the vehicle hubs instead of extracting power from the rolls that usually is the case. During emission measurements a common practice is to measure the related fuel consumption at the same time. In Brace and Moffa (2009) a statistical approach is used for identifying factors that influence the fuel consumption of a vehicle. Here a 48 inch chassis dynamometer is used and the largest effect was recognized to be a discharged battery.

Except for conducting legislative certification driving cycles for emissions, a chassis dynamometer can also be used for other experiments or tests such as performance tests of the powertrain and noise tests, of vibration and harshness (NVH) to mention a few. In the latter case usually larger diameters of the rolls are required to ensure that the contact surface between the tire and roll are large enough.

3   Laboratory Overview

The vehicle propulsion laboratory is housed in the facility L-huset at Linköping University which was finished mid 2011. The L-huset can be viewed in Figure 2 and contains in total approximately 220 m^2 laboratory space and also some office space. The focus of this paper is on the vehicle propulsion laboratory being one of three labs in the building. The chassis dynamometer in the propulsion laboratory was chosen because of its flexibility, simplicity, and cost of ownership and installation. Nevertheless, during construction of the lab, some criteria had to be fulfilled to support the chassis dynamometer installation. The main specific criterion during the construction of the lab-building was that the electrical power transmission had to be dimensioned to support the four 160 A 230 V three phase power supplies for the regenerative motor drives and the 125 A power supply for the head wind fan. The second criterion was that the exhaust gases need to be taken care of with suitable ventilation. Other than that, the laboratory building is simply a regular building with garage.

Figure 2: The building L-huset where the vehicle propulsion laboratory is housed.

3.1 The vehicle propulsion laboratory

The vehicle propulsion laboratory consists of an 80 m² lab area divided between a control room and the actual lab space. An overview picture of the vehicle propulsion laboratory can be seen to the left in Figure 3. The usable ceiling height is approximately 5 m and the garage doors are of a height of 4 m. This way even light-duty-trucks can be brought into the laboratory. The panoramic window in

Figure 3: Left: View of the vehicle propulsion laboratory with four mobile dynamometers, head wind fan and exhaust ventilation. Right: View from the corridor.

the corridor, which can be seen to the right in Figure 3, gives spectators and staff a view of the laboratory and yields the possibility to easily demonstrate the facility for visitors. In the control room, which can be seen in Figure 4, a supervisor can control the experiments and at the same time have a visual supervision of the activity in the laboratory.

Due to that the wheels need to be removed during the mounting of the dynamometers a jack or preferable a lift needs to be used to lift the vehicle. Because the dynamometer units are mobile the choice of lift requires some consideration. The laboratory is currently equipped with a movable hydraulic scissor lift (not shown in the figures) that can be used and stowed away easily, maintaining the flexibility of the dynamometers. One drawback with the current solution is, however, that not all cars have enough ground clearance for the lift.

Because the dynamometer can be used at high vehicle loads for long time measurements the exhaust gases can reach high temperatures. To cope with the high temperatures the ventilation system is dimensioned to suck excess air, thus diluting the hot exhaust gases at the source. Currently a selection of pipes with different lengths and shapes are used to fit the ventilation to vehicles with different exhaust pipe layouts but a more flexible solution is sought for.

Figure 4: View of the vehicle propulsion laboratory control room.

3.2   EQUIPMENT

The propulsion laboratory is equipped with a chassis dynamometer, as well a data acquisition hardware, network infrastructure, and communication software. Pictures of the laboratory can be seen in Figure 3 and a schematic overview of the system can be seen in Figure 5. The main parts of the equipment are

The chassis dynamometer   which is the main equipment of the vehicle propulsion laboratory and consists of four mobile units, as well as other control and supply components. The chassis dynamometer is thoroughly described further down.

A PC for measurement and control   located in the control room. This computer is currently running a standard Linux distribution that can be adapted to running real time software, e.g. for look-ahead-control purposes. Measurements are either performed directly at the dynamometer systems Control PC or by this measurement computer through CAN, serial port OBDII or UDP. This way data that is measured by other means than by the dynamometer or vehicle control systems can easily be forwarded to the measurement computer.
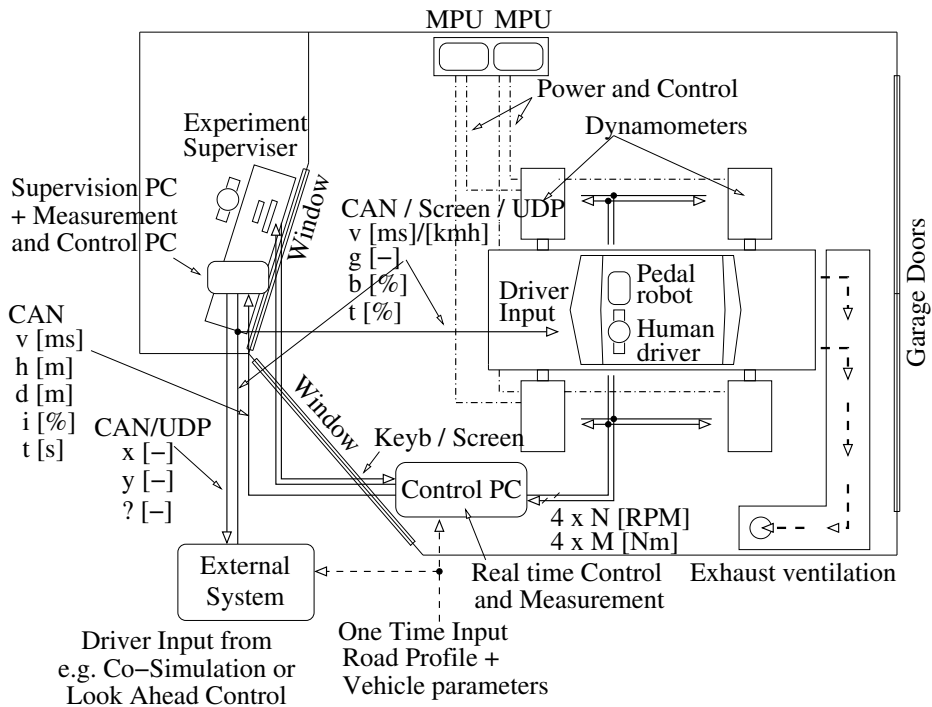
Figure 5: The lab area, where the dynamometer units are located, and a control room, from where an experiment supervisor controls the experiment, are separated with a large panoramic window. The garage doors, shown in the right part of the picture, are large enough to allow full size trucks to enter the lab area.

A supervision PC   located in the control room. This computer is used for supervision and communication using Confero (Johanson, 2010) which is a teleconference software which can be used independently without an external Internet connection.

Ethernet connections   to a local switch room with single mode fiber to neighboring facilities. The Ethernet network is separated between a local high speed measurement network, also available from the offices, a dedicated single mode fiber extension currently connected to the moving base simulator facility at the Swedish Road and Transportation Research Institute, VTI, as well as a number of standard university networks for use with regular research and student activities.

Direct cable connections   between the control room and the lab area for Ethernet, CAN, serial RS232 connections or other equipment suitable for CAT5e cables, e.g. keyboard video and mouse extenders, USB extenders or OBDII adapters.

The power supply   of the laboratory, which consists of

- A 125 A 230 V three phase European power socket for the head wind fan.

- Four 160 A 230 V three phase power supplies for the regenerative motor drives.

- Two 16 A 230 V three phase European power sockets for use with the vehicle lift and other typical tools.

Finally, for personal safety the laboratory is equipped with a hand-carried CO_2 sensor as well as CO_2 and CO sensors connected to an emergency evacuation fan.

4   DYNAMOMETER SYSTEM

4.1   SYSTEM DESCRIPTION

The chassis dynamometer equipment consists of

- Four mobile dynamometer units, (Rototest Energy 230 4WD).

- Two main power units housing the regenerative motor drives. These are placed in a protective cabinet which is vented with outside air to avoid smoke damages in case of a small fire.

- A mobile control rack consisting of the master control unit, a real time control system, as well as a user interface module which is built on an ordinary PC.

- A mobile head wind fan capable of wind speed up to 100 km/h (about 62 mph)

Depending on the system mode the dynamometer units can operate as either motors or generators, and can thus both brake and propel the vehicle. This can for example be used when simulating downhill driving where the vehicle is accelerated even if the engine does not provide any tractive force.

The dynamometer units are mobile and can be moved to fit different vehicle sizes and configurations, such as 1WD (motorcycles), 2WD, or 4WD vehicles. The vehicle is fitted to the dynamometer by removing the driven wheels and mounting the vehicle to the dynamometer using adapter plates directly on the wheel hubs. Switching vehicles can be performed in less than 30 minutes which enables the use of the laboratory for parallel projects.

Configuration for component testing

Because of the system's flexibility it is also tempting to use the system for other purposes than as a chassis dynamometer. An application is to use the dynamometer units as parts of a transmission test rig which can be used in early stages of for example clutch and transmission control evaluation.

Head wind fan

A head wind fan is used to simulate the head wind which cools the engine and its components. The headwind fan, which can be seen in the left part in Figure 3, can either be manually controlled or it can be set to follow the simulated vehicle velocity in the interval 0-100 km/h. One benefit with the dynamometer equipment is that the noise is relatively low. The single noisiest component is the head wind fan with a peak noise level of 120 dBA at full speed. In the speed range 0-70 km/h the noise is low enough to hear the powertrain components as one would in a normal driving situation. This way, experiments where drivetrain noise is important can be performed.

Sensors

The outputs of the dynamometer are wheel torques and speeds but also vehicle speed and other quantities that can be calculated using the internal vehicle model. The torques are measured using string gauges fitted to the drive suspension of the dynamometer units and the torque measurement accuracy is within 0.1% of measured value.

Setup

Before starting an experiment a number of vehicle parameters are needed. Depending on operation mode they are

- Axle weight, m_a, and effective wheel diameter, d_w, for calculation of safety limits.

- Gear ratios, $r_{g,i}$, for all gears including the final drive, for calculation of engine speed.

- Vehicle mass, m_v, front area, A_f, drag coefficient, c_d, and rolling resistance, c_r, for driving resistance calculation in the road force simulation mode.

For the road profile simulation mode an elevation map, including turn radii, for the road is also needed.

In a typical test setup the driver steps into the vehicle as would be the case for a normal driving mission. Because of the mobile dynamometer setup the driver can turn the steering wheel. In another scenario a pedal robot is used, e.g. when connected to an external system as discussed below. In both setups the experiments are directed from the control room, and the dynamometer is controlled either trough the Control PC or via CAN remote control which adds for extra safety when connected to an external systems.

4.2   DYNAMOMETER PERFORMANCE

The performance of the chassis dynamometer equipment is in the speed range $0 - 1000$ rpm limited to an axle torque of 1180 Nm continuous and up to 2200 Nm momentarily. In the speed range $1000 - 2100$ rpm the torque is limited by the power. The continuous power that the equipment can output is 124 kW (166 bhp) and up to 230 kW (308 bhp) momentarily per axle. Thus, for four wheel driven vehicles the continuous power that the vehicle can either be braked or propelled by is 248 kW. In Figure 6 the continuous and momentarily limitations are shown together with the modeled required power to overcome the rolling and aerodynamic resistance at a flat road for different speeds of a typical car. The operating points (torque vs speed) from three tests with different drivers are also shown. For these tests the drivers where instructed to drive at highway speeds on a simulated highway with moderate traffic. This indicates the possibility of interesting investigations of driver behavior.

4.3   MOUNTING PROCEDURE

To mount a vehicle in the laboratory a vehicle is driven into the lab through the garage doors and the vehicle is then raised with either a jack or a lift. The vehicle is connected to the dynamometer units by removing the driven wheels, and with the help of adapter plates the vehicle is fitted to the equipment. The adapter plates are bolted on the wheels hubs and are then connected to the dynamometer unit for each wheel hub. After the bolts are tightened the vehicle is lowered and the vehicle then rests on the dynamometer. The connection to the dynamometer is similar to Wang et al. (1997), where the car wheel rests on small rolls while the torque is extracted from the wheel hubs, but here the
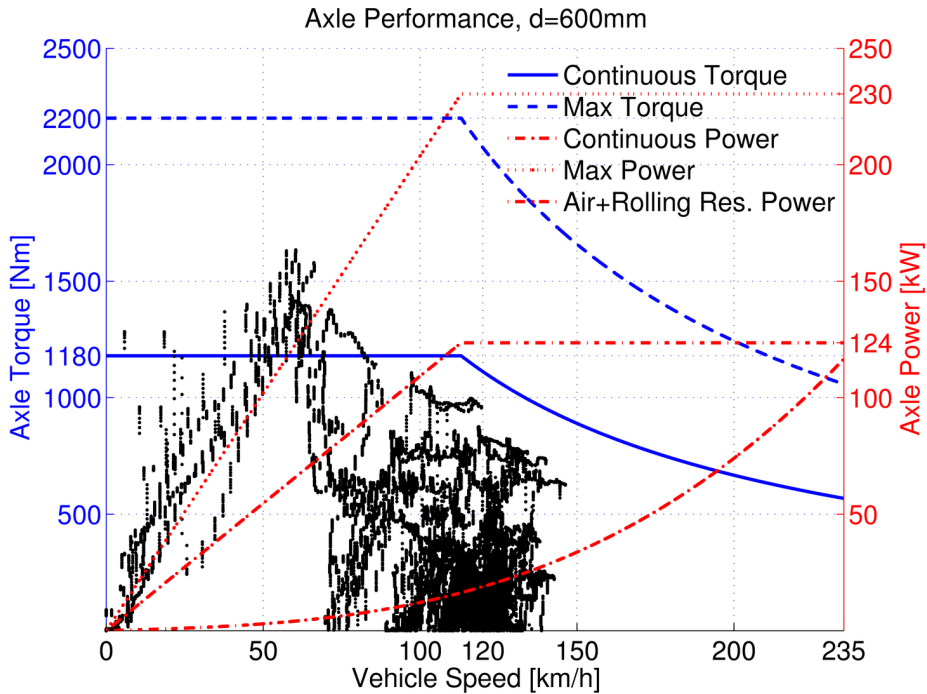
Figure 6: In the speed range $0 - 1000$ rpm the dynamometer can deliver 1180 Nm of continuous torque and up to 2200 Nm momentarily per axle. In the speed range $1000 - 2100$ rpm the power is the limiting factor. The continuous power is 124 kW and up to 230 kW momentarily can be exerted per axle. A reference trajectory of the required steady-state power for a typical 2WD car is shown together with measured torque from three experiments.

driven wheels are removed so that the driven wheel hubs are resting on the dynamometer units instead.

4.4   Test modes

The chassis dynamometer equipment can be used in a variety of ways depending on the purpose of the experiments. One test mode is constant speed while measuring the torque exerted by the powertrain. In another test mode the forces a vehicle is exposed to during normal driving are simulated, e.g. used when simulating driving cycles. This is also the foundation for the road profile test mode, a product from the ongoing joint collaboration. In this mode the system is pre-programmed with an elevation map. In the next sections the different test modes of the equipment are explained.

Constant Speed

In constant speed tests the chassis dynamometer are set to achieve a pre-defined velocity of the vehicle. The dynamometer units act as motors or generators to maintain the vehicle at this speed. A typical example is performance test where the vehicle manufacturer/owner want to measure how much power/torque the vehicle is producing at certain speeds. In Figure 7 the maximum torque and power for different vehicle speeds and gears have been measured. The tested vehicle was a Golf V with a 1.4l multifuel engine.

Road Forces Simulation

An alternative to on-road tests is the use the chassis dynamometer in the road forces simulation mode. In this mode the simulated forces that a vehicle has to overcome at the wheels are the aerodynamic drag force F_{air}, the rolling resistance, F_{roll}, the gravitational resistance, F_{grav}, in case that the simulated road is not flat, i.e. has non-zero incline. If the propulsion force at the wheels, F_{prop}, produced by the powertrain exceeds these modeled losses the mounted vehicle will accelerate with an acceleration, a, according to

$$m \cdot a = F_{\mathrm{prop}} - F_{\mathrm{res}}$$
$$F_{\mathrm{prop}} = \sum_i \frac{T_{\mathrm{wheel},i}}{r_{\mathrm{wheel}}},$$

where m is the vehicle mass, F_{prop} the propulsion force calculated from the measured torque on each driven wheel, $T_{\mathrm{wheel},i}$, and the wheel radius constant, r_{wheel}. The resistance force F_{res} can either be a polynomial function in vehicle
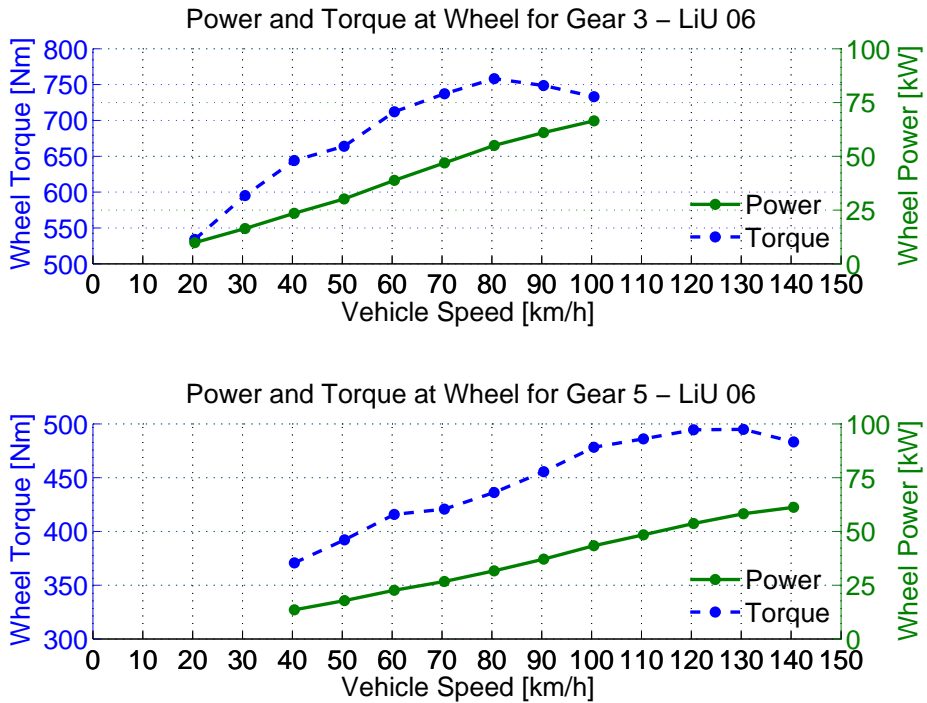
Figure 7: Measurements of the maximum torque and power that can be exerted at the wheels for a Golf V with a 1.4l multifuel engine. The upper figure is for the 3rd gear and the lower figure is for the 5th gear engaged.

speed or a standard model for driving resistance

$$F_{\text{res}} = F_{\text{roll}} + F_{\text{air}} + F_{\text{grav}}$$
$$F_{\text{roll}} = c_{\text{r}} \cdot m \cdot g$$
$$F_{\text{air}} = \frac{1}{2} \cdot \rho_{\text{a}} \cdot c_{\text{d}} \cdot A_{\text{f}} \cdot (v + v_0)^2$$
$$F_{\text{grav}} = m \cdot g \cdot p,$$

where c_{r} is the rolling friction coefficient, g the gravitational constant, ρ_{a} the density of air, c_{d} drag coefficient, A_{f} the frontal area of the vehicle, p incline of the road, and v_0 is the relative wind speed during the experiment. In case a polynomial function is used the air drag and rolling resistance is replaced with

$$F_{\text{air}} + F_{\text{roll}} = F_0 + F_1 v + F_2 v^2 + F_3 v^3 + F_4 v^4.$$

Depending on the sign of $F_{\text{prop}} - F_{\text{res}}$ the simulated vehicle will accelerate or decelerate . If the incline is set to zero the test will simulate driving on a flat road, and the forces the vehicle has to overcome depends on the vehicle parameters and the velocity the simulated vehicle is traveling at.

DRIVING CYCLES

A driving cycle is a speed profile (speed vs time) that can be used to test or certify vehicles regarding exhaust emissions and fuel consumptions. Usually the driving cycle is driven at a flat road, i.e. with zero incline. This test mode is an application of the road force simulation where a pre-defined speed profile is to be tracked. During these tests either a driver in the vehicle is shown the profile and tries to follow it or a pedal robot is used to automate the testing.

ROAD PROFILE

A new test mode has been developed which simulates the forces for a road with varying road profile and hence varying incline depending on how far the simulated vehicle has traveled in the driving mission. Figure 8 shows the results of such an experiment where the driver was instructed to drive at highway speed. In the upper figure the vehicle speed is shown. In the lower figure road profile as function of distance is shown.

The speed of the vehicle determines the traveled distance which sets the current incline. Thus, depending on the driver input the distance and incline at a certain time is not necessary the same for another driver on the same driving mission.

This mode is a requirement for projects such as look-ahead control, co-simulation with a moving base simulator and studies of driver feel and behavior. These are new and more complex usages than standard constant speed tests and road force simulations, and thus puts new requirements on interfaces and behavior of the test equipment. Some also require access to internal vehicle control. To
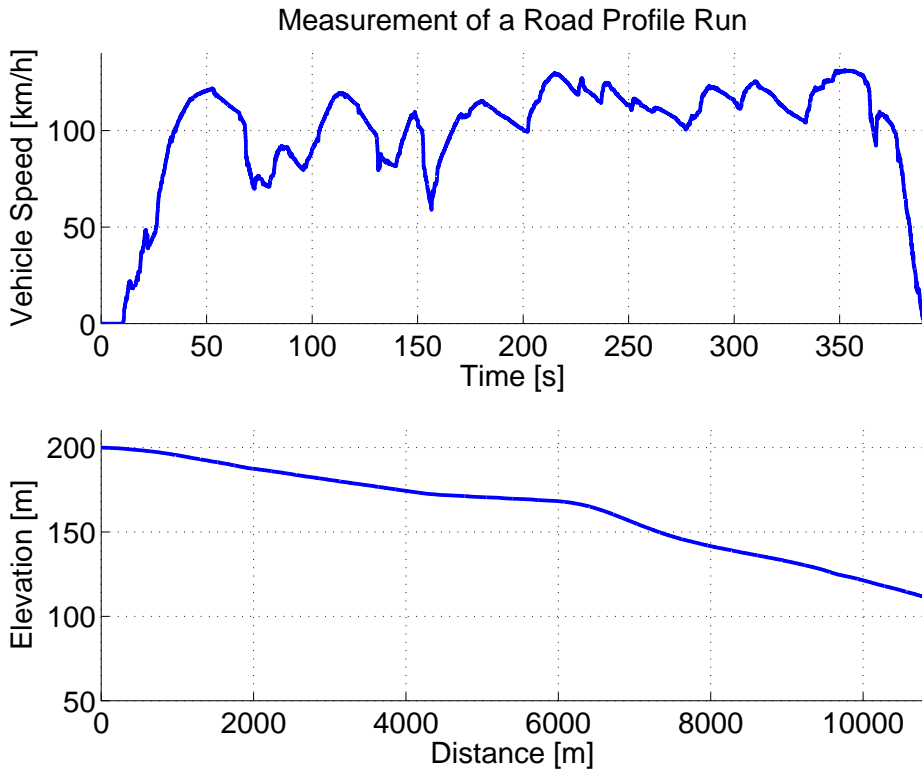
Figure 8: Velocity profile with elevation over sea level from an example measurement in road profile mode.

develop this new functionality we have collaborated with the dynamometer supplier, automotive companies, the Swedish Road and Transportation Research Institute, and our local Internet service provider.

LOOK-AHEAD CONTROL

A natural continuation of the road profile test mode is to use the system for look-ahead control related research. Look-ahead control using GPS navigation has previously been used for heavy vehicles where fuel savings are possible if the road topography is known (Hellström et al., 2009, 2010). An interesting prospect is to use the same techniques applied to hybrid electric or plug in hybrid electric vehicles where optimal battery charging strategies can be calculated using road topography, speed limit, traffic lights, and other road information.

Given the simulation possibilities of the vehicle propulsion laboratory such techniques can easily be evaluated for a large variety of situations and it is possible to answer questions such as what is the most relevant information to have access to or how will the algorithm be affected by dense traffic etc.

5   PERFORMED STUDIES

The system has already been used for a number of different projects such as

- NVH-analysis where the drivetrain and engine induced oscillations are analyzed achieving separation from the tire in an attempt to refine a tire pressure indicator system.

- Demonstrating appropriate excitation for modeling and control of co-surge for a 6-cylinder bi-turbo engine.

- Traditional engine mapping made possible for a group of students participating in the Formula student competition, having a slim budget.

- Chassis dynamometer road force co-simulation with a moving base simulator, where a pedal robot replaces the human driver, demonstrating functional interfaces to the lab.

5.1   MODELING OF ENGINE AND DRIVELINE RELATED DISTURBANCES ON THE WHEEL SPEED IN PASSENGER CARS

Tire vibrations measured from the wheel speed sensors can be used to monitor tire pressure since the dynamics of the tire depends on the pressure. However, other sources of vibrations, such as the drivetrain are also visible in the sensor data. An interesting problem therefore is to model and decouple the vibrations that origins from the drivetrain.

In cooperation with an industry partner the vehicle propulsion laboratory has been used to investigate how a wheel mounted dynamometer can be used

to separate the tire vibrations in an effort to model these drivetrain vibrations (Johansson, 2012). This would not have been possible when using a chassis dynamometer with rolls. Another benefit with the hub-mounted dynamometer is that the body of the vehicle does not need to be fixed to the lab which means that regular cars of the market can be used without modification. For the experiments two different four wheel drive cars, a diesel Audi A4 and a petrol Audi A5, were used.

In Johansson (2012) the drivetrain is modeled as a series of masses, dampers, and springs and experiments are performed to parametrize the model. An example of a validation of the drivetrain model for the Audi A4 is shown in Figure 9. During these experiments the constant speed mode was used for a number of different engine speeds while the drivetrain oscillations were measured. The engine torque that was used for these experiments was 50 Nm. More details of the project are found in Johansson (2012). The fact that Figure 9 shows well defined peaks means that the equipment is appropriate for this type of investigation in terms of its own inertia, control performance, and noise levels.

5.2 Modeling and control of co-surge in bi-turbo engines

Bi-turbocharged supercharger configurations can give faster torque response and help to better utilize exhaust energy for V-type engines by allowing more efficient placement of the turbocharger (Thomasson and Eriksson, 2011). In a recent project the propulsion laboratory was used to study, model, and control a special surge phenomenon, co-surge, that can occur in these configurations. An example of co-surge is shown in Figure 10 where a 6-cylinder bi-turbo equipped vehicle was forced into co-surge by inducing a small 0.3 s throttle disturbance at time t=0. The disturbance causes oscillations in the mass flows of the two air-paths which can be seen in the upper figure.

For the experiments the constant speed mode was used for the dynamometer. Using this operation mode a set of operating points with different engine-speed and load was spanned. The bi-turbocharged engine was mounted in a car together with its auxiliary systems, making it possible to perform experiments and calibrate the control design in a realistic setting. The experiments show that it was possible to excite and study individual components in the car using the equipment in the laboratory. This made the development process efficient. Another benefit to be noticed was the short start-up time of the project compared to a conventional engine test bed. More information about the project can be found in Thomasson and Eriksson (2011).

5.3 Formula student, mapping

The propulsion laboratory has also been used by the newly started Formula student team at Linköping University. The Formula student is a competition where the competing teams develop, design and build a small race car and
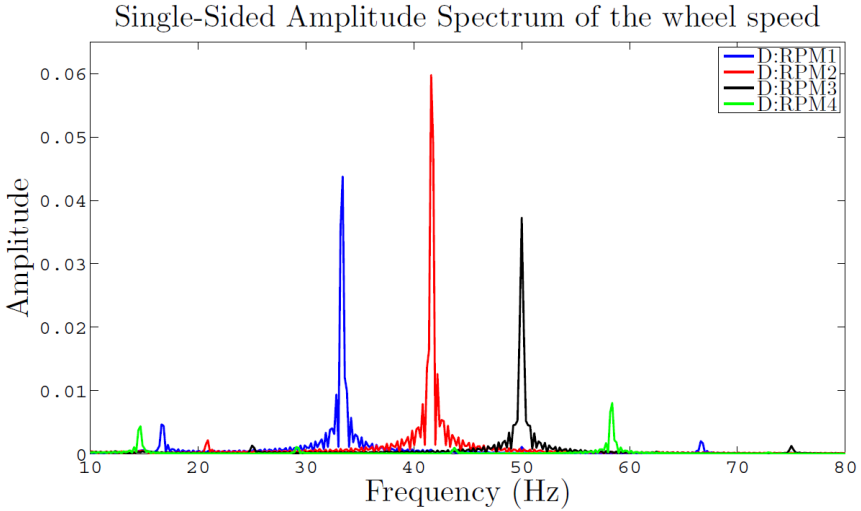
(a) Spectrum of the **simulated** wheel speed disturbances at different engine speeds for gear four.
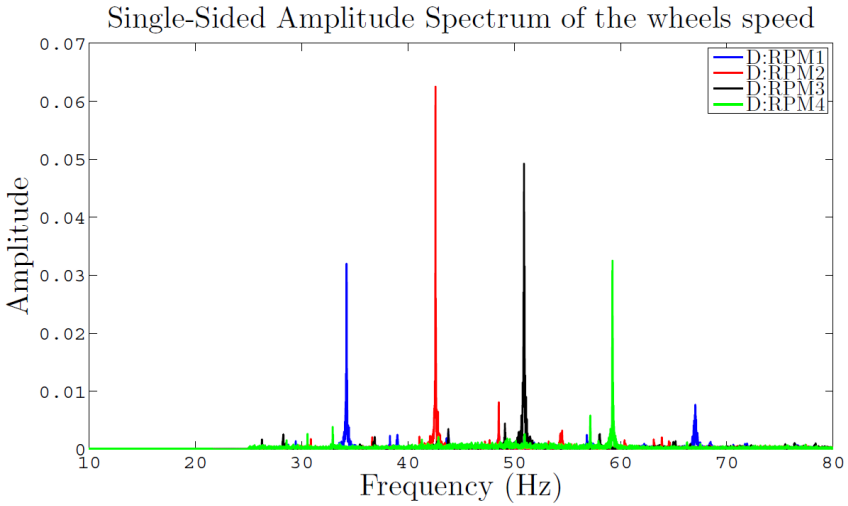
(b) Spectrum of the **measured** wheel speed disturbances at different engine speeds for gear four.

Figure 9: Example of model validation for the drivetrain model. Simulated wheel speed disturbances, a), are compared to measured, b), for different engine speeds at forth gear. (Courtesy of Robert Johansson, c.f. (Johansson, 2012))
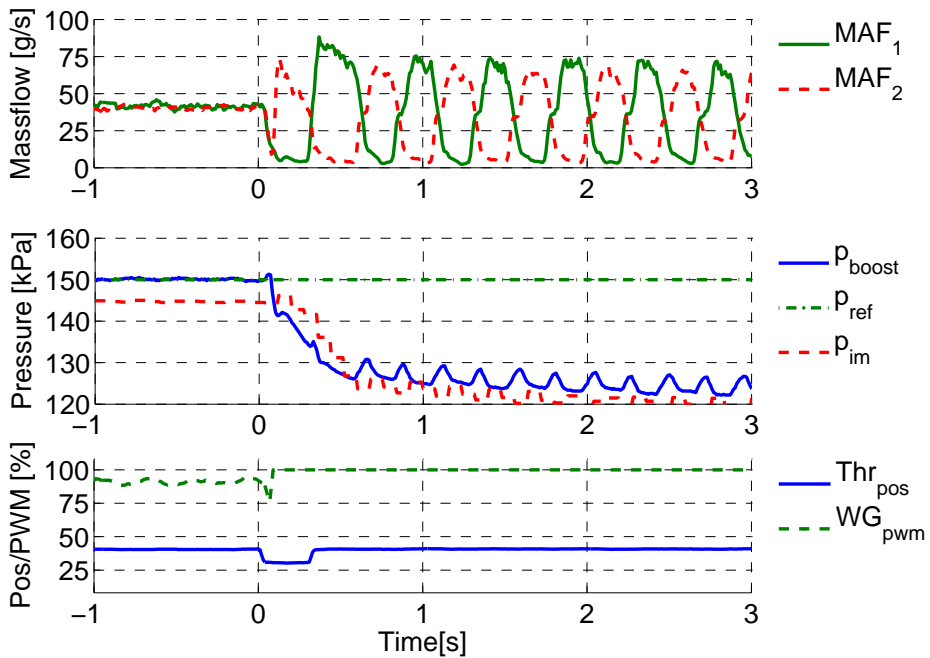
Figure 10: Mass flow rates for the two air-paths (upper), intake manifold and boost pressure (middle), and throttle position (lower). A 0.3 s throttle disturbance at time t=0 induces co-surge in the system. The mass flows starts to oscillate and will keep oscillating until the operating point it changed or a controller damps out the oscillations.

competes with other universities once a year. The mapping of the engine was performed by measuring the torque at the wheel hubs at different engine speeds. Changes in the ignition timing and amount of fuel injected were executed. The fuel-to-air-ratio, λ value, was measured with an external λ-sensor and the torque was measured at the wheel hubs.

Given a complete vehicle it was beneficial to perform the mapping of the engine with the chassis dynamometer. The reason is that it is low-effort-work compared to constructing appropriate engine mounts and running it in an engine test bed, and even more important for a project with low budget it is significantly more cost-efficient. Another difference is that the complete powertrain is tested instead of only the engine, which can be beneficial sometimes.

5.4   Chassis dynamometer road force co-simulation with a moving base simulator

In cooperation with the Swedish Road and Transportation Research Institute, VTI, a hardware-in-the-loop setup with a pedal robot to replace the human driver has recently been investigated (Andersson et al., 2013). The idea is to use co-simulation to let a driver in the VTI moving base simulator, Sim-iii, experience an actual powertrain instead of the traditional models that are used, and to study the possibilities to enhance the fidelity of the simulator. Another possible benefit from such a setup is that the vehicle in the chassis dynamometer is exposed to more realistic loads because the driver input is likely to be closer to actual driving than when used independently.

In the project a pedal robot, shown in Figure 4, was developed for this purpose. During the experiments the pedal robot was fed driver inputs from Sim-iii via a low latency dedicated single mode fiber connection and the resulting forces and wheel speeds from the chassis dynamometer where returned to the Sim-iii simulator.

An actual driving mission using the pedal robot can be seen in Figure 12 where the driver sitting in the moving base simulator Sim-iii was instructed to drive at highway speeds with varying incline and traffic. At around 180 seconds the driver was exposed to traffic which can also be seen in the upper figure where the speed becomes more varying for the rest of the test. The elevation profile can be seen in the lower left figure and the measured wheel torque from the powertrain can be seen in the lower right figure. More information about this project can be found in Andersson et al. (2013).

Figure 11: The pedal robot that was used to actuate the gas and brake pedal according to the input from the driver in the Sim-iii simulator.
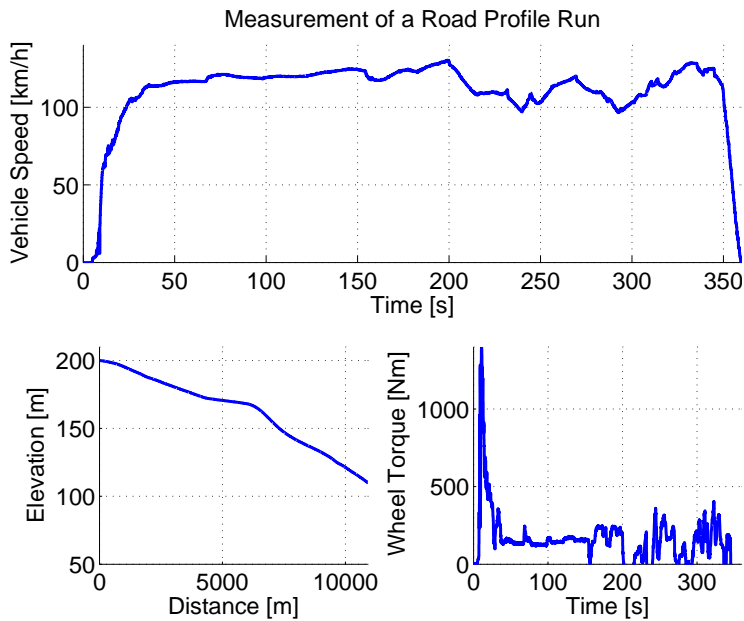
Figure 12: Velocity profile with elevation over sea level and wheel torque from a measurement in road profile mode and driver input from the pedal robot connected with the Sim-iii simulator. During the launch from zero velocity the high torque origins from low gear and high engine torque.

The overall conclusion is that the interfaces and coordination with other systems, such as pedal robot and moving base simulator, work well. This includes measurement and communication systems.

6   Future Projects Aims and Goals

A natural continuation is development of future test methods for concept evaluation, driving feel, performance, and driver behavior. Specifically we are aiming for the following topics

- Continued development of co-simulation with moving base simulator.

- Behavioral studies.

- Integrated model chain (see below).

- Driving cycle research (see below).

Integrated Model Chain

In a neighboring laboratory, dynamic vehicle models are used to evaluate vehicle behavior for different purposes (Lundahl et al., 2011; Nickmehr et al., 2012). The aim here is an integrated chain for testing of vehicle concepts consisting of

- Modeling.

- Automatic parameter estimation from measurements.

- Evaluation of driver behavior.

A first step is to automatically parametrize the models using measurements from regular driving while the complete movements, e.g. speed and acceleration, are measured. As a second step the dynamics of these models can be experienced in a moving base simulator, e.g. the previously mentioned Sim-iii at VTI, as well as in the vehicle propulsion laboratory studying driving feel, driver behavior and performance. Another possible use is to simulate a hybrid powertrain using the parametrized vehicle model to evaluate how a thought hybrid system would have performed in an actual driving mission of a regular car.

Driving Cycle Research

In another application a pedal robot, e.g. like the one in Figure 4, can be used to eliminate the drivers impact on experiment repeatability. This is interesting for example when following a driving cycle where it is beneficial that the drivers direct impact on the vehicle is eliminated. Here the research focus on test repeatability with respect to driving cycle deviation.

Research questions that need to be answered is for example, how long should a driving cycle be and what should it look like to represent real world driving.

Another research topic deals with how to construct a driving cycle to excite specific phenomena, e.g. for control system tuning. Both these examples requires a controlled environment with a predictable driving cycle tracking performance.

7 Summary

The vehicle propulsion laboratory has been operational for about one year. It is still under continuous development both in collaboration with the manufacturer and with vehicular applications. The flexibility of the lab with its wheel mounted configuration yields an opportunity to use regular cars of the market without prior modifications and has proved useful to shorten the start-up times for projects such as the investigation of co-surge for bi-turbocharged V-type engines and for the traditional engine mapping, when used by the Formula student team. The experiments for the co-surge project also show that it was possible to excite and study individual components in the car using the equipment in the laboratory. This made the development process efficient.

Further, the wheel mounted configuration of the dynamometer is advantageous in investigations used to separate the tire vibrations in an effort to decouple the vibrations that origins from the drivetrain. The fact that it is possible to see well defined peaks in the measured data means that the equipment is appropriate for this type of investigation in terms of its own inertia, control performance, and noise levels.

The jointly developed road profile test mode, where topography maps are used together with the road force simulation, is a key component that enables new and more complex usages than standard constant speed tests and road force simulations, and thus puts new requirements on interfaces and behavior of the test equipment. As an example, the road profile test mode is used in the moving base simulator/chassis dynamometer co-simulation project. The overall conclusion is that the interface and coordination with other systems, such as pedal robot and moving base simulator, work well. This includes measurement and communication systems.

The road profile test mode thus yields unique opportunities, such as research on look-ahead control and driving cycle related research, and with infrastructure to neighboring facilities the usefulness of the lab can be extended even further, e.g. as in the co-simulation project.

References

A. Andersson, P. Nyberg, H. Sehammar, and P. Öberg. Vehicle powertrain test bench co-simulation with a moving base simulator using a pedal robot. In *SAE World Congress*, number 2013-01-0410, Detroit, USA, 2013.

M. André. The ARTEMIS European driving cycles for measuring car pollutant emissions. *Science of the Total Environment*, 334-335:73–84, 2004.

C J. Brace and J. Moffa. Increasing accuracy and repeatability of fuel consumption measurement in chassis dynamometer testning. *Journal of Automobile Engineering*, 223(9):1163–1177, 2009.

E. Hellström, M. Ivarsson, J. Åslund, and L. Nielsen. Look-ahead control for heavy trucks to minimize trip time and fuel consumption. *Control Engineering Practice*, 17(2):245–254, 2009.

E. Hellström, J. Åslund, and L. Nielsen. Design of an efficient algorithm for fuel-optimal look-ahead control. *Control Engineering Practice*, 18(11):1318–1327, 2010.

M. Johanson. Multimedia communication, collaboration and conferencing using alkit confero. Whitepaper, Alkit Communications, 2010. URL `http://confero.alkit.se/confero_whitepaper.pdf`.

R. Johansson. Modeling of engine and driveline related disturbances on the wheel speed in passenger cars. Master's thesis, Linköping University, 2012.

K. Lundahl, J. Åslund, and L. Nielsen. Investigating vehicle model detail for close to limit maneuvers aiming at optimal control. 22nd International Symposium on Dynamics of Vehicles on Roads and Tracks (IAVSD), Manchester, UK, 2011.

N. Nickmehr, J. Åslund, L. Nielsen, and K. Lundahl. On experimental-analytical evaluation of passenger car ride quality subject to engine and road disturbances. 19th International Congress on Sound and Vibration, Vilnius, Lithuania, 2012.

L. Pelkmans and P. Debal. Comparison of on-road emissions with emissions measured on chassis dynamometer test cycles. *Transportation research part D*, 11:233–241, 2006.

A. Thomasson and L. Eriksson. Modeling and control of co-surge in bi-turbo engines. In *IFAC World Congress*, Milano, Italy, 2011.

W.G. Wang, N.N. Clark, D.W. Lyons, R.M. Yang, M. Gautam, R.M. Bata, and J.L. Loth. Emissions comparisons from alternative fuel buses and diesel buses with a chassis dynamometer testing facility. *Environmental science & technology*, 31:3132–3137, 1997.

Paper B

Vehicle Powertrain Test Bench Co-Simulation with a Moving Base Simulator Using a Pedal Robot⋆

B

Vehicle Powertrain Test Bench Co-Simulation with a Moving Base Simulator Using a Pedal Robot

Andreas Andersson*, Peter Nyberg**, Håkan Sehammar*, and Per Öberg**

*Vehicle Technology and Simulation,
VTI, SE-583 30 Linköping, Sweden.

**Vehicular Systems, Department of Electrical Engineering,
Linköping University, SE-581 83 Linköping, Sweden.

ABSTRACT

To evaluate driver perception of a vehicle powertrain a moving base simulator is a well-established technique. We are connecting the moving base simulator Sim III, at the Swedish National Road and Transport Research Institute with a newly built chassis dynamometer at Vehicular Systems, Linköping University. The purpose of the effort is to enhance fidelity of moving base simulators by letting drivers experience an actual powertrain. At the same time technicians are given a new tool for evaluating powertrain solutions in a controlled environment. As a first step the vehicle model from the chassis dynamometer system has been implemented in Sim III. Interfacing software was developed and an optical fiber covering the physical distance of 500 m between the facilities is used to connect the systems. Further, a pedal robot has been developed that uses two linear actuators pressing the accelerator and brake pedals. The pedal robot uses feedback loops on accelerator position or brake cylinder pressure and is controlled via an UDP interface. Results from running the complete setup showed expected functionality and we are successful in performing a driving mission based on real road topography data. Vehicle acceleration and general driving feel was perceived as realistic by the test subjects while braking still needs improvements. The pedal robot construction enables use of a large set of cars available on the market and except for mounting the brake pressure sensor the time to switch vehicle is approximately 30 minutes.

1   INTRODUCTION

One major part of any vehicle is the powertrain. This is what enables a vehicle to move forward providing energy conversion to torque at the wheels to overcome rolling resistance, aerodynamic drag and/or climbing resistance. The powertrain has also been under a lot of development recently as the environmental demands increase (Chan, 2007). To cope with the increasing demands the amount of hybrid vehicles using multiple sources for energy have increased (Chan, 2007; Offer et al., 2010). This introduces several clever solutions providing good environmental performance at the cost of more complex and expensive systems. It is thus interesting to see how these solutions are perceived by a driver. Also, battery cost is a major issue for hybrid electric and plug-in hybrid electric vehicles and it is therefore interesting to see how the driver behavior influences battery lifetime (Wu et al., 2012). To improve the possibilities to evaluate driver perception of a vehicle powertrain one idea is to use a moving base simulation. In these situations the powertrain is usually simulated using a vehicle model. To enhance the fidelity of the powertrain one possibility is to use a harware-in-the-loop, HIL, powertrain. This enables a driver in a moving base simulator to experience an actual powertrain and for technicians to try new powertrain solutions while letting a driver run a test in a controlled environment. There exists a lot of HIL setups which would benefit if they could be used cooperatively. Previous work has been done by Ersal et al. (2011, 2012) where an internet distributed setup with an engine was investigated.

In this work we have connected the moving base simulator, Sim III, at the Swedish Road and Transportation Research Institute, VTI, with the vehicle propulsion laboratory, presented in Öberg et al. (2013), at Linköping University, LiU.

Co-simulating a moving base simulator with a vehicle powertrain test bench using a test vehicle over a network connection is an area where little work has been done although individual parts have been well investigated. Therefore it's interesting to evaluate if this can be used to increase fidelity of current designs even further. The question we here initially investigate is if we think it is possible to obtain a realistic driving experience using a vehicle powertrain test bench in co-simulation with a moving base simulator.

2   EXPERIMENTAL SETUP

The main parts of the experimental setup are the vehicle propulsion laboratory at LiU, the moving base simulator Sim III, the pedal robot used to control the test vehicle in the propulsion laboratory, and the connection between the research facilities at LiU and VTI. In the following section these systems are all described. Further, the synchronization between the vehicle models and the driving mission used for the test driving is discussed.

2.1 Chassis dynamometer lab

A new chassis dynamometer lab has recently been built at the Division of Vehicular Systems, Linköping University (Öberg et al., 2013), in the vehicle propulsion laboratory a chassis dynamometer setup is installed. The dynamometer provides four wheel motors/generators that can provide both positive and negative torque at the wheels of a vehicle, and a control computer. This control computer can be given road profile data to simulate driving for an installed vehicle. An overview of the lab can be seen in Figure 1.
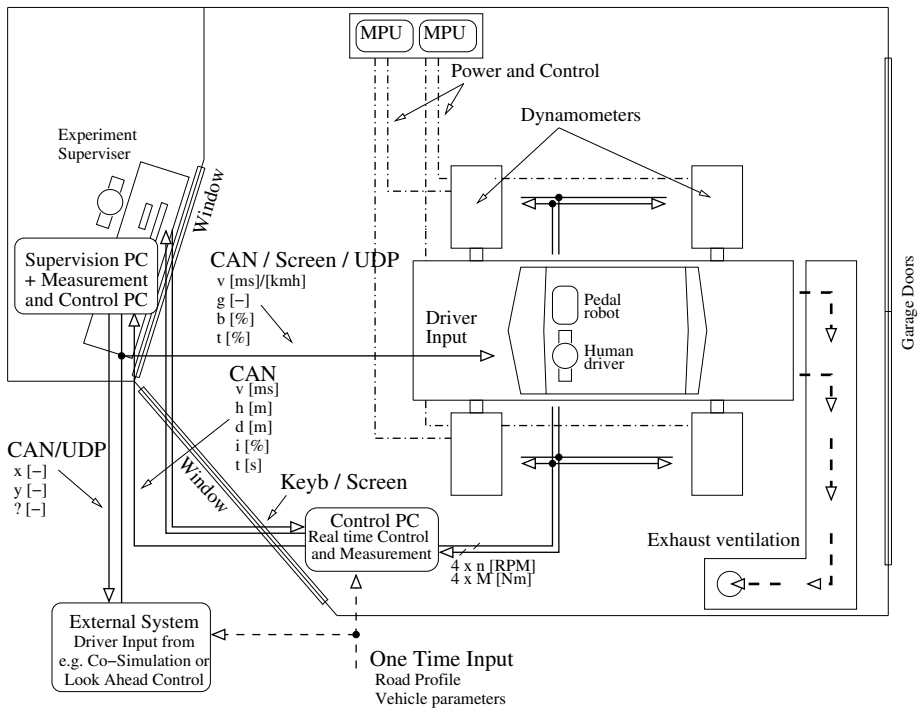
Figure 1: Schematic overview of the propulsion laboratory. The car is driven into the lab through the garage doors on the right and the dynamometers are then mounted to respective wheel hub. Road topography and vehicle parameters are then entered in the chassis dynamometer control PC. During the experiment the measurement and control PC in the control room forwards CAN messages from the chassis dynamometer to an external system via UDP. The external system then returns driver input to a human driver or, as in this case, a pedal robot.

SYSTEM DESCRIPTION

The dynamometer units can operate as both motors and generators depending on the system mode and can thus both brake and propel the vehicle. The dynamometer units are mobile and can be moved to fit different vehicle sizes and configurations, such as 1WD (motorcycles), 2WD, or 4WD vehicles. The vehicle is fit to the dynamometers by removing the driven wheels and mounting the vehicle to the dynamometer using adapter plates directly on the wheel hubs.

In a typical test setup the driver steps into the car as would be the case for a normal driving mission. In another scenario a pedal robot is used, e.g. when connected to an external system as discussed in this work. In both setups the experiments can be directed from the control room and the dynamometer can be controlled either through the Control PC or via CAN remote control which adds for extra safety because the external system can be used to automatically stop the dynamometer.

The outputs of the dynamometer are wheel torque and rotational speed but also vehicle speed and other quantities that can be calculated using the internal vehicle model. The torques are measured using string gauges fit to the drive suspension and the torque measurement accuracy is within 0.1% of measured value.

SYSTEM SETUP

Before starting an experiment a number of vehicle parameters is needed. Depending on operation mode they are

- Axle load in kg, m_a, and effective wheel radius, r_w, for calculation of safety limits

- Gear ratios, $r_{g,i}$, for all gears including the final drive, for calculation of engine speed

- Vehicle mass, m_v, front area, A_f, drag coefficient, c_d, and rolling resistance, c_r, for driving resistance calculation in the road force simulation mode

- Road topography map, including turn radii, for the road.

The chassis dynamometer equipment can be used in a variety of ways depending on the purpose of the experiments. One test mode is constant speed while measuring the torque exerted by the powertrain. In another test mode the forces a vehicle is exposed to during normal driving are simulated, e.g. used when simulating driving cycles. This is also the foundation for the road profile test mode that is used in this work.

ROAD FORCES SIMULATION

The simulated forces that a vehicle has to overcome at the wheels are the aerodynamic drag force F_{air}, the rolling resistance, F_{roll}, the climbing resistance,

F_{climb}, in case that the simulated road is not flat, i.e. has non-zero incline. The propulsion force at the wheels, F_{prop}, produced by the powertrain and the resistance forces determines the acceleration, a, of the mounted vehicle according to following model

$$F_{\mathrm{tot}} = m_{\mathrm{v}} \cdot a = F_{\mathrm{prop}} - F_{\mathrm{res}}$$

$$F_{\mathrm{prop}} = \sum_i \frac{T_{\mathrm{w},i}}{r_{\mathrm{w}}}$$

where m_{v} is the vehicle mass, F_{prop} the propulsion force calculated from the measured torque on each driven wheel, $T_{\mathrm{w,i}}$, and the measured wheel radius r_{w} which is constant during simulation. The resistance force F_{res} can either be a polynomial function in vehicle speed or a standard model for road resistance

$$F_{\mathrm{res}} = F_{\mathrm{roll}} + F_{\mathrm{air}} + F_{\mathrm{climb}} \tag{1}$$

$$F_{\mathrm{roll}} = c_{\mathrm{r}} \cdot m_{\mathrm{v}} \cdot g$$

$$F_{\mathrm{air}} = c_d \cdot A_{\mathrm{f}} \cdot \frac{\rho_{\mathrm{air}} \cdot (v + v_0)^2}{2}$$

$$F_{\mathrm{climb}} = m_{\mathrm{v}} \cdot g \cdot p$$

where c_{r} is the rolling friction coefficient, g the gravitational acceleration constant, ρ_{a} the density of air, c_{d} aerodynamic resistance coefficient, A_{f} the frontal area of the vehicle, p incline of the road, and v_0 is the relative wind speed during the experiment. In case a polynomial function is used the air drag and rolling resistance is replaced with

$$F_{\mathrm{air}} + F_{\mathrm{roll}} = c_0 + c_1 \cdot v + c_2 v^2 + c_3 \cdot v^3 + c_4 \cdot v^4.$$

Depending on the sign of $F_{\mathrm{prop}} - F_{\mathrm{res}}$ the simulated vehicle will thus accelerate or decelerate . If the incline is set to zero these equations will simulate driving on a flat road. The forces the vehicle has to overcome thus depends on the vehicle parameters and the velocity the simulated vehicle is traveling at.

Vehicle Dynamics Parameters

The parameters that are needed for the vehicle dynamics part when calculating braking force for the road simulation are

m_{v} - Mass of vehicle in kg

A_{f} - Front area m^2

c_{d} - Drag coefficient

c_{r} - Rolling coefficient

Built in parameters are

ρ_{air} - Air density (1.202 kg/m^3 at an altitude of 200 m)

g - Gravitational acceleration (9.81 m/s^2)

TEST VEHICLE

For this study a 2009 Volkswagen Passat Ecofuel DSG was used. This car has a dual clutch semi-automatic transmission and runs on both gasoline and methane. The maximal power of the car is 110 kW (150 hp) for both fuel options. In Figure 2 the car is shown mounted in the vehicle propulsion laboratory. Because it is a front-wheel driven car only the front wheels need to be connected.

Figure 2: The Volkswagen Passat that is used in the experiment mounted in the chassis dynamometer of the vehicle propulsion laboratory.

Before the experiments a brake pressure sensor was installed on the main brake cylinder. To be able to mount the pedal robot the driver chair was removed. The parameters that were used for the vehicle are listed in Table 1.

Table 1: Vehicle model parameters used in the study.

Parameter	Value	Unit
m_v	1 401	kg
c_d	0.320	-
A_f	2.0	m^2
c_r	0.01	-
r_w	0.3	m

Input and Output During Simulation

During simulation the input to the chassis dynamometer is those that a driver can give, namely

- Accelerator pedal position in the range $[\,0 - 1\,]$.

- Brake pedal pressure, measured in the range $[\,2.98 - 7\,]$ volts.

The outputs are in form of CAN messages sent either at 10 or 100 Hz. Status messages, such as temperature etc, are sent in 10 Hz and simulation output messages are sent either at 10 Hz or 100 Hz. The outputs available through these CAN messages are summararized in Table 2

Table 2: Available output signals from the simulator rig.

Signal	Unit	Frequency	Description
n_i	rpm	100 Hz	Wheel speed
T_i	Nm	100 Hz	Wheel torque
v_l	km/h	10 Hz	Longitudinal vehicle speed
v_v	km/h	10 Hz	Vertical vehicle speed
r_{road}	m	10 Hz	Road curvature radius
H	°	10 Hz	Heading, relative origin
h	m	10 Hz	Elevation of road
p	°]	10 Hz	Incline
d_{TP}	m	10 Hz	Distance since start
t_{TP}	s	10 Hz	Time since start
T_i	°C	10 Hz	Dynamometer temperature
$S_{d,i}$	-	10 Hz	Dynamometer status
S	-	10 Hz	System status

2.2 VTI simulator III

The Swedish Road and Transportation Research Institute, VTI, is an independent research institute in the transport sector. The principal task of VTI is to conduct research and development related to infrastructure, traffic and transport. The institute has technically advanced equipment, and part of this equipment are the driving simulators. For this work, particularly the advanced moving base simulator, VTI Simulator III, or Sim III was used.

Sim III uses state of the art techniques for simulation of road conditions (Bolling et al., 2011) and has earlier been used in, amongst others, studies related to effects of yaw stability at side impact (Andersson and Jansson, 2011). A picture of Sim III can be seen in Figure 3.

The linear motion system of Sim III's has four degrees of freedom and offers both linear and tilt motion at an acceleration of 8 m/s². Realistic lateral motions are obtained by linking the cradle's motion to the vehicle's lateral

Figure 3: The moving base driving simulator Sim III at VTI.

position. Sim III can be rotated 90 degrees to enable studies with focus on acceleration and braking instead of lateral forces.

To give the driver a field of vision of 120 degrees during the simulation six projectors are used and to simulate the rear-view mirrors three LCD displays are used. High-frequency vibrations can be provided using a vibration table. This can be used for example to simulate road unevenness during experiments with rumble strips. Both a passenger car and a truck can be fitted to the simulator and for the purpose of this project a Saab 9-3 cabin was used.

Software for running Sim III is largely developed at VTI. The software consists of algorithms for graphics, sound, simulation kernel, motion queuing, vehicle model and more. In this work the focus is on the vehicle model which is modified to accept inputs from the vehicle propulsion laboratory at LiU. This means that the chassis dynamometer at the propulsion laboratory controls the propulsion of the vehicle during the simulation but that other parts of the simulator is intact providing a realistic environment to the driver.

2.3 Pedal robot

To control the vehicle speed a pedal robot has been constructed which uses two electrical linear actuators pressing the accelerator and brake pedals. Together with a vehicle with an automatic transmission this setup gives basic control of the vehicle powertrain. The pedal robot control logic has been created using

Figure 4: Pedal robot installed in the Volkswagen Passat test vehicle.

Matlab Simulink with Stateflow and xPC-Target and the pedal robot uses a two-way UDP communication interface to Sim III. The actions taken by the driver in the simulator are sent as command signals to the pedal robot and the pedal robot controller sends status information back to the simulator software. A picture of the pedal robot is shown in Figure 4. As can be seen, the construction is made such that the actuators can be moved sideways and up and down which makes it easily adaptable for different vehicles.

Each actuator is of ball screw type and is driven by a 24 volts DC motor, equipped with an encoder for positioning. The actuator is also equipped with two adjustable circuit breakers defining the maximal and minimal allowed position of the piston. Each actuator has a working range of 300 mm.

Accelerator pedal control

The pressure needed for pushing the accelerator pedal is relatively low and thus the main requirement for the actuator is high speed rather than high dynamic load. The chosen actuator has a dynamic load of 210 N and a maximum speed of 250 mm/s.

When mounting the accelerator pedal actuator the circuit breakers are first adjusted to define the maximum allowed range. The control application then starts with a calibration phase where the actuator is slowly moved up and down between the limits defined by the circuit breakers. In this way the circuit

breakers are used to set the safety limits for the controller. The working range is finally set with a safety marginal of 3 mm to these limits. An important aspect of the calibration process is to adjust the circuit breakers so that the zero position for the accelerator pedal is within the region limited by the safety limit and the position where the pedal does not cause any engine activity.

Once the calibration phase is completed a PI controller, shown in Figure 5, is used. Input to the controller is the desired accelerator position in mm. This position is calculated from the range limits and the input signal which is sent from the simulator at a frequency of 200 Hz.
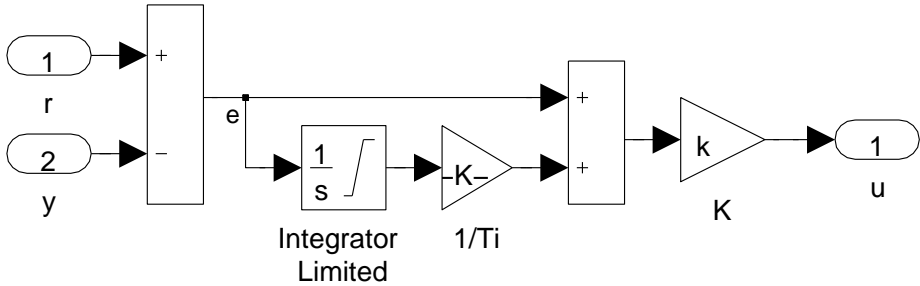
Figure 5: Position control of accelerator pedal with limits on integrator to avoid wind-up using Matlab Simulink.

Brake pedal control

The actuator controlling the brake pedal will be subjected to a significant resistance force when a large braking pressure is commanded from the simulator. It is thus desirable that the mounting of the pedal robot in the vehicle is as stiff as possible. For the constructed robot all four front chair screw holes where used to ensure a sufficiently stiff mounting. For this actuator, maximum load has been prioritized and the dynamic load is 420 Nm while the maximum speed is 215 mm/s.

As control signal measured brake pressure in Sim III was scaled linearly between measured brake pressure limits in the Volkswagen Passat test vehicle. The measured maximum and minimum brake pressure in Sim III was thus scaled to measured maximum and minimum brake pressure in test vehicle. In case of measurement spikes the brake pressure measurement was limited to the maximum pressure limit. Zero and maximum pressure in Sim III was measured from 0 kPa to 14000 kPa, and in the test vehicle it was measured from 3 to 7 volts.

As for the accelerator pedal the circuit breakers are first adjusted to define the maximum allowed range of the brake pedal. The brake pedal actuator control application then also starts with a calibration phase where the circuit breakers are used for defining the working range of the actuator. For the brake pedal

control the circuit breakers are adjusted to give maximum and minimum allowed pressure in the brake cylinder of the vehicle. To close the control loop the vehicle has been equipped with a pressure sensor, measuring the pressure in the brake master cylinder. One important aspect of the calibration is to adjust the zero pressure limit so that when the simulator commands zero pressure the brake pedal is not activated. This is necessary because if the pedal is even slightly activated the vehicle's own logic may prevent the car from accelerating.

Once the calibration phase is completed a PI controller for pressure in the main brake cylinder is used. This controller is sufficient when the command signal is greater than zero since this will make the actuator push against the brake pedal. When commanded pressure is zero there is no control of the actuator position and nothing will prevent it from drifting backwards into the circuit breaker. This will cut the power to the actuator for safety reasons. Therefore the pressure controller is complemented by a position controller, which is also a PI controller. This controller uses output from the motor encoder and kicks in when the actuator has no contact with the brake pedal. This way the pedal is prevented from drifting into the circuit breaker.

A problem with the brake pressure measurement is that the voltage switching from the PWM motor control has a negative influence on the measured brake pressure which interferes with the controller. To overcome this problem a second order low-pass filter is used. The filter was tuned to remove the pressure spikes that were present in the pressure signal which introduced a signal delay of approximately 15 ms.

2.4 Connection between facilities

To be able to use the powertrain setup at LiU together with the Sim III simulator a connection had to be established between the two facilities. As the physical distance is rather short, approximately 500 meters, an optical fiber link was established which connects the network at the chassis dynamometer facility with the Sim III network. To ensure that no external interference occurred during the simulations this network was closed off by turning off the power to routers connecting hardware which was not used during these experiments. Because UDP has a lower overhead than TCP and because that the need for an acknowledge is not needed when no packet loss is expected UDP was chosen as communication protocol.

2.5 Synchronizing vehicle models

Both the chassis dynamometer in the propulsion laboratory and Sim III need to know the wheel speed of the vehicle. The chassis dynamometer uses the speed for the road force simulation and Sim III needs it for the driver experience.

The chassis dynamometer at the vehicle propulsion lab uses a vehicle model to calculate vehicle speed according to the model in (1). The modeled wheel speed is used as reference and the amount of torque that the powertrain excerts

at the wheel hubs are measured. Using this torque the vehicle speed is then increased or decreased according to (1).

For the moving base simulator there is thus at least two different ways to calculate vehicle speed. One option is to use the rotational velocity measured at the wheels in the propulsion laboratory and another option is to instead use the measured torque to calculate the acceleration which is then integrated to vehicle speed using the model equations in (1) using the same model parameters as for the dynamometer.

In Figure 6 we show an acceleration phase of the vehicle when starting from stand still on a motorway. Here the velocity is calculated using the two described options. The speed limit on a Swedish motorway is typically 110 km/h. At time
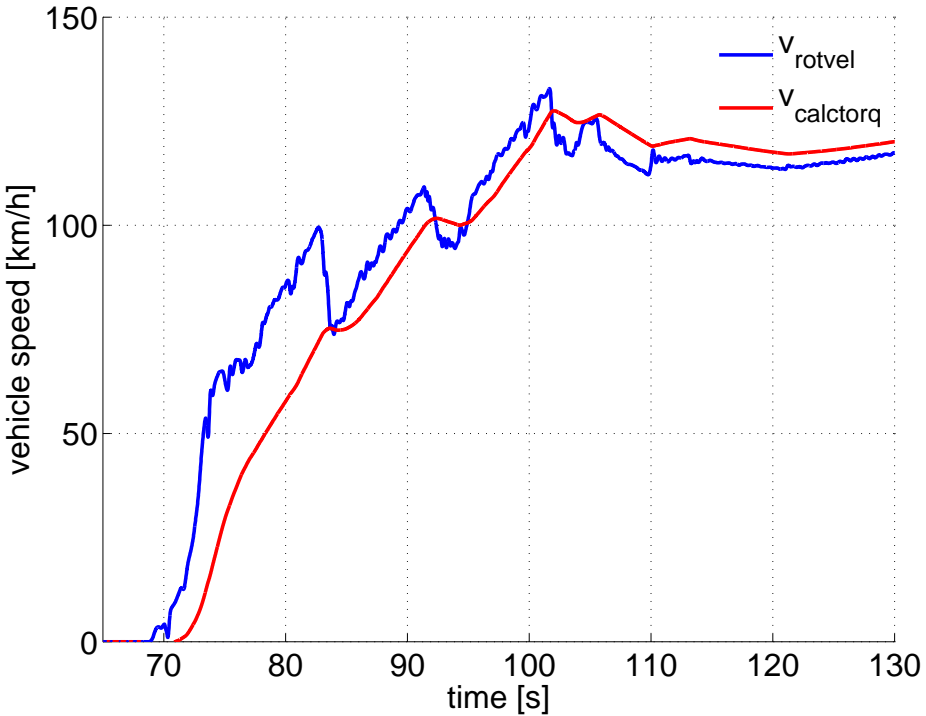
Figure 6: Measured velocity from dynamometers rotational speed compared with calculated speed using (1) from measured dynamometers torque.

83 s in the data the transmission performs a gear shift and we see a large drop in measured rotational speed. Thus, we see that if we only use the measured rotational speed we get a large variation in speed during the gear shift. If we on the other hand would use measured torque the models deviate due to different implementation choices.

To overcome this model deviation while at the same time suppressing large speed variations due to gear shifts our approach is to use an observer to merge

the two signals. By tweaking the observer gain, K, it is possible to smooth out the speed variation while keeping the two models synchronized. The equations for the vehicle speed using discrete notation is

$$
\begin{aligned}
\dot{v}[i] = {} & - c_{\mathrm{r}} \cdot g \cdot \min(v[i-1], 1.0) \\
& + \frac{T_1 + T_2}{m_{\mathrm{v}} \cdot r_{\mathrm{w}}} \\
& - c_{\mathrm{d}} \cdot A_{\mathrm{f}} \cdot \rho_{\mathrm{air}} \cdot \frac{v^2[i-1]}{2 \cdot m_{\mathrm{v}}} \\
& + K\left(\frac{\pi}{30}\frac{n_1 + n_2}{2} r_{\mathrm{w}} - v[i-1]\right) \\
v[i] = {} & v[i-1] + \dot{v}[i] \cdot \Delta t
\end{aligned}
$$

where T_1 and T_2 are torque measured at the chassis dynamometer rig for the front wheels, n_1 and n_2 are measured rotational speed at the chassis dynamometer and Δt is the timestep between samples. Here effects of incline and speed offset due to wind have been neglected.

2.6 Driving mission

A driving mission with the goal to test the complete setup and at the same time get first impressions feedback was constructed. Other objectives was to evaluate if the obtained performance fulfilled our expectations. The used driving mission consisted of approximately 10 km of driving on a previously measured part of the E4 motorway between Linköping and Norrköping. About 3 km of the drive was without traffic while 7 km was with light surrounding traffic. The height profile of the road is shown in Figure 7 where it can bee seen that the motorway is going slightly downwards. The road curvature of the used road segment is small and is thus approximated to be straight. At the start of the driving mission the position for Sim III and the chassis dynamometer are synchronized.

For the initial testing test drivers were recruited at VTI and LiU and their instructions were to maintain a speed between 60 km/h and 140 km/h while trying to get a feeling of the system without having too unnatural behavior. This means that most of the test drivers, even though they were not involved in this work had heard of it, and thus were biased. The large linear motion in Sim III was used for lateral motion and the cylinders were used to present acceleration and deceleration. When a driving mission was complete the test driver was asked to fill in a questionnaire and after that the test leader had an informal discussion until the next test person arrived, which was typically in around 5 minutes.
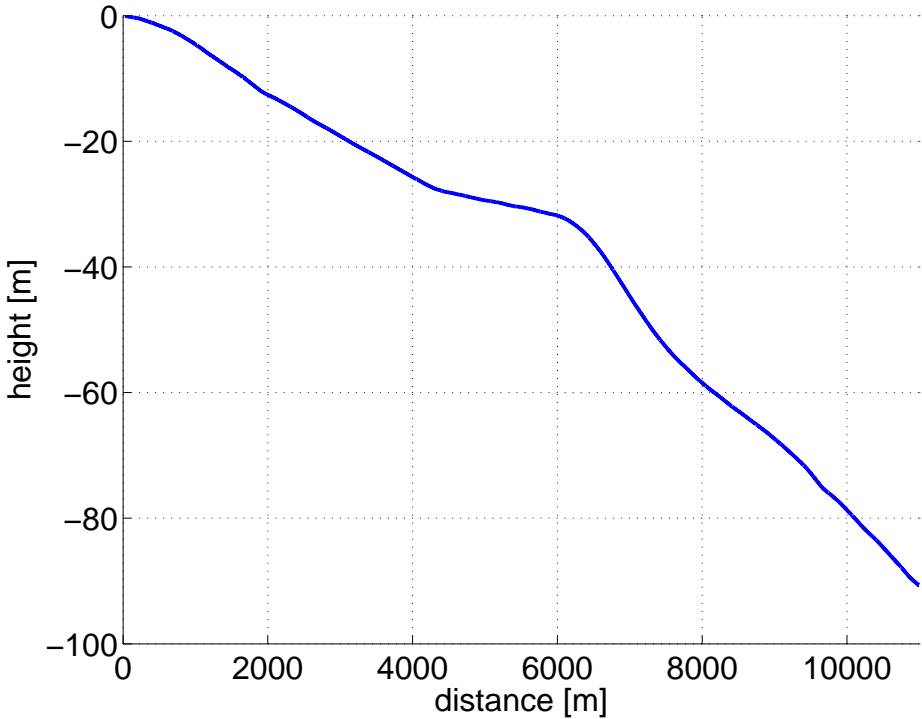
Figure 7: Longitudinal height profile of the used road segment.

3   Results

3.1   Network performance

A round trip time, RTT, test was used to test the performance of the network. A test packet similar to the actual packages sent during simulations was created to ensure that the testing conditions were similar to those of an actual driving mission. The test packets represents actual packets sent from Sim III with some extra data to ensure that the packets had decent sizes, see Table 3. For the RTT test each packet is timestamped and id-tagged with an increasing counter value before being sent off. This was to ensure that packets were received in order. The packets are then sent at 200 Hz from Sim III, which is the same speed at which the simulator core is running, and upon reception at the vehicle propulsion laboratory they are sent back without modification. When the packet returns to Sim III it is once again timestamped and stored to disc. Typically experiments does not involve driving for to long and about one hour of driving were considered enough as a little above normal. Therefore, during the test one million packets were sent which corresponds to a little more than 83 minutes.

The RTT test programs were running at Linux computers and to ensure

Table 3: Packet structure that was used in the RTT test between the two facilities.

Type	Name
time_t	send_sec
suseconds_t	send_usec
time_t	recv_sec
suseconds_t	recv_usec
long	counter
float	data[70]

Table 4: Statistics for the RTT test between the facilities.

Statistic	Value
Number of Packets	1 000 000
Min delay	0.20 ms
Max delay	2.17 ms
Median delay	0.22 ms
Dropped packets	none
Spikes above 0.5 ms	18

as low latencies as possible the programs ran with higher priority than normal processes. This way the test was performed in the exact same way as would be the case during a driving mission.

The round trip times for one of these test can be seen in Figure 8 and statistic measures of the delays are shown in Table 4. No packets were received in the wrong order for any of the tests which is the expected result as the largest obtained packet delay was 2.17 ms and a complete simulation loop is 5 ms. 99.9 percent of the packages had a delay of 0.27 ms or faster.

3.2 Step response tests of pedal robot

To evaluate the accelerator pedal response time a number of step response tests were performed. The step response tests were about two minutes each and for these test the accelerator pedal was fed reference values of 0, 0.25, 0.75 and 1.0. In Figure 10 five step responses from two different tests are shown on top of each other. The first tests shows a step from 0 (released) to 1 (maximally depressed) and the second shows steps between 0.25 to 0.75 of maximally depressed accelerator pedal.

Step response tests were conducted for the brake as well. For these tests approximately four minutes of step responses were recorded for two different types of step responses, one test between minimum and maximum pressure and one test between 0.25 to 0.75 of maximal brake pressure. Five steps are shown on top each other in Figure 11, where also the two different control strategies
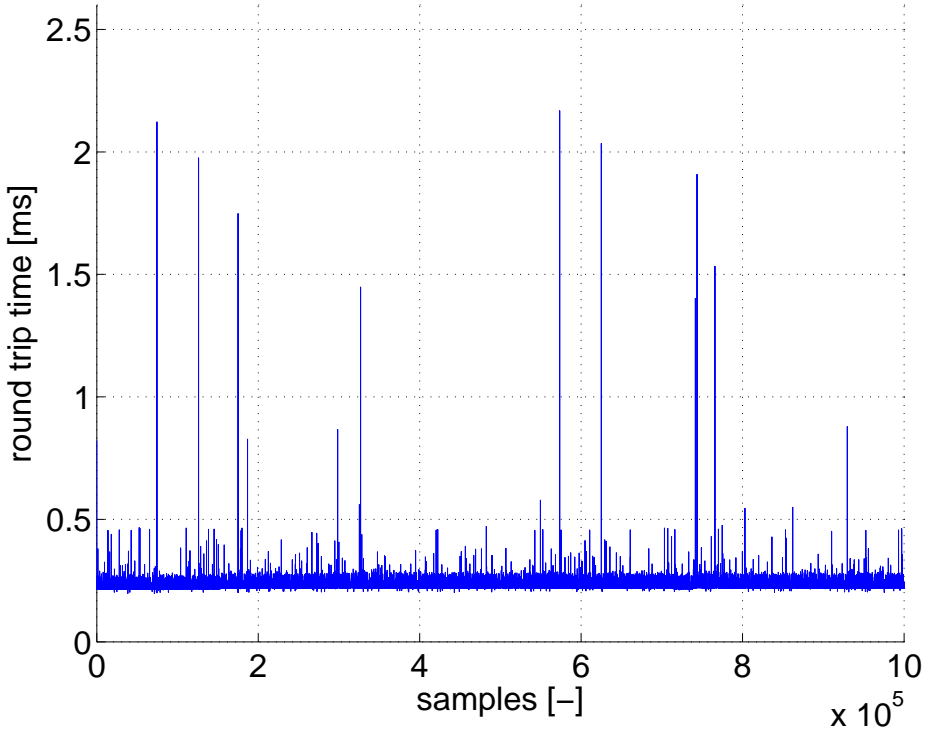
Figure 8: Round trip time, RTT, between the propulsion lab at LiU and Sim III using the fibre optics link.

for the fully released brake pedal and the not fully released brake pressure can be seen.

3.3   RUNNING THE COMPLETE SYSTEM

The study with our driving mission contained five test drivers were data were logged. Here we show data from the different driving missions and summarizes feedback from the test drivers.

ACCELERATOR AND BRAKE PEDAL

The performance of the accelerator and brake pedals is analyzed by evaluating the correspondence between the desired and obtained output. Using these values a control error $\epsilon = u_{ref} - u$ is calculated. Logged data from one of the test drivers is shown in Figure 9 and Figure 12 together with respective control error.
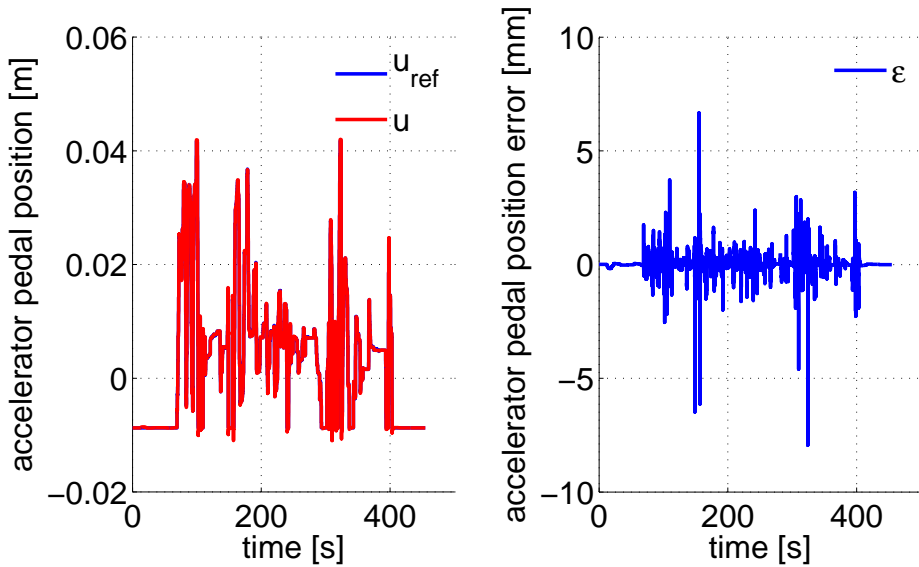
Figure 9: Accelerator pedal position reference value compared with actuated position value for one of the test drivers.
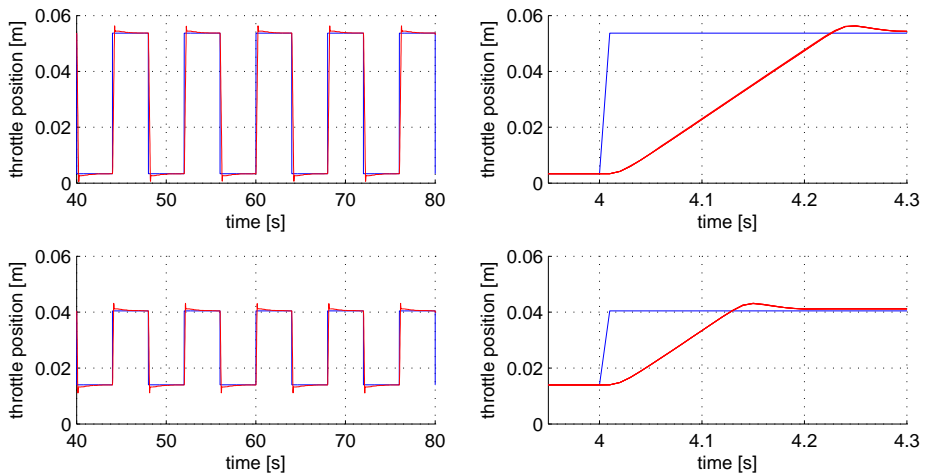
Figure 10: Step response tests made with the accelerator. The steps are from 0 (released) to 1 (maximally depressed) and from 0.25 to 0.75 of maximally depressed accelerator pedal. In the right figures five steps are shown on top of each other.
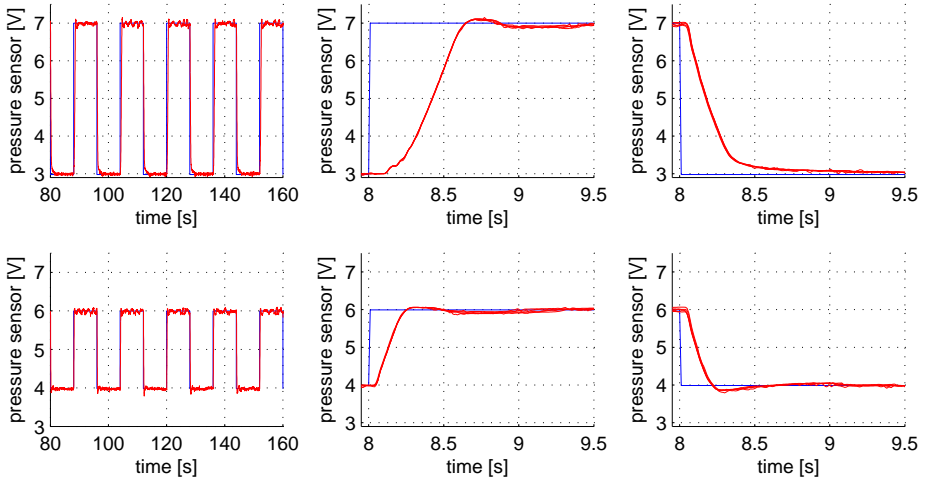
Figure 11: Step response tests made with the brake pedal. Steps are from minimum to maximum brake pressure (upper) and between 0.25 to 0.75 of maximum brake pressure (lower). Note the different control strategy for releasing the brake in the upper rightmost figure.
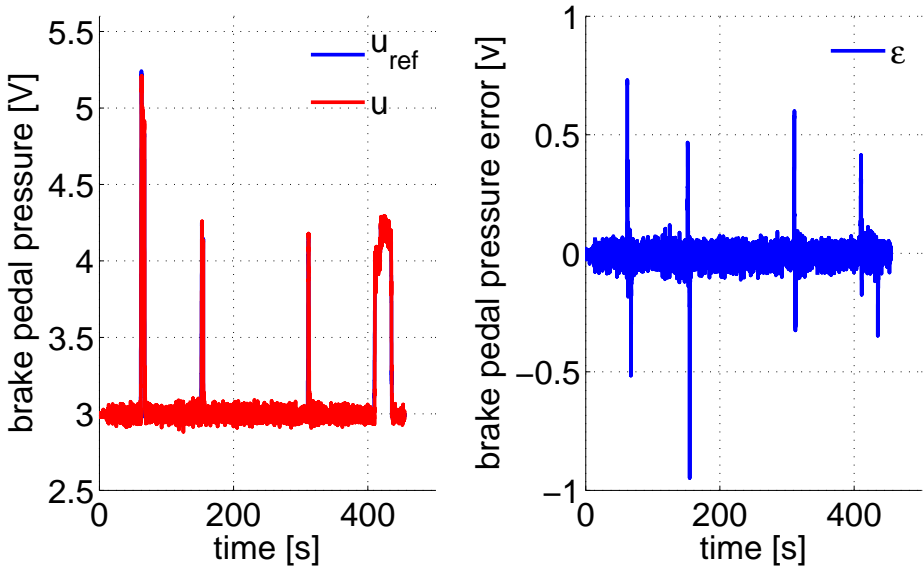
Figure 12: Brake pedal pressure reference value compared with actuated pressure value for one of the test drivers.

As can be seen, both the accelerator and brake pedals closely follows their reference signals. The RMS of the control errors are between 1.87e-4 to 6.44e-4 for the accelerator pedal and between 4.82e-2 to 5.96e-2 for the brake pedal. As the working range of the accelerator pedal is approximately 5 cm this translates to a RMS error of about 1 percent, while for the brake pedal with a working range of 4 V the RMS error is about 1.5 percent. However, because the brake pedal is rarely used during normal driving these values needs to be interpreted with care.

For the accelerator pedal, which is used most of the time during driving, the conclusion is that the controller is sufficiently fast while for the brake pedal the RMS is averaged over large periods where the pedal is never used and where the control error is almost zero. The brake pedal RMS therefore measures mostly noise.

VEHICLE RESPONSE IN SIM III

To tune the trade-off for the observer parameter K a few test drives were conducted before the study. In these tests the value of K was adjusted until a reasonable trade-off was obtained. The velocities that were obtained for the chassis dynamometer and Sim III using the chosen K for one of the test drivers driving the test vehicle is shown in Figure 13. Here it can be seen that the
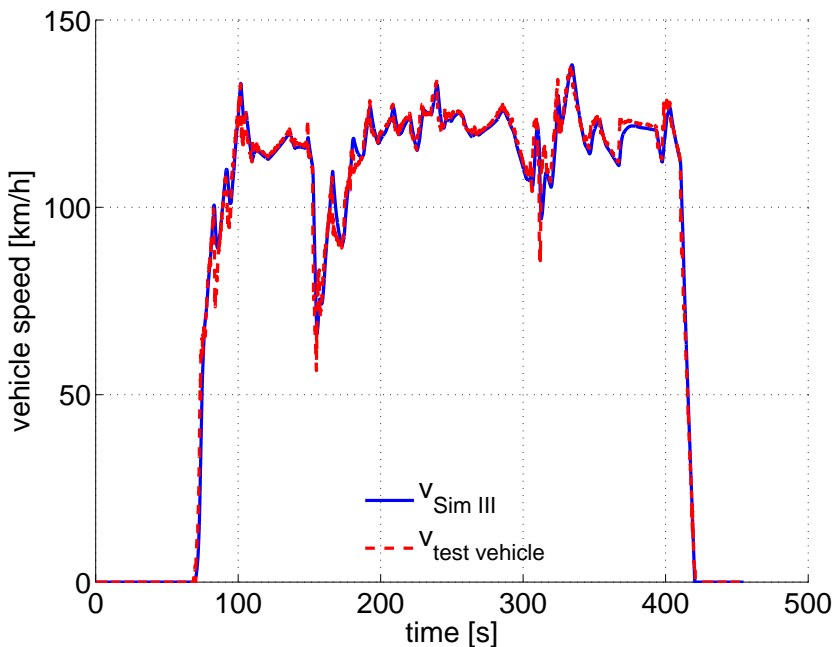
Figure 13: Comparison of the Sim III vehicle speed with the chassis dynamometer vehicle speed for the test vehicle for the chosen K.
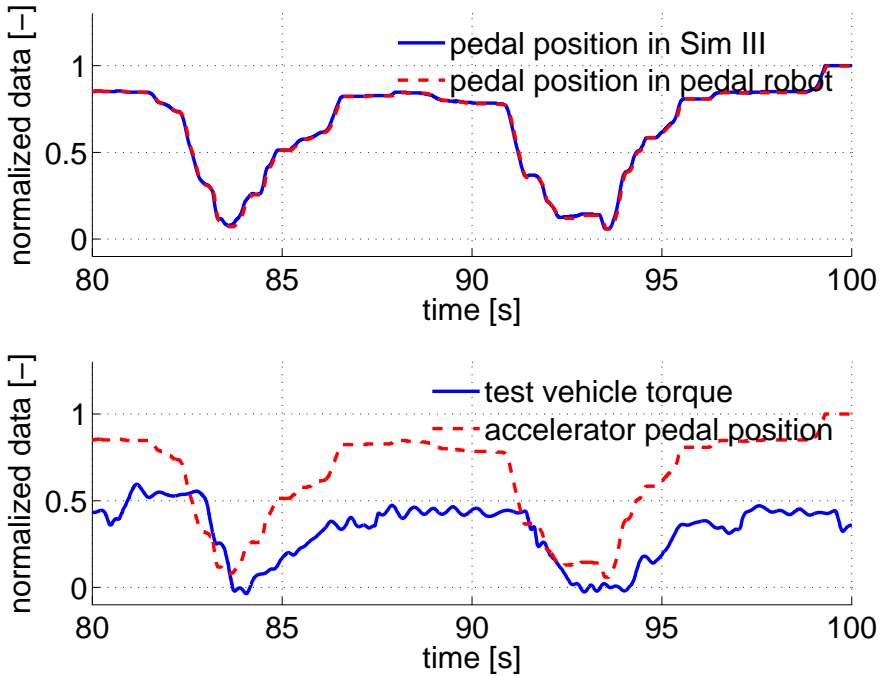
Figure 14: Response times from pedal position in Sim III to pedal robot position (upper) and from pedal robot position to test vehicle torque (lower).

velocity in Sim III is smoother than for the test vehicle, while we also see that the difference in velocity is small. This difference in velocity results in a position error which is approximately 1 percent of driven distance, meaning driving 100 m yields an offset in position by 1 m.

Another important aspect are the time delays for the system. In Figure 14 the time delay from an accelerator pedal change until the pedal robot has actuated desired position is about 0.05 to 0.1 s, which was expected from the step response test. Similar results are obtained for the brake pedal. The time delay from releasing the accelerator pedal, at about 92 s in the figure, until a change in measured torque is about 0.6 s.

TEST DRIVER FEEDBACK

The driver behavior differed between drivers as some drivers were driving between 60 km/h to 140 km/h and some drivers maintained 110 km/h only changing speed due to traffic conditions. This can be seen in the reference values for the accelerator and brake pedal and also in the velocity and acceleration of the vehicle in Sim III.

The general feeling of the vehicle was found sufficiently good by the test

drivers. There were however some complaints of which the main two were

- Lack of engine sound feedback.

- The brakes seemed slow.

The reason for the lack of engine sound is that engine speed was not measured at the propulsion laboratory and hence the sound feedback couldn't be adjusted according to engine speed. Therefore it was decided to rather have no sound than erroneous sound. This is, however, something that will be fixed in future experiments. As a result of the missing sound test drivers probably exaggerated accelerator use.

4 CONCLUSIONS

The connection between the facilities is fast enough for our purposes. The amount of lost packets are none meaning that every packet will reach its destination. The maximum delay is shorter than the simulation loop time which means that data from the chassis dynamometer will always be recent. This conclusion is also drawn when looking at the logged data where the delay from the network is so small compared to other delays that it can not be seen.

The constructed pedal robot works well. This is seen both in the results from the step response test and in the data from the test driving. For the construction, one intention was to minimize the time of switching vehicles and when mounting the pedal robot it was confirmed that even though the front chair had to be removed the mounting took about 30 minutes. As the perception of braking was considered in need of improvement this would be one of the first part to improve along with the engine sound which is most easily implemented.

Data obtained from our driving mission experiment with test drivers show that the complete setup is functional and that the synchronization of the models for the different systems works. For a typical driving mission this initial experiment setup already indicates small, meaning around 1 percent, control errors in the vehicle position and in accelerator pedal position for motorway driving.

Put together, interviews with test drivers and data from the example driving mission shows that the current co-simulation setup has the potential of obtaining a realistic driving experience.

References

A. Andersson and J. Jansson. A moving base simulator investigation of effects of a yaw stability system caused by a side impact. *ASME/Journal of Computing and Information Science in Engineering*, 11(4), 2011.

A. Bolling, J. Jansson, M. Hjort, M. Lidström, S. Nordmark, H. Sehammar, and L. Sjögren. An approach for realistic simulation of real road condition in a moving base driving simulator. *ASME/Journal of Computing and Information Science in Engineering*, 11(4), 2011.

C.C. Chan. The state of the art of electric, hybrid, and fuel cell vehicles. *Proceedings of the IEEE*, 95(4):704–718, 2007.

T. Ersal, M. Brudnak, A. Salvi, J.L. Stein, Z. Filipi, and H.K. Fathy. Development and model-based transparency analysis of an internet-distributed hardware-in-the-loop simulation platform. *Mechatroncis*, 21:22–29, 2011.

T. Ersal, M. Brudnak, J. L. Stein, and H. K. Fathy. Statistical transparency analysis in internet-distributed hardware-in-the-loop simulation. *IEEE/ASME transactions on mechatronics*, 17(2), 2012.

G.J. Offer, D. Howey, M. Contestabile, R. Clague, and N.P. Brandon. Comparative analysis of battery electric, hydrogen fuel cell and hybrid vehicles in a future sustainable road transport system. *Energy policy*, 38(1):24–29, 2010.

C. Wu, J. Wan, and G. Zhao. Addressing human factors in electric vehicle system design: Building an integrated computational human-electric vehicle framework. *Journal of power sources*, 214:319–329, 2012.

P. Öberg, P. Nyberg, and L. Nielsen. A new chassis dynamometer laboratory for vehicle research. In *SAE World Congress*, number 2013-01-0402, Detroit, USA, 2013.

Paper C

Driving Cycle Adaption and Design Based on Mean Tractive Force*

C

Driving Cycle Adaption and Design Based on Mean Tractive Force

Peter Nyberg, Erik Frisk, and Lars Nielsen

Vehicular Systems, Department of Electrical Engineering,
Linköping University, SE-581 83 Linköping, Sweden.

Abstract

Driving cycles are used for certification, for comparison of vehicles, and to an increasing extent as an engineering tool in vehicle design. A situation with only a few fixed driving cycles to use would then lead to the risk that a test or design would be tailored to details in the driving cycle instead of being representative. Due to this, and due to the increased use in the development process, there is now a strong need for methods to achieve representative driving cycles that in a wide sense are similar but not the same. To approach this problem area, we define equivalence between driving cycles based on mean tractive force, and develop algorithms and methods for equivalence-modification and equivalence-transformation of driving cycles. There are a number of applications for these methods but one example that is demonstrated is to transform the well-known FTP75 into an equivalent NEDC, and the other way around, to transform the NEDC into an equivalent FTP75.

1   INTRODUCTION

A driving cycle is a representation of how vehicles are driven and is usually represented by a set of data points of vehicle speed versus time. It is used for certification, for comparison of vehicles, or as an engineering tool in vehicle design (André, 1996), (Lin and Niemeier, 2002), or (Stockar et al., 2010). Regardless of application, the general idea behind a driving cycle is that it should be representative for driving behavior in the region it is used, and perhaps also that it should capture different driver behavior and different traffic situations. A representative driving cycle usually means that some statistical criteria of interest is sufficiently close to data from real-world driving.

There are many examples of driving cycles, and as an example a common one, is the New European Driving Cycle (NEDC), is seen in Figure 1. This particular driving cycle has low levels of acceleration compared to several examples of real-world driving, and thus, the NEDC is not representative of real-world driving conditions (Zaccardi and Le Berr, 2012). The NEDC also underestimate the CO_2 emissions compared to real-world driving (Fontaras and Dilara, 2012). Further, design parameters that are optimized for a certain driving cycle are not necessarily optimal for another driving cycle (Schwarzer and Ghorbani, 2013), and a reason for this is that vehicle manufacturers need only to focus on a limited operating regions of the engine (Kågeson, 1998). If another driving cycle excites the operating regions differently, different exhaust gas emissions and fuel consumption characteristics are obtained, and thus if the driving cycle is not representative, the optimization on a single driving cycle, will be a sub-optimal solution for real-world driving (Schwarzer and Ghorbani, 2013; Kågeson, 1998). With this background, and the increased importance of using driving cycles in the vehicle product development process, it is natural that there are new proposals for finding representative driving cycles, see for example (Lee and Filipi, 2011), (Lin and Niemeier, 2002), (Schwarzer and Ghorbani, 2013), or (Kamble et al., 2009).

To avoid the single cycle problem, it would be highly beneficial to have mechanisms to generate similar driving cycles that are not the same. The approach taken here is to define the concept of equivalent driving cycles, and this is done by using integral measures on the driving cycles, with mean tractive force (MTF) (Guzzella and Sciarretta, 2007) as the main example in this paper.

The main objective is to find algorithms that can modify a given driving cycle into a different driving cycle that is equivalent in the measure, or to modify a given driving cycle into another one with a specified equivalence measure. Formulating and approaching these problems are the main topic of this paper.

2   DRIVING CYCLE EQUIVALENCE

A driving cycle excites and tests vehicles, and a vehicle's particular parameters determine the impact the driving cycle has on the powertrain. To compare
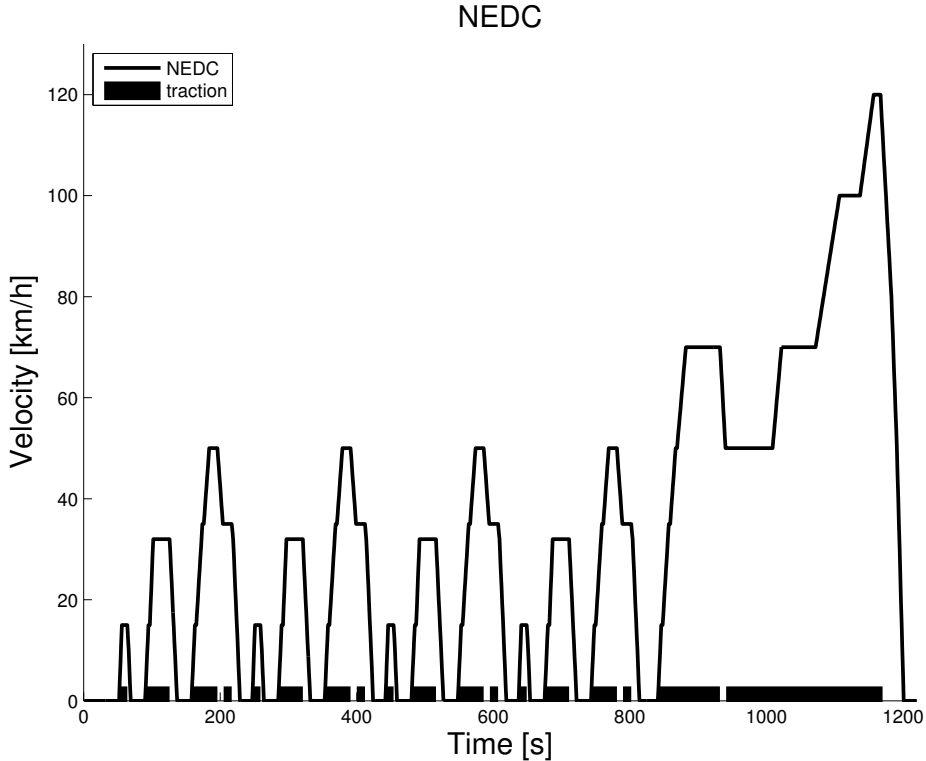
Figure 1: The NEDC with marked traction regions which indicates the instants where the powertrain needs to deliver positive power to the wheels so that the vehicle is able to track the driving cycle.

the performance obtained in two different driving cycles is difficult since the cycles have different characteristics. A naive way could be to scale the driving cycles so they have the same mean vehicle speed. However, this does not make the cycles equivalent, since acceleration characteristics may still be radically different. Thus, a more insightful characterization of driving cycles is needed.

2.1 MEAN TRACTIVE FORCE EQUIVALENCE

The required torque at the wheels, from acceleration, is higher in the FTP75 compared to the NEDC since the FTP75 has more aggressive acceleration sequences. The EUDC (the highway part of the NEDC), has higher mean velocity than the FTP75 which yields that the rolling resistance, which is dependent on the rolling coefficient of the tires of the vehicle, has a higher impact on the vehicle power. Hence, the torque and power are dependent on the driving cycle, the vehicle mass and other parameters of the vehicle.

Using a measure on a driving cycle it is possible to define equivalence among driving cycles and also to make comparison between cycles possible. A measure can be defined on the whole time interval $\tau = [0, t_{\text{final}}]$, but the characterization used here is based on the mean tractive force (MTF) (Guzzella and Sciarretta, 2007). The integration intervals for MTF are determined by the vehicle traction regions where the powertrain of the vehicle provides positive power ($F(t) > 0$), i.e. $\bar{F}_{\text{trac}}$ is defined on a subset $\tau_{\text{trac}} = \{t \in \tau : F(t) > 0\}$, and the measure is

$$\bar{F}_{\text{trac}} = \frac{1}{x_{\text{tot}}} \int_{t \in \tau_{\text{trac}}} F(t) \cdot v(t) \, dt, \tag{1}$$

where x_{tot} is the distance traveled in the driving cycle, $F(t)$ is the sum of the forces at the wheels, and $v(t)$ is the speed of the vehicle. The measure (1) can be used for a preliminary estimate of the fuel consumed by the propulsion system (Guzzella and Sciarretta, 2007).

For flat roads the forces at the wheels origins from aerodynamic drag resistance force (F_{air}), rolling resistance force (F_{roll}), and also forces due to acceleration/deceleration of the vehicle (F_{m}). These forces are here modeled as

$$F(t) = F_{\text{air}} + F_{\text{roll}} + F_{\text{m}} \tag{2}$$
$$F_{\text{air}} = \frac{1}{2}\rho_a c_d A_f v^2(t)$$
$$F_{\text{roll}} = mc_r g$$
$$F_{\text{m}} = ma(t),$$

where ρ_a is the air density, c_d is the drag coefficient, A_f is the frontal area. The rolling resistance is modeled as proportional to the vehicle weight. The weight is the product of vehicle mass (m), and the gravitational constant g. The proportional constant is denoted c_r. Finally, the force from acceleration is the mass times the acceleration $a(t)$.

The MTF quantity $\bar{F}_{\text{trac}}$ in (1), can be partitioned into three different parts originating from aerodynamic drag resistance, rolling resistance, and acceleration resistance,

$$\bar{F}_{\text{trac}} = \bar{F}_{\text{air}} + \bar{F}_{\text{roll}} + \bar{F}_{\text{m}} \tag{3}$$

$$\bar{F}_{\text{air}} = \frac{1}{x_{\text{tot}}} \int_{t \in \tau_{\text{trac}}} \frac{1}{2}\rho_a c_d A_f v^2(t) \cdot v(t) \, dt = \kappa\alpha \tag{4}$$

$$\bar{F}_{\text{roll}} = \frac{1}{x_{\text{tot}}} \int_{t \in \tau_{\text{trac}}} mgc_r \cdot v(t) \, dt = mgc_r\beta \tag{5}$$

$$\bar{F}_{\text{m}} = \frac{1}{x_{\text{tot}}} \int_{t \in \tau_{\text{trac}}} ma(t) \cdot v(t) \, dt = m\gamma, \tag{6}$$

where $\kappa = \frac{1}{2}\rho_a c_d A_f$. The force components in (4 - 6) have been split into two parts where the first part consists of constants and vehicle parameters. The other part is driving cycle specific, but is however influenced by the vehicle

parameters indirectly due to their influence on the coasting velocity in (10), which affects the traction regions, τ_{trac}. The parameters related to the driving cycle are

$$\alpha = \frac{1}{x_{\text{tot}}} \int_{t \in \tau_{\text{trac}}} v^2(t) \cdot v(t) \, dt \tag{7}$$

$$\beta = \frac{1}{x_{\text{tot}}} \int_{t \in \tau_{\text{trac}}} 1 \cdot v(t) \, dt = \frac{x_{\text{trac}}}{x_{\text{tot}}} \tag{8}$$

$$\gamma = \frac{1}{x_{\text{tot}}} \int_{t \in \tau_{\text{trac}}} a(t) \cdot v(t) \, dt. \tag{9}$$

Based the introduced MTF in (4 - 6) we are ready to define a equivalence measure for driving cycles

Definition 1. *For a given vehicle, two driving cycles, $v_1(t)$ and $v_2(t)$, are said to be* equivalent, *denoted $v_1(t) \sim v_2(t)$, if the following is fulfilled*

$$\alpha(v_1(t)) = \alpha(v_2(t))$$
$$\beta(v_1(t)) = \beta(v_2(t))$$
$$\gamma(v_1(t)) = \gamma(v_2(t)).$$

2.2 DETERMINING TRACTION REGIONS

A vehicle is in traction if the powertrain need to provide positive power ($F(t) > 0$ in (2)). The other two modes are coasting ($F(t) = 0$) and braking ($F(t) < 0$). Another way to determine if the vehicle is in traction is to calculate the coasting velocity which is determined by (2). Using $\dot{v}(t) = a(t)$ and $F(t) = 0$, the vehicle coasting speed (v_{coast}) is determined by

$$0 = F_{\text{air}} + F_{\text{roll}} + F_{\text{m}} \Rightarrow$$
$$\dot{v}_{\text{coast}}(t) = -\frac{1}{2m} \rho_a c_d A_f v_{\text{coast}}^2(t) - c_r g$$
$$= -k_1^2 v_{\text{coast}}^2(t) - k_2^2 \Rightarrow$$
$$v_{\text{coast}}(t) = \frac{k_2}{k_1} \tan(\arctan(\frac{k_1}{k_2} v_{\text{coast}}(t_0)) - k_1 k_2 \cdot t). \tag{10}$$

For discrete driving cycles and given an initial speed $v(t_0 = t_{k-1})$ in the driving cycle, the vehicle is in traction at time t_k if $v(t_k) > v_{\text{coast}}(t_k)$, otherwise the vehicle is in coasting ($v(t_k) = v_{\text{coast}}(t_k)$), or in braking ($v(t_k) < v_{\text{coast}}(t_k)$). The traction regions in the NEDC for a certain vehicle is seen as the marked regions near the x-axis in Figure 1.

2.3 PHYSICAL INTERPRETATION OF THE MTF COMPONENTS

The parameters β and γ have physical meanings as follows. The parameter β in (8), which is related to the MTF measure for the rolling resistance, is

the quotient between the distance traveled during traction, x_{trac}, and the total driven distance x_{tot}.

The MTF component (6) can be written as

$$
\begin{aligned}
\bar{F}_{\text{m}} = m\gamma &= \frac{1}{x_{\text{tot}}} \int_{t \in \tau_{\text{trac}}} m\dot{v}(t) \cdot v(t)\, dt \\
&= \frac{1}{x_{\text{tot}}} \int_{t \in \tau_{\text{trac}}} \frac{m}{2} \cdot \frac{dv^2(t)}{dt}\, dt \\
&= \frac{1}{x_{\text{tot}}} \sum_{i}^{\#trac} \left[\frac{m \cdot v^2(t)}{2} \right]_{t_{i,\text{start}}}^{t_{i,\text{end}}},
\end{aligned}
\tag{11}
$$

where it is clearly seen that it is proportional to the sum of the difference in kinetic energy for all the traction intervals. The number of traction intervals is denoted $\#trac$ and each traction interval has its start, $t_{i,\text{start}}$, and end point $t_{i,\text{end}}$. Given that x_{tot} is the same for two driving cycles, they have the same $\bar{F}_{\text{m}}$ if $\sum_{i}^{\#trac} \left[\frac{m \cdot v^2(t)}{2} \right]_{t_{i,\text{start}}}^{t_{i,\text{end}}}$ are equal. If the start and end points of the traction regions are not changed and x_{tot} is kept constant this measure will be the same before as after any changes in the driving cycle. This observation will be used in the algorithms further on.

3   PROBLEM FORMULATION

A key problem studied is how to transform a given driving cycle, into another driving cycle that is equivalent in the sense of Definition 1. The first basic problem is thus

Problem P0: Given a driving cycle $v(t)$, find $\tilde{v}(t) \neq v(t)$ so that $\tilde{v}(t) \sim v(t)$.

A second strongly related problem is to incorporate a specified driving cycle segment, v_{spec} defined on $\tau_{\text{spec}} \subset \tau$, within the driving cycle, where $\tilde{v}(t) = v_{\text{spec}}(t), t \in \tau_{\text{spec}}$.

Problem P1: Given a driving cycle $v(t)$, find $\tilde{v}(t) \neq v(t)$ so that (i) $\tilde{v}(t) \sim v(t)$ and (ii) $\tilde{v}(t) = v_{\text{spec}}(t),\ t \in \tau_{\text{spec}}$.

Another problem is when a driving cycle is given, but it is desired to change the excitation of the vehicle properties, while maintaining as much of the vehicle speed characteristics of the original driving cycle as possible. This can be done by changing the MTF quantity to the new desired target values $(\alpha', \beta', \gamma')$. The problem formulation is

Problem P2: Given a driving cycle $v(t)$ and a target $(\alpha', \beta', \gamma')$. Find $\tilde{v}(t)$ so that $|\alpha(\tilde{v}(t)) - \alpha'| \leq \epsilon_\alpha$, $|\beta(\tilde{v}(t)) - \beta'| \leq \epsilon_\beta$, $|\gamma(\tilde{v}(t)) - \gamma'| \leq \epsilon_\gamma$.

The target MTF could be the values for another driving cycle $v_2(t)$, $(\alpha(v_2(t))$, $\beta(v_2(t)), \gamma(v_2(t)))$, and the resulting driving cycle, $\tilde{v}(t)$, should resemble real-world driving and not be unrealistic. The next section will describe algorithms for the above mentioned problems.

4   ALGORITHM

A trivial solution to alter the driving cycle while maintaining the same MTF components would be to shuffle around the micro-trips to create a new driving cycle. This cycle is obviously altered but it is basically the same cycle. Instead we seek a solution that alter the driving cycle by doing iterative changes and at the same time maintaining the MTF quantities (3-6). To simplify the derivation of the algorithms, the total distance traveled, x_{tot}, and the traction regions will not be changed.

4.1   CORE COMPONENT: ANALYTICAL LOCAL MODIFICATIONS

Denote the original driving cycle as v_0 (where the time dependence is omitted) and a slightly altered driving cycle, $\tilde{v}$, with a speed difference vector δv that contains n non-zero elements, $\delta v_i = \delta v(t_i) = \delta_i$, $i = 1, 2, ..., n$. The altered driving cycle is thus $\tilde{v} = v_0 + \delta v$. The algorithm will not change the start or end points of traction intervals. This results in that the MTF component (6) is kept constant according to (11). This yields that only the integrals in (7 - 8) need to be considered, and thus two driving cycles has the same MTF if

$$\int_{t \in \tau_{\text{trac}}} v_0^3 \, dt = \int_{t \in \tau_{\text{trac}}} (v_0 + \delta v)^3 \, dt \tag{12}$$

$$\int_{t \in \tau_{\text{trac}}} v_0 \, dt = \int_{t \in \tau_{\text{trac}}} (v_0 + \delta v) \, dt. \tag{13}$$

It is possible to alter two speed points (v_{01}, v_{02}) and still maintain the MTF. However, the solution is then the trivial solution, the speed points change position ($\tilde{v}_{01} = v_{02}$ and $\tilde{v}_{02} = v_{01}$). Hence, switching or sorting speed points will not change the MTF as long the traction modes remain unchanged, and the start and end points in each traction region is not changed.

An issue is that the speed difference vector δv is not allowed to be chosen freely. The fact that the traction regions shall be intact implies that a change in the driving cycle is forced to not change the traction mode for any points. An illustration of the boundaries for any change in speed $v(t_k)$ is seen in Figure 2. The upper boundary origins from a limitation in the maximum acceleration, a_{max}, at point $v(t_k)$ and also that the next speed point $v(t_{k+1})$ does not lose traction. The lower boundary comes from that the current speed point will not loose traction and that the acceleration for the next speed point is kept within the maximum acceleration.
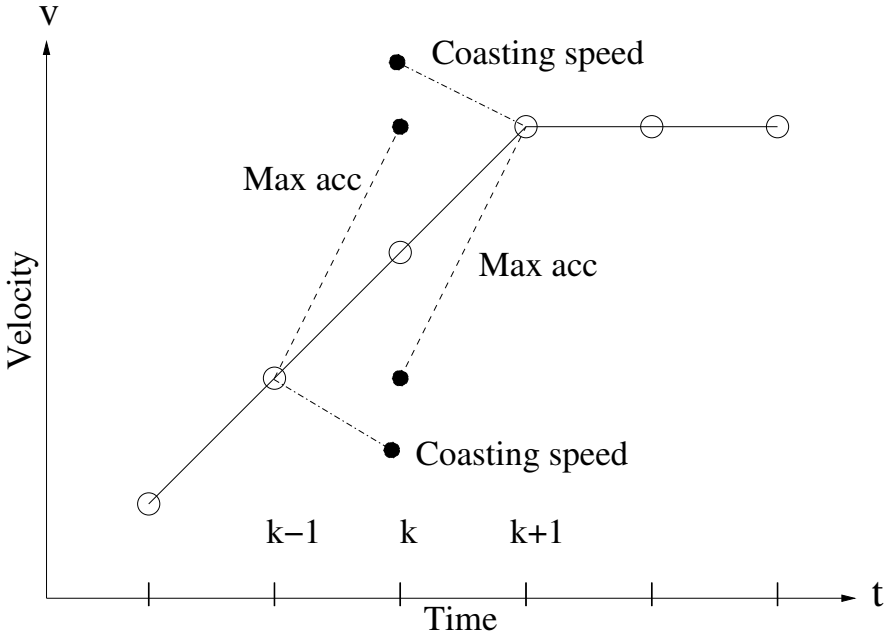
Figure 2: Limitations of changes of $v(t_k)$ which origins from maintaining the traction regions and also considering that the maximum acceleration is not exceeded.

If three speed points are considered $(n = 3)$, an extra degree of freedom is introduced. The variable that is free is δ_2, and when it is set it determines δ_1 and δ_3. For discrete driving cycles, the solution of (12-13) are

$$\sum v_0 = \sum v_0 + \delta v \Rightarrow$$
$$\delta_3 = -(\delta_1 + \delta_2) \tag{14}$$
$$\sum v_0^3 = \sum (v_0 + \delta v)^3 \Rightarrow$$
$$0 = \delta_1^2 \cdot a(\delta_2) + \delta_1 \cdot b(\delta_2) + c(\delta_2) \Rightarrow$$
$$\delta_1 = \frac{b}{2a} \pm \sqrt{\frac{b^2}{4a^2} - \frac{c}{a}}, \tag{15}$$

where δ_2 is the free variable and its dependency on the factors a, b, and c is omitted in (15). Thus, by picking a suitable δ_2 (considering Figure 2) and using (14-15), an altered driving cycle is achieved without changing the MTF measures. The reason for this is that the traction regions are intact, and (14) results in that the average speed is unchanged, hence the distance traveled during the traction regions is kept constant. Thus, x_{tot} will not be changed and the measures (3-6) will be the same.

The core component is this analytical solution to make local modifications of a given driving cycle without changing the MTF. In the most straightforward way the three speed points are randomly selected. This can be iteratively done and the results would be a driving cycle that varies around the original driving cycle, and thus, a solution to problem P0. In the next section this core component will be used to make global modifications of the driving cycle.

4.2   Algorithm 1: Global modifications of the driving cycle

Using the solution from the previous section iteratively produces an altered driving cycle that is of little use. It has the same MTF measures but due to the random selection of the speed points the resulting driving cycle is the original one with some fluctuations within it.

However, if the points that are changed in each iteration would be chosen more wisely, it is possible to alter the driving cycle in a more systematic way. For example, given a driving cycle, v, and a specified segment of a driving cycle, v_{spec}, with corresponding time points τ_{spec}, Algorithm 1 will produce an equivalent driving cycle $\tilde{v}$ such that $\tilde{v}(t) = v_{\text{spec}}(t), t \in \tau_{\text{spec}}$, and hence, a solution for problem P1. The algorithm uses the analytical solution in (14-15) as a base to change the driving cycle iteratively until the specified driving cycle segment is achieved. The pseudo-code for Algorithm 1 is seen in Figure 3.

procedure $\text{ALG1}(v, v_{\text{spec}}, \tau_{\text{spec}})$
    while any $v(t_i) \neq v_{\text{spec}}(t_i), \forall t_i \in \tau_{\text{spec}}$ **do**
        $bounds = f(v, a_{\max}, v_{\text{coast}}(v))$
        Choose at random $t_1, t_3 \in \tau_{\text{trac}} \setminus \tau_{\text{spec}}$
        Choose $t_2 \in \tau_{\text{spec}}$
        Set δ_2 to reduce $\sum_i |v(t_i) - v_{\text{spec}}(t_i)|$
        $\delta_1 = \frac{b}{2a} \pm \sqrt{\frac{b^2}{4a^2} - \frac{c}{a}}$ $\triangleright$ according to (15)
        $\delta_3 = -(\delta_1 + \delta_2)$ $\triangleright$ according to (14)
        $v(t_1) = v(t_1) + \delta_1$
        $v(t_2) = v(t_2) + \delta_2$
        $v(t_3) = v(t_3) + \delta_3$
    end while
end procedure

Figure 3: Algorithm 1 change a given driving cycle, v, iteratively, so that a specified driving cycle segment is incorporated within v, while maintaining the MTF.

4.3   Algorithm 2: Transforming to target α, β, and γ

The core component and the previous algorithm consider only that the driving cycle should maintain the MTF. To change how a driving cycle excites the vehicle properties a novel algorithm is proposed that, iteratively changes one measure at the time until the MTF of the altered driving $\tilde{v}$ is sufficiently close to target values $(\alpha', \beta', \gamma')$.

Step 1: Transforming β

As previously discussed, the quantity β in (8) is the ratio between traveled distance during traction regions and the total driven distance in the driving cycle. To change the driving cycle such that $|\beta(\tilde{v}) - \beta'| \leq \epsilon_\beta$ the speed points within the traction regions will be altered. This will change x_{trac} in (8) until the difference between $\beta(\tilde{v})$ and β' is sufficiently small.

Step 2: Transforming γ

If the traction regions are intact and x_{tot} is held constant, it is only possible to alter $\gamma(\tilde{v})$ by changing the speed at the start and end of each traction interval. By iteratively changing the end points it is possible to achieve $|\gamma(\tilde{v}) - \gamma'| \leq \epsilon_\gamma$. Every change in the end points need to be compensated so that the average speed is kept constant and hence also x_{tot}. If the traction region shall remain intact it may be necessary to scale certain traction intervals. Keeping x_{tot} constant is still vital for not changing $\beta(\tilde{v})$.

Step 3: Transforming α

Finally, to modify the driving cycle to get $|\alpha(\tilde{v}) - \alpha'| \leq \epsilon_\alpha$ while maintaining both $\beta(\tilde{v})$ and $\gamma(\tilde{v})$, can be achieved by expanding or contracting of the speed points (keeping the average speed) in the driving cycle. If the average speed is kept constant and the traction regions are maintained it will result in that x_{tot} is the same and hence will not affect $\beta(\tilde{v})$. If addition the start and end points of each traction regions is kept constant this will neither affect $\gamma(\tilde{v})$.

Algorithm summary

The algorithm is summarized in Figure 4, and is a solution for problem P2. For illustration of the use of Algorithm 2, the NEDC, v_1, will be transformed to the target MTF of the FTP75, v_2. Hence, producing an altered version of the NEDC, denoted $\tilde{v}_1$ which has an MTF that is sufficiently close to the MTF of v_2. A comparison between the original NEDC, the output from the intermediate step 2 (after the second while-loop in Figure 4), and the output after the last step is seen in Figure 5. The dash-dotted line correspond to a driving cycle that has similar MTF components as the FTP75 for (8) and (9). The solid line correspond to a driving cycle that has similar MTF as the FTP75. As can be

procedure ALG2($v, \alpha', \beta', \gamma'$)
    while $|\beta(v) - \beta'| > \epsilon_\beta$ **do**
        $bounds = f(v, a_{max}, v_{coast}(v))$
        Choose $t \in \tau_{trac}$
        Set δ_β regarding $bounds$, $\beta(v) - \beta'$
        $v(t) = v(t) + \delta_\beta$
    end while
    while $|\gamma(v) - \gamma'| > \epsilon_\gamma$ **do**
        $bounds = f(v, a_{max}, v_{coast}(v))$
        Choose $t_1 \in \tau_{trac}$, within end points
        Choose $t_2 \in \tau_{trac}$
        Set δ_γ regarding $bounds$, $\gamma(v) - \gamma'$
        $v(t_1) = v(t_1) + \delta_\gamma$
        $v(t_2) = v(t_2) - \delta_\gamma$
    end while
    while $|\alpha(v) - \alpha'| > \epsilon_\alpha$ **do**
        $bounds = f(v, a_{max}, v_{coast}(v))$
        Choose $t_1 \in \tau_{trac}$
        Choose $t_2 \in \tau_{trac}$
        Set δ_α regarding $bounds$, $\alpha(v) - \alpha'$
        $v(t_1) = v(t_1) + \delta_\alpha$
        $v(t_2) = v(t_2) - \delta_\alpha$
    end while
  end procedure

Figure 4: Algorithm 2 transform a driving cycle to pre-defined target measures (α', β', γ'). The acceptable difference are determined by thresholds ($\epsilon_\alpha, \epsilon_\beta, \epsilon_\gamma$).

seen in the figure, the resulting driving cycle is unrealistic since it varies to much. To get a smooth driving cycle an MTF invariant low-pass filtering algorithm can be used and it will be explained in the next section.

4.4 ALGORITHM FOR REDUCING FLUCTUATIONS

The algorithms that have been proposed have problems that the resulting driving cycle fluctuates to much and can be unrealistic. These problems origins from the random selection of the point, in the algorithms, that causes the acceleration from point to point to not be so smooth. To remedy this, we propose a filtering step that sorts the points in each traction interval so the change in acceleration from point to point is smoother. Such a smoothing of the driving cycle does not affect the MTF as long as the start and end points of each traction region are not altered and the traction region intervals are not changed.

The algorithm is applied on each traction interval and sorts and smooths the speed points depending on the speed of the start and end points, $v(t_{i,\text{start}})$ and $v(t_{i,\text{end}})$. For example, for the case $v(t_{i,\text{start}}) \leq v(t_{i,\text{end}})$ and the interval $I_i =$
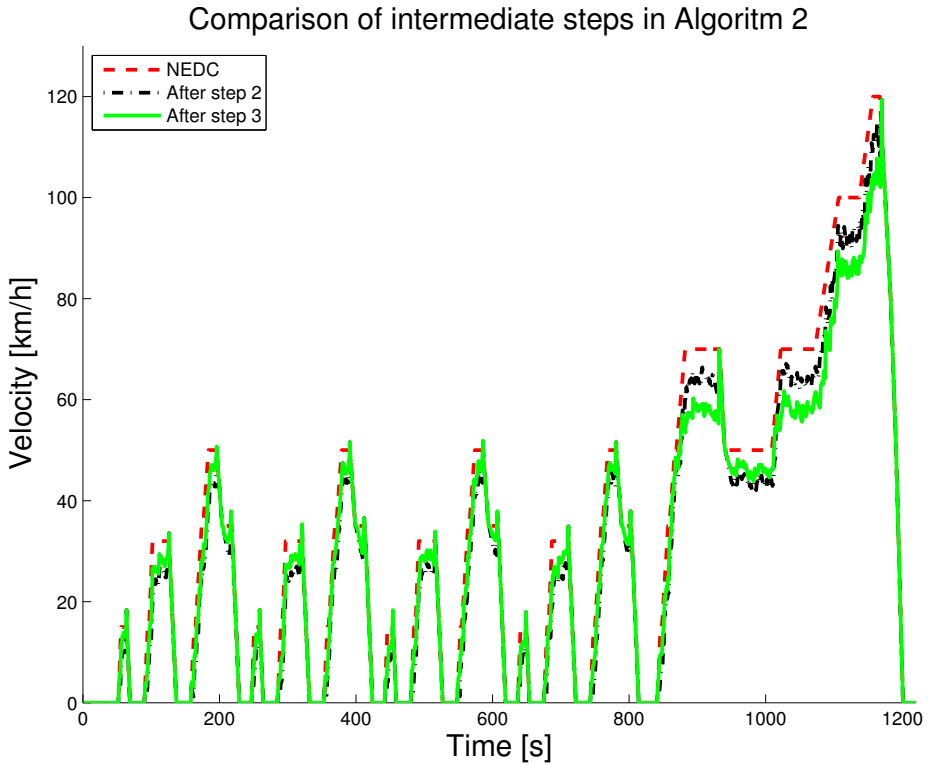
Figure 5: Comparison between different stages in algorithm 2 where the NEDC is transformed so that it gets similar MTF as the FTP75. Intermediate step after transforming β and γ (dash-dotted), final step after also transforming α (solid) and the NEDC (dashed).

$(t_{i,\mathrm{start}}, t_{i,\mathrm{end}})$ the filtering becomes a sorting in ascending order if $v(t_{i,\mathrm{start}}) \leq v(t \in I_i) \leq v(t_{i,\mathrm{end}}), \forall t \in I_i$. If there exists speed points such that $v(t_{i,\mathrm{start}}) > v(t \in I_i)$ or $v(t \in I_i) > v(t_{i,\mathrm{end}})$ these points will be partitioned in such a way that the change in acceleration, from point to point, will be reduced in each traction interval. The outcome of the filtering step is seen in Figure 7 compared to the non-filtered (solid line) in Figure 5.

5   CASE EXAMPLES

Solving problems P0-P1, can be done using Algorithm 1. Assume, for the sake of illustration, that the highway part of the NEDC is wanted to be more aggressive to test some transient behavior, but the new test cycle should still be equivalent to NEDC. In the example, $\tau_{\mathrm{spec}} = [1009, 1180]$, and the new speed profile in that segment, v_{spec}, with more aggressive acceleration is seen in Figure 6 as the solid curve. In addition, the rest of the cycle, defined on $[0, 1008]$, needs to be modified so that the complete driving cycle, defined on $[0, 1180]$, still affects the vehicle parameters in a similar way. By giving v_{spec} to Algorithm 1 the output will be a driving cycle that is equivalent to the NEDC, and that has the desired driving cycle segment, v_{spec}, within it during $\tau_{\mathrm{spec}} = [1009, 1180]$. The result of this, including a filtering step for reducing fluctuations, is seen in Figure 6.

Given a driving cycle, v, and specified equivalence measures $(\alpha', \beta', \gamma')$, Algorithm 2 transforms the driving cycle until the $\alpha(v)$, $\beta(v)$, and $\gamma(v)$ are sufficiently close to target measures, and thus a solution for problem P2. For illustration of the use of Algorithm 2, the NEDC, $v_1(t)$, is transformed to the target measures of the FTP75, $v_2(t)$. The filtered results from Algorithm 2 is seen in Figure 7. The values for the FTP75 for a certain vehicle are $(\alpha(v_2(t)), \beta(v_2(t)), \gamma(v_2(t))) = (231, 0.83, 0.14)$ and corresponding values for the NEDC are $(\alpha(v_1(t)), \beta(v_1(t)), \gamma(v_1(t))) = (324, 0.85, 0.11)$. Due to $\beta(v_1(t)) > \beta(v_2(t))$ the speed points during traction intervals have to be lowered, and this can also be seen in Figure 7 where the average speed of the equivalent driving cycle is lower than the original NEDC. When the first step in Algorithm 2 has been performed, the MTF measures have been changed. Denote γ_{step1} to be the γ-value after step 1. Due to $\gamma_{step1} < \gamma(v_2(t))$ the end points of each traction region need to be raised. Finally due to $\alpha_{step2} > \alpha(v_2(t))$, the speed during traction has to be contracted to fully be transformed to a driving cycle that has an MTF sufficiently close to the FTP75.

The other way around (from FTP75 to NEDC) is seen in Figure 8. Notice that due to $\beta(v_1(t)) > \beta(v_2(t))$ this will result in that the average speed in the transformed FTP75 driving cycle will be raised even if the average speed of the NEDC is lower than the FTP75 from start. The reason for this is that (8) is proportional to the ratio between distance traveled in the traction regions and the total distance traveled. It is a fairer measure of the tractive power at the wheels than the average speed, which does not consider the coasting or braking regions.
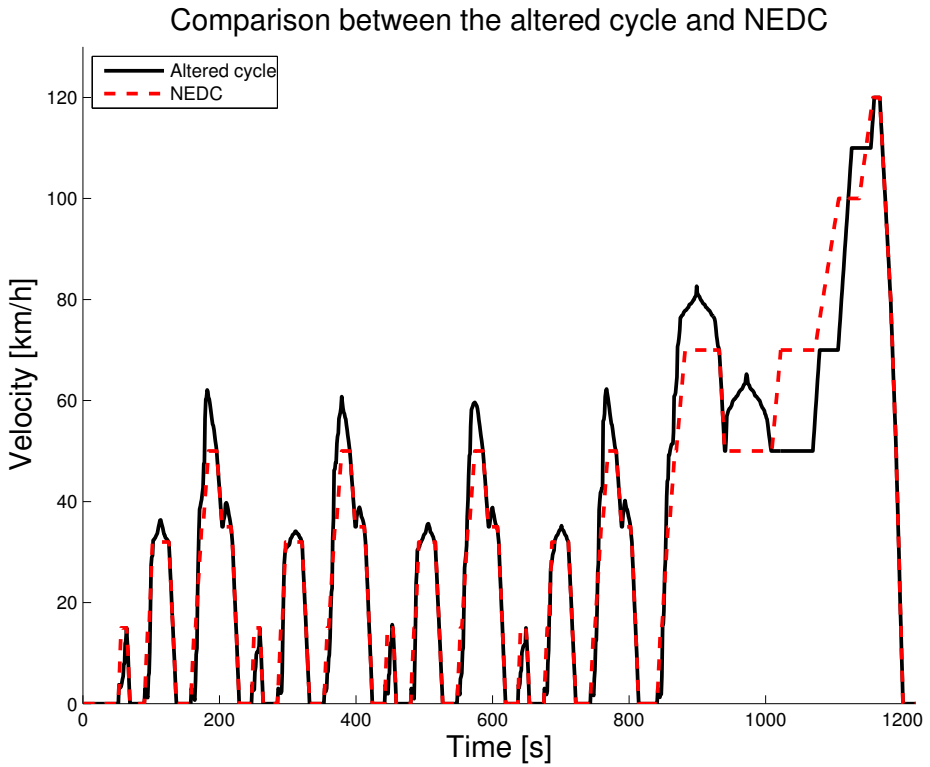
Figure 6: Results from Algorithm 1 when a specified driving cycle segment is wanted within an existing driving cycle, while the MTF are kept constant.
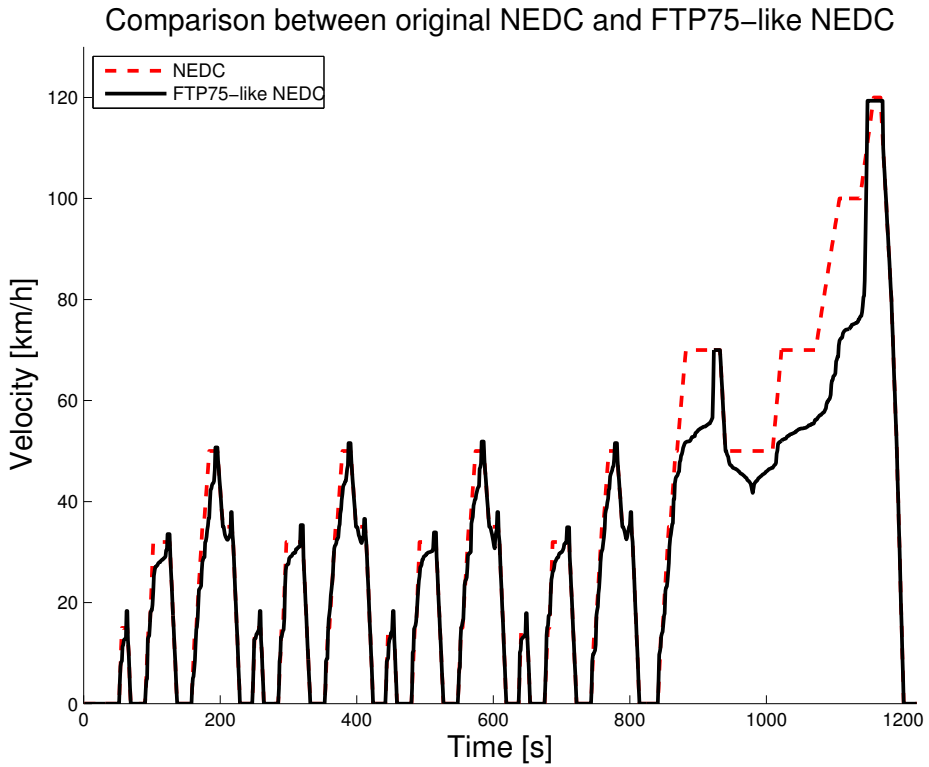
Figure 7: Comparison between NEDC (dashed) and an altered driving cycle (solid) which has MTF values close, in the sense of $(\epsilon_\alpha, \epsilon_\beta, \epsilon_\gamma)$, to the FTP75.
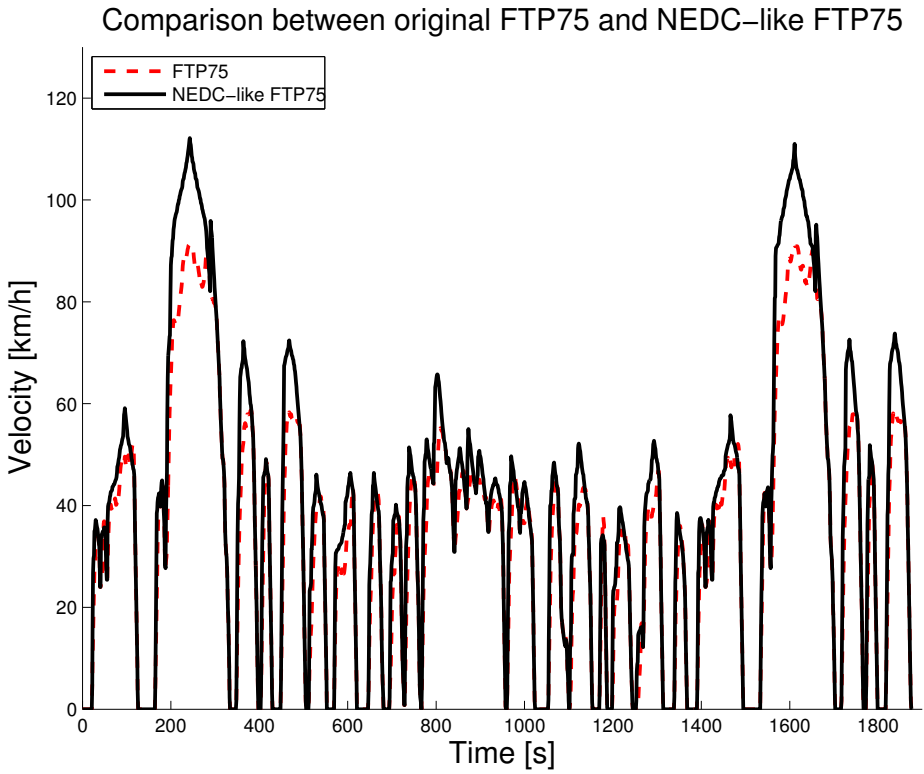
Figure 8: Comparison between FTP75 (dashed) and an altered driving cycle (solid) which has MTF values close, in the sense of $(\epsilon_\alpha, \epsilon_\beta, \epsilon_\gamma)$, to the NEDC.

6   Conclusions

Driving cycles are used for certification, for comparison of vehicles, and as an engineering tool in vehicle design. Due to the increased use and importance of driving cycles, especially in the vehicle development process, there is a strong need for methods to find or design representative driving cycles, but also to work with them and to modify them in the engineering process. A key step taken here was to define the concept of equivalent driving cycles based on mean tractive force. Using this measure two main problems were defined, namely how to modify a driving cycle into a different one but with the same equivalence measure, and how to modify a driving cycle so that its measure comes sufficiently close to a predefined equivalence measure. Algorithms solving these problems were presented, a core component where used for local modification and using this repeatedly achieved global modifications of the driving cycle. This fits well with the engineering situation when there is a representative driving cycle at hand, and the wish is to modify it slightly without loosing its characteristics. With our approach the level of modification can be controlled, and, furthermore, the modifications can be directed to parts of the driving cycle of specific interest. One such example is to request for a little different behavior in a certain transient, but where one would still like to have an MTF-equivalent driving cycle to get comparable results. Even though the algorithms are not yet optimized they show the feasibility of the methods and also gives interesting results. Two examples that were demonstrated was to transform the well-known FTP75 into an equivalent NEDC, and the other way around, to transform the NEDC into an equivalent FTP75. We foresee further development and more applications for the ideas and methods presented.

References

M. André. Driving cycles development: Characterization of the methods. In *SAE Technical Paper 961112*, 1996.

G. Fontaras and P. Dilara. The evolution of European passenger car characteristics 2000-2010 and its effects on real-world CO_2 emissions and CO_2 reduction policy. *Energy Policy*, 49(0):719 – 730, 2012.

L. Guzzella and A. Sciarretta. *Vehicle Propulsion System: Introduction to Modeling and Optimization*. Springer, 2007.

S.H. Kamble, T.V. Mathew, and G.K. Sharma. Development of real-world driving cycle: case study of Pune, India. *Trans. Research Part D*, 14(2):132–140, 2009.

P. Kågeson. Cycle-beating and the EU test cycle for cars. *European Fed. for Trans. and Envir. T&E*, 98(3), 1998.

T-K. Lee and Z.S. Filipi. Synthesis of real-world driving cycles using stochastic process and statistical methodology. *Int. J. Vehicle Design*, 57(1):17–36, 2011.

J. Lin and D.A. Niemeier. An exploratory analysis comparing a stochastic driving cycle to California´s regulatory cycle. *Atmospheric Envir.*, 36:5759–5770, 2002.

V. Schwarzer and R. Ghorbani. Drive cycle generation for design optimization of electric vehicles. *IEEE Transactions on Vehicular Technology*, 62(1):89 –97, 2013.

S. Stockar, P. Tulpule, V. Marano, and G. Rizzoni. Energy, economical and environmental analysis of plug-in hybrids electric vehicles based on common driving cycles. *SAE Int. Journal of Engines*, 2(2):467–476, 2010.

J-M. Zaccardi and F. Le Berr. Analysis and choice of representative drive cycles for light duty vehicles - case study for electric vehicles. *Proc. of the Inst. of Mech. Engineers, Part D: J. of Automobile Engineering*, 2012.

Paper D

Robust Driving Pattern Detection and Identification with a Wheel Loader Application⋆

D

Robust Driving Pattern Detection and Identification with a Wheel Loader Application

Tomas Nilsson, Peter Nyberg, Christofer Sundström,
Erik Frisk, and Mattias Krysander

*Vehicular Systems, Department of Electrical Engineering,
Linköping University, SE-581 83 Linköping, Sweden.*

Abstract

Information about wheel loader usage can be used in several ways to optimize customer adaption. First, optimizing the configuration and component sizing of a wheel loader to customer needs can lead to a significant improvement in e.g. fuel efficiency and cost. Second, relevant driving cycles to be used in the development of wheel loaders can be extracted from usage data. Third, on-line usage identification opens up for the possibility of implementing advanced look-ahead control strategies for wheel loader operation. The main objective here is to develop an on-line algorithm that automatically, using production sensors only, can extract information about the usage of a machine. Two main challenges are that sensors are not located with respect to this task and that significant usage disturbances typically occur during operation. The proposed method is based on a combination of several individually simple techniques using signal processing, state automaton techniques, and parameter estimation algorithms. The approach is found to be robust when evaluated on measured data of wheel loaders loading gravel and shot rock.

1 INTRODUCTION

Wheel loaders are used for a wide variety of tasks, ranging from use as snow-plows to loading gravel or pallets onto trucks. This work concerns characterization of a specific customer's vehicle usage. For example, experience shows that proper matching of machine configuration, such as sizing of the thermal management system (Park et al., 2011), and customer profile can have significant influence on machine efficiency and reduce fuel consumption. Since many customers operate their wheel loaders mainly for specific tasks throughout the entire lifespan, there is a potential for significant efficiency improvement. Other motivating examples where knowing the driving behavior is beneficial are advanced predictive engine control and automatic gear shifting algorithms. Good estimates on future power trajectories can be utilized in controls to further improve efficiency resulting in lower purchase cost, higher productivity, and lower fuel consumption. A third area where knowing the customers usage profile is beneficial is during development and evaluation of control algorithms. Good knowledge of customer usage makes it possible to simulate representative driving cycles and thereby obtaining more relevant evaluation results.

Today, a common situation is that only rough estimates, typically averaged quantities over long periods of time, about customer usage is available. Therefore, for example customer adaption is based on qualified guesses and test drive experience and no adaptation to a particular customers needs is possible. This situation is the main motivation for the objective here; to develop an algorithm that, using production sensors only, automatically extracts detailed information from customers vehicles during operation. The output of the algorithm should support improved matching of vehicle configuration and customer usage, provide driving information for online adaption of engine control and automatic gear shifting, and provide data for generating relevant driving cycles to simulate during product development, such as ride comfort considerations (Rehnberg and Drugge, 2008). For the control application, the algorithm must run in real time on board the vehicle. Main challenges are then to first define what information that is relevant and then to perform online usage identification robust against significant usage disturbances.

Related works for on-road automotive vehicles are for example (Engstrom and Victor, 2001) and (Johannesson, 2009; Manzie et al., 2007) showing a potential to increase vehicle efficiency by use of driving pattern knowledge. For construction machines this task is more complicated since, for example, the vehicle does not follow a given road. Control algorithms for hybrid electric vehicles based on pattern recognition are developed in Lin et al. (2004); Jeon et al. (2002). A main difference here is that the key objective is to analyze usage patterns, not to design a control algorithm. The key contribution of this paper is an algorithm, that seamlessly integrates techniques from automata theory (Kelley, 1998; Mitrovic, 2005) and system identification (Ljung, 1999), to obtain an algorithm that is robust against large usage disturbances that inherently affects vehicle operation.
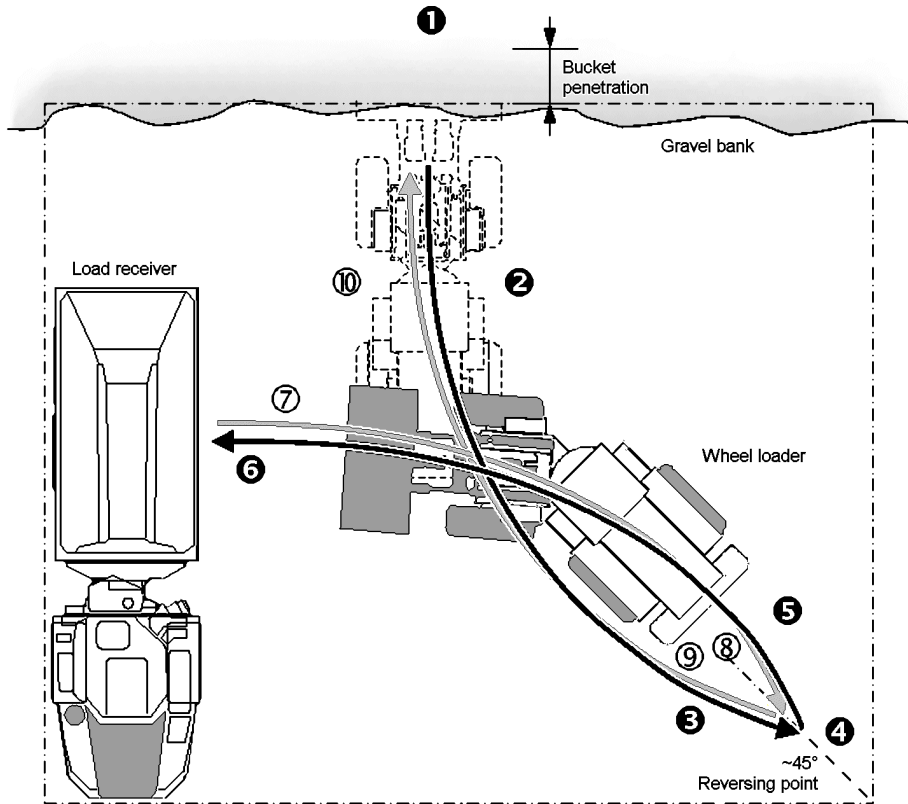
Figure 1: A view of a short loading cycle (Filla, 2012).

2 Problem Formulation and Challenges

Before the main problem is formulated, together with some of the main challenges, a brief introduction of typical wheel loader usage and sensor configuration is shown.

2.1 Wheel loader usage

Figure 1 illustrates common usage of a wheel loader, where gravel is loaded onto an articulated hauler. This loading mission consists of repeating the cycle of filling the bucket at the pile and emptying it at the receiving hauler. In the figure, the loader is starting from point 4, driving towards the pile for filling the bucket at point 1. The bucket is pushed into the pile, lifted and tilted up at loading. After reversing the loader to point 4 it approaches the receiver at point 6. The loaded bucket is lifted during the re-positioning from the pile to the

hauler. After emptying the bucket the loader reverses to point 4 while lowering the bucket.

The load receiver is often, just as in Figure 1, a truck or a hauler. In this case, when the hauler is full, there will be a pause in the loading. During this pause the machine is often cleaning the working site or waiting in a dormant state for a new hauler to arrive for loading.

2.2   SENSORS CONFIGURATION AND MEASUREMENT DATA

Figure 2 shows a schematic view of the vehicle where important measured signals are included. The production sensors used here are measuring the lift angle θ and the tilt angle ϕ of the bucket, the pressure p_{Ls} in the load sensing hydraulic pump, and the angular speed $|\omega_{ds}|$ of the drive shaft. The vehicle has a four speed gearbox and a forward/reverse gear in series, and both selected gear and gear direction is known. Finally, the driver inputs, such as hydraulics controls usage, are available. The sensor measuring pressure p_{θ} in the lift cylinder of the bucket is not a production sensor and will therefore only be used as a reference.

Figure 3 shows measurements of vehicle velocity and the bucket lift and tilt angle during typical wheel loader operation. The data is collected during a sequence of loading cycles, similar to the one described in Section 2.1, and cleaning cycles in which dropped gravel is moved back to the pile. This type of data is the input to the cycle identification algorithm.

It is common that a significant part of the total energy consumption is required for lifting the bucket with its load and knowledge of load weight is therefore important for engine control. Also, since moving material is the purpose of the operation described in Figure 1, relevant efficiency measures are the weight of the material moved divided by the time needed or the fuel used. It is therefore important to keep track of the amount of material handled. The bucket load is not measured directly, and estimating the load is not trivial, especially if no additional sensors can be introduced.

2.3   PROBLEM FORMULATION

This paper treats the development of an algorithm for online cycle detection and identification using only production sensors. The intended ouput of the algorithm is illustrated in Figure 3 where cycle detection has been performed. In addition to the identified cycles, important usage parameters such as the bucket load are also automatically estimated.

2.4   CHALLENGES

The cycle identification problem is challenging because the specification of different types of cycles are based on what the driver think is done in a given mission. Figure 3 shows six loading cycles which all perfectly match the description, but have significantly different signal trajectories with respect to amplitudes and
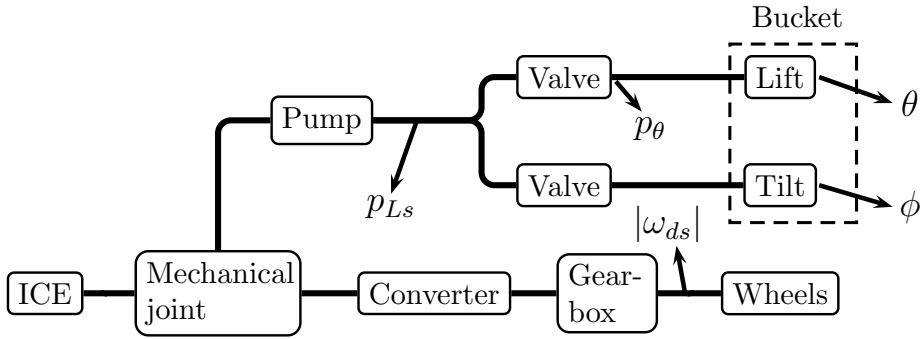
Figure 2: The configuration of the vehicle powered by the internal combustion engine, ICE. The pressure in the lift cylinder of the bucket p_θ and the Ls pressure p_{Ls} are two pressures in the system where only p_{Ls} is known in production loaders. The bucket lift and tilt angles, and the angular speed of the drive shaft are denoted θ, ϕ, and $|\omega_{ds}|$, respectively.
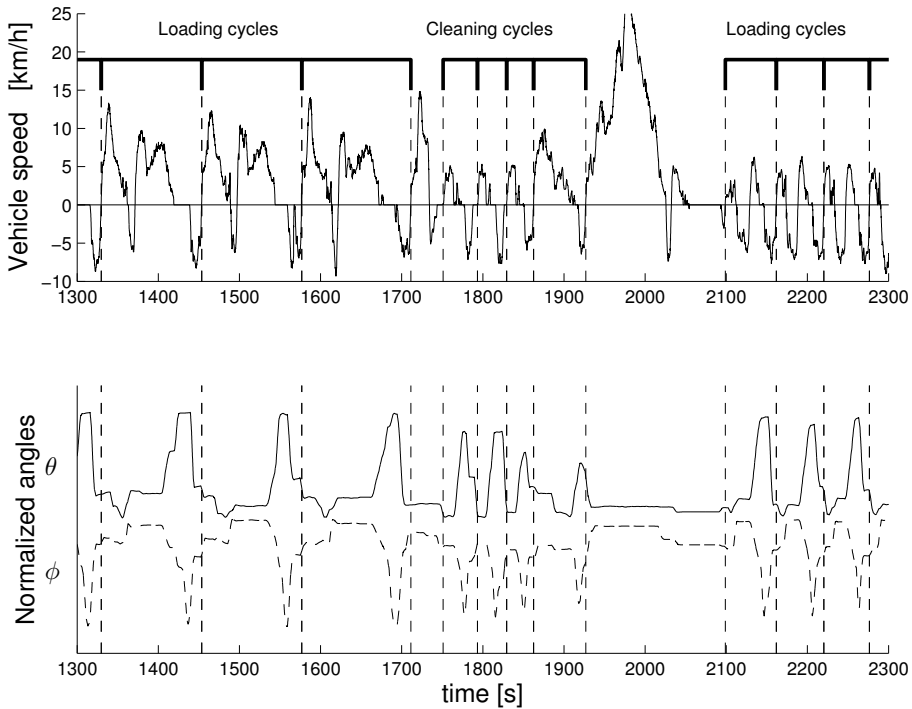
Figure 3: Data collected during typical wheel loader operation. in this case there are six loading cycles and four cleaning cycles.

lengths in parts of the cycle. In this case the differences are caused by the operator not driving perfectly repetitive, but in general also the driving style differs, different material handled such as shot rock or gravel requires different operations and the geometry of the site of operation differs. For successful cycle identification the algorithm must be robust against these types of disturbances.

The benefits of the cycle detector in parameter estimation will be exemplified with bucket load estimation. Figure 4 shows a loading cycle, according to Figure 1, with a 50 s transportation between points 4 and 6. The first peak in p_{Ls} is caused by the bucket filling and the second peak is caused by the raising of the bucket before emptying. Estimating the bucket load from the pressure p_θ in the bucket lift cylinder when the machine carries a load would be straightforward but pressure p_θ is not measured in production vehicles which means that the estimation algorithm can only use the load sensing pressure p_{Ls}. This makes the estimation problem more challenging since p_{Ls} supplies all hydraulics including lifting and tilting. Furthermore, the pressures p_θ and p_{Ls} are only similar at specific operating modes, as illustrated in Figure 4. This indicates that intelligent partitioning of the measurements are needed to extract exactly those parts that are useful for bucket load estimation.
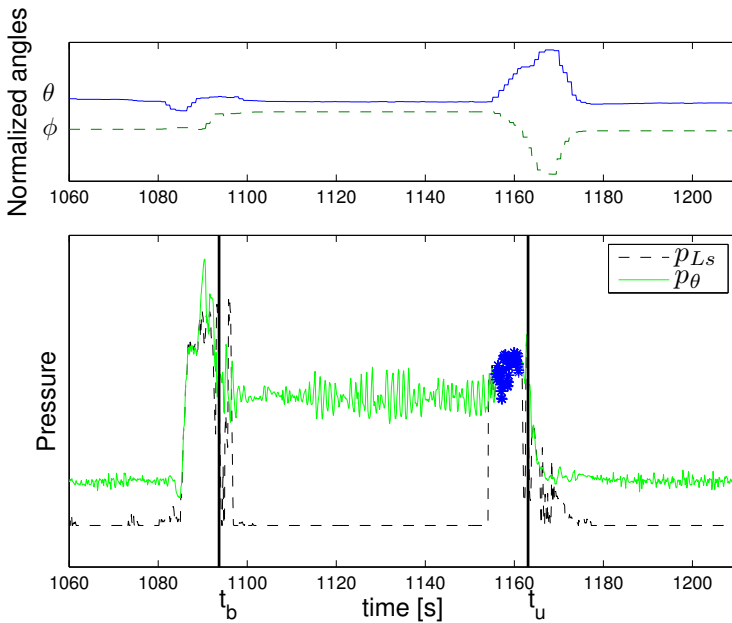
Figure 4: The load sensing pump and lift cylinder pressures, p_{Ls} and p_θ, during a transport. The bucket is loaded during the first pressure peak and unloaded at the second pressure peak. Time $t = t_b$ corresponds to where the wheel loader starts reverse motion and $t = t_u$ when the bucket is unloaded.

3 MODELING

The objective of this section is to introduce a simple way of modeling operation of the wheel loader. Key properties of such a model are 1) it should be possible to model cyclic behavior and 2) support the extraction of important operation parameters such as bucket load weight and distance traveled etc. This paper propose modelling the cycles as sequences of discrete events, in which the events are at a low enough complexity for robustly being detected while diverse enough to uniquely describe the driving cycles. This structure of building cycles from events enable using standard automata theory (Kelley, 1998) to devise cycle detection methods in Section 4. Automatic extraction of models directly from measured data would be interesting, for example using symbolic data mining techniques (Han et al., 2007). Here, it is assumed that the models are made by hand using engineering knowledge. Due to the high level of abstraction of the models, this has proven to be a relatively easy task. The models presented here are focused on bucket handling, but the methodology has also been used for other types of cycles, e.g., timber and pallet handling in Ohlsson-Öhman (2012), by additional modeling of events and cycles.

3.1 EVENTS

The principal modeling object that is used is called an *event* which represents a specific occurrence in time. First a set of events need to be introduced. These should be simple enough to be robustly, with respect to usage disturbances, detected using measurement data and still diverse enough to describe the cycles.

The primary operation described in this paper is handling of gravel and shot rocks using a bucket. An analysis indicates that six events can be used to describe the driving cycles in this type of operation. These are:

- transition from dormant to action - a

- transition from action to dormant - d

- transition from backward to forward motion - f

- transition from forward to backward motion - b

- bucket loading - l

- bucket unloading - u

In the illustration shown in Figure 1, f events happens at point 4, and point 1 and 6 are positions where event b happens. Event l occurs near point 1, and event u near point 6. The events a and d usually occur when the receiver has been filled, and the wheel loader is dormant while waiting for a new receiver to arrive.

3.2   EVENT DESCRIPTIONS

For the formal statement of the events models, introduce the notation x_k for an event x at time $t = t_k$ and $z_k = z(t_k)$. If the velocity v is 0 and if the lift angle θ and the tilt angle ϕ are constant during the $\epsilon + 1$ last time samples t_i where $i \in \{k - \epsilon, k - \epsilon + 1, \cdots, k\} =: \mathcal{I}_k$ then a transition $d_{k-\epsilon}$ from action to dormant operation is detected at time t_k. The parameter ϵ is a model parameter and will be discussed in Section 4.1. Formally, an event $d_{k-\epsilon}$ is generated if

$$(v_j = 0 \text{ and } \theta_i = \theta_j, \text{ and } \phi_i = \phi_j) \forall i, j \in \mathcal{I}_k \tag{1}$$

Note that the dormant event $d_{k-\epsilon}$ is detected in the end of the interval, i.e. at time t_k, but time stamped with the starting time $t_{k-\epsilon}$.

An activation event a_k is detected if the vehicle has been dormant according to the definition in (1) and starts to move, i.e. if (1) holds for $\mathcal{I}_{k-1}$ and

$$v_k \neq 0 \text{ or } \theta_{k-1} \neq \theta_k \text{ or } \phi_{k-1} \neq \phi_k \tag{2}$$

The events f and b are straightforward to define since v is a processed signal that has no zero-crossing noise. An event f_k is generated if there exists an interval

$$\mathcal{I} = [t_j, t_{j+1}, \ldots, t_k]$$

where the velocity is negative at the start of the interval, positive at the end of the interval, and 0 in the, possibly empty, time in between. Formally, this translates into

$$v_j < 0 \text{ and } v_{j+1} = \cdots = v_{k-1} = 0 \text{ and } v_k > 0 \tag{3}$$

where v is the vehicle velocity, computed from the drive shaft angular speed $|w_{ds}|$ and if a forward or reverse gear is selected. Note that the length of the interval is not fixed, but will depend on the number of consecutive time instances with 0 velocity. A corresponding condition for b_k is then

$$v_j > 0 \text{ and } v_{j+1} = \cdots = v_{k-1} = 0 \text{ and } v_k < 0 \tag{4}$$

A bucket unloading event u is detected when the tilt angle ϕ is small enough, i.e.

$$u_k \text{ is generated if } \phi_{k-1} \geq \xi \text{ and } \phi_k < \xi \tag{5}$$

where ξ is a model parameter. As can be seen in Figure 3, the tilt angle ϕ is given in discrete levels and not affected by noise which means that only a single unloading event is generated when the tilt angle is monotonously decreased.

The bucket loading event l is a bit more complex and is assumed to have happened if both the lift angle θ and the tilt angle ϕ has increased significantly over a time window while the machine is moving forward, i.e.

$$l_{k-L} \text{ is generated if } \theta_k - \theta_{k-L} > \alpha \text{ and } \phi_k - \phi_{k-L} > \beta \text{ and } v_{k-L} > 0 \tag{6}$$

where α and β are model constants and L the length of the time window. Note that this event is time-stamped at the start of the time window and not at the end. In contrast to the unloading event, the loading event can be generated multiple times during one bucket loading.

With the event descriptions (1)-(6) measurement data of velocity $v(t)$, lift angle $\theta(t)$, and tilt angle $\phi(t)$ can be transformed into a sequence of symbols from the alphabet $\Sigma = \{a, b, d, f, l, u\}$ with corresponding time stamps.

3.3 Cycles

As discussed in Section 2, repetitive behavior called cycles is of special importance. Here, cycles will be modeled using the events defined in Section 3.1 as a state automaton. The start time, $t_{c,s}$, of a cycle is determined by the first event and the end time, $t_{c,e}$, is determined by the event next after the last event in the cycle.
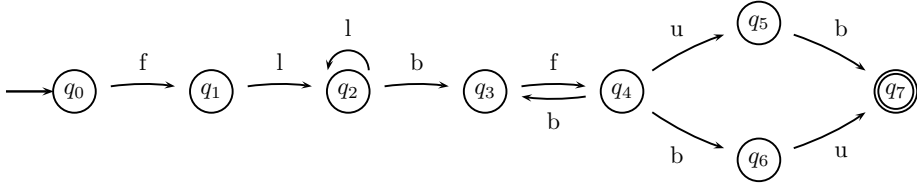
Figure 5: Transition diagram of the automata describing a loading cycle. The initial state is q_0 and the accepting states is q_7.

One can model any number of cycles using automatons and here two common types of behavior will be modeled, first a *loading cycle* and second a *cleaning cycle*. A loading cycle is intuitively described by the sequence of events $flbfub$ which is accepted by the automaton in Figure 5 by going through the states q_0, q_1, q_2, q_3, q_4, q_5, and q_7. The rationale behind the model can be realized by going through the event sequence typically generated in the loading cycle shown in Figure 1. The event f is generated at point 4, l at point 1, b at point 1, f at point 4, u at point 6, and finally b at point 6. However if we only search for the ideal sequence $flbfub$, the order of events are crucial to get a fit. Due to minor changes in operator behavior, the events ub become bu and the reason is that these events occur near each other in time and small cycle-to-cycle variations effect the order of the events. For example, in Figure 1 this is common at point 6. Also possible multiple bucket loading events, l, generated at point 1 stresses that the patterns need to be robust against these disturbances. Due to the automaton modeling language used, regular expressions, it is straightforward to take such variations into account as is depicted in the full automata in Figure 5. The model for a cleaning cycle is slightly smaller but follows a similar structure as shown in Figure 6 and dormant operation is modeled as in Figure 7.
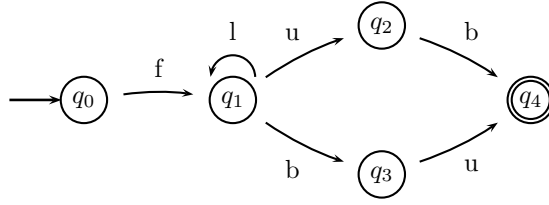
Figure 6: Transition diagram of the automata of the cleaning cycle.
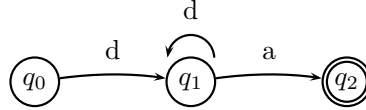
Figure 7: Transition diagram of the automata describing dormant operation. The initial state is q_0 and the accepting state is q_2.

4   METHOD

In this section it is described how the models from last section can be used in an online algorithm for identifying wheel loader usage including cycle detection and usage parameter estimation. An overview of the different parts and the information flow of the algorithm is shown in Figure 8. The input to the algorithm is measurement data and the high-level cycle descriptions provided as automata like the ones given in Figures 5-7. The algorithm can be divided into 3 main parts: low-level event detection, cycle identification, and parameter estimation.
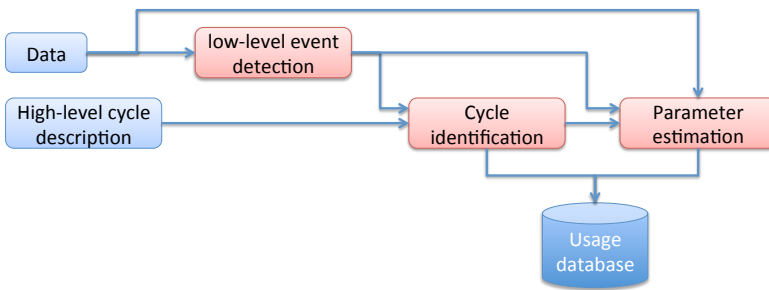
Figure 8: Data comes from sensors. The events are generated from the rules (1)-(6). The high-level description are the patterns that are fed to the cycle identification along with the generated events. Finally, parameters are estimated and stored together with cycle information in an usage database.

4.1 EVENT DETECTION

The event detectors (1)-(6) take measurement data as input and generate a sequence of time-stamped events. The event sequence is then used, instead of whole data series of measurements, in the cycle identification to achieve robustness against user disturbances. In order to achieve reliable detection there are a few parameters in the event detectors that must be tuned. The choice of the constants has been made with the aim of robustness in the detection of the events. The tuning was made by comparing recorded sequences of wheel loader usage to the corresponding sensor data.

The time needed to robustly decide that the vehicle is dormant is determined by the parameter ϵ in (1). If ϵ is set low it means a risk of detecting dormant events in for example loading cycles and thus missing detection of these cycles. A large value of ϵ implies that a short period of dormant operation would not be detected.

The value of ξ in (5) should be set at about the angle at which load would slide out of the bucket. The recorded data show no example of drivers tilting the bucket this low except when emptying and in that case the angle is usually much lower since this makes the emptying quicker. The sensitivity to the value of ξ is therefore low.

Common sizes of lift angle change, tilt angle change, and loading time have been determined from recorded sequences of data. This can be used as α, β and L in (6). However, variations in these variables are large. This is primarily accounted for by increasing the sensitivity of loading detection by decreasing α, β, and increasing L. The high sensitivity of the detector leads to multiple alarms and this is considering when designing the cycle models shown in figures 5 and 6 to achieve robust cycle identification.

4.2 CYCLE IDENTIFICATION

The inputs to the cycle identification algorithm is an event sequence and a set of automata each describing a cycle type. The cycle identification is then performed each time a new event is detected.

Recall that events such as the loading event l and the dormant event d are not immediately detected. This means that when a new event is detected it is not sure that it will be the last one in the generated event sequence. In order to handle the non-causal behavior of incoming events all events after the latest matched cycle are the input to the cycle identification algorithm. The output is the set of states in the different cycles that is consistent with the considered event sequence. Consider as an example if the input event sequence is $flbfb$ then the output will be q_3 and q_6 in the loading cycle automaton in Figure 5 and q_3 in the cleaning cycle automaton in Figure 6. The string matching is done similar to the algorithms given in Mannila et al. (1997); Das et al. (1997).

There are words matching the loading cycle automaton such that the last part of the word also matches the cleaning cycle automaton and this causes a

non-unique identification of cycles. To illustrate this, consider the word $flbfub$ which matches the loading cycle automaton in Figure 5. The last part of this word, i.e. the 3 events fub also match the cleaning cycle automaton in Figure 6. To get a unique identification, the patterns are ordered according to a priority. Patterns with higher priority is matched first and for example, here the loading cycle has higher priority than the cleaning cycle, i.e., if the cleaning cycle is part of a longer sequence that can be interpreted as a loading cycle the latter interpretation is preferred. In this way matching coverage is maximized in this case.

User disturbances can lead to different event sequences, or variations of the sequences, for repetitions of the same type of cycle. To get a match even with cycle variation the automaton of the loading cycle in Figure 5 is made with this variation in mind. However, if the sequence of events does not match the automaton the algorithm regard this as a mismatch even if there is just a single difference between them. It works for this application but if there would be more and stochastic variations, approximate string matching techniques would be of interest (Navarro, 2001; Antoniou et al., 2006).

4.3   Parameter estimation

There are several parameters that are of interest in the analysis of how the vehicle is operated. Most of these are trivial, such as vehicle speed and gear selection, and need not be treated further. In this paper a suggested parameter for separation between short and long loading cycles and an estimation of the bucket load weight are presented since these require some additional analysis.

Separation between short and long loading cycles

The trivial way of estimating whether the loading cycle is short or long is to use the cycle time. If the time is above a threshold, the cycle is a long loading cycle, otherwise it is short. With this criteria a short loading cycle including a stop in the middle or with a toggle between the states q_3 and q_4 in Figure 5 could be classified as a long loading cycle. To get a more robust classification parameter for distinguishing between short and long cycles the longitudinal distance from the time t_l of the first loading event to the time t_u of the unloading event is used, i.e. if $v(t)$ is the velocity of the vehicle the classification parameter is

$$r = \int_{t_l}^{t_u} v(t) \ \mathrm{dt} \tag{7}$$

In a short loading cycle the loader reverses approximately the same distance as it is driving forward and r is close to zero. In a long loading cycle the loader is driving forward more than reversing and r is a positive number. Therefore, r is calculated for every loading cycle and is compared to a threshold, ψ, and the

classification of short and long cycles is determined according to

$$\text{short loading cycle:} \quad r \leq \psi$$
$$\text{long loading cycle:} \quad r > \psi,$$

here the threshold is set to $\psi = 30$ m.

BUCKET LOAD ESTIMATION

The bucket load weight is estimated once for each loading cycle. When estimating the load in the bucket, an affine relation between the pressure in the lift cylinder, p_θ, and the mass, m_{load}, relation is used

$$m_{load} = f(p_\theta) = a_\theta p_\theta + b_\theta \tag{8}$$

where a_θ and b_θ are constants. As stated previously, there is no sensor in series production loaders for measuring p_θ, but only the system pressure, p_{Ls}, at the hydraulic pump is known. The bucket load only effects p_{Ls} when the valve connecting the lifting cylinder to the pump is opened, i.e. during transient operation of the bucket. This can be seen in Figure 4, where these two pressures are given for a loading cycle, and at the two peaks in pressure, p_{Ls} is a good approximation of p_θ. However, it is beneficial to only base the load estimation on the second pressure peak where the bucket is lifted before it is unloaded. The reason is that when the bucket is lifted during loading, the pressure varies depending on if there are, e.g., roots in the pile or the material handled. The event and cycle identification algorithm is used to find the time interval to use in the estimation of the lift cylinder pressure, that later is used in the estimation of the bucket load. The time period of interest is stated to be after the first reverse event after the loading event is generated in the loading cycle, t_b, and the unloading event is generated, t_u. The equality $p_{Ls} = p_\theta$ in the time interval $t \in [t_b, t_u]$, is assumed to be valid when two conditions are fulfilled. The first condition is based on that the driver lifts the bucket. The estimated angular velocity, $\hat{\theta}$, is used and the signal is smoothed by a low-pass Butterworth filter. The interval of interest is defined as

$$\mathcal{I}_1 = \left\{ t_i : \hat{\theta}(t_i) > \gamma \cdot \max_{t_k \in [t_b, t_u]} \left\{ \hat{\theta}(t_k) \right\} \right\} \tag{9}$$

where $\gamma < 1$ is a tuning parameter. The condition uses a relative threshold to achieve as good performance as possible of the estimated pressure in the lift cylinder, $\hat{p}_\theta$, for different driving situations. Due to robustness the second condition for the assumption $p_\theta = p_{Ls}$ is the interval

$$\mathcal{I}_2 = \left\{ t_i : p_{Ls}(t_i) > \delta \cdot \max_{t_k \in [t_b, t_u]} \left\{ p_{Ls}(t_k) \right\} \right\} \tag{10}$$

where $\delta < 1$ is a tuning parameter. For time points in $\mathcal{I}_1 \cap \mathcal{I}_2$, we estimate the pressure p_θ according to

$$\hat{p}_\theta = \frac{1}{|\mathcal{I}_1 \cap \mathcal{I}_2|} \sum_{t_k \in \mathcal{I}_1 \cap \mathcal{I}_2} p_{Ls}(t_k) \tag{11}$$

The bucket load estimate is then

$$\hat{m}_{load} = f(\hat{p}_\theta) = a_\theta \hat{p}_\theta + b_\theta \tag{12}$$

The samples where conditions $\mathcal{I}_1$ and $\mathcal{I}_2$ are fulfilled are marked with stars in Figure 4. Both γ and δ are used for removing data that is less accurate due to low signal amplitudes. Values close to 0 means most data is accepted and close to 1 that most data is rejected. As long as these extremes are avoided the sensitivity to the values is small. Here $\gamma = 0.65$ and $\delta = 0.50$ has been used.

5   EVALUATION

It is hard to quantify how well the algorithm fulfills the requirements since it may be subjective which operation a wheel loader is performing in a particular situation. In addition, it is not obvious what should be considered to be usage disturbances within a specific cycle type and what should be considered to be completely different cycles. For example, it is common to adjust the position of the machine and/or shake the bucket during unloading, but the amount of deviation that should be allowed within a cycle is subjective. The proposed algorithm has been evaluated against real data where several drivers have used a machine, handling different materials, while being filmed. The resulting data and films have been used for evaluation of the algorithm. The drivers have been given a driving scenario, such as loading shot rock onto an artificial hauler, and told to drive as they would on a regular working day. The drivers have in most cases operated the vehicle in a cyclic behavior as described in Section 3, with occasional cleaning of the working site. Visual examination of these films has been used for creating a reference which can be compared to the result of the algorithm.

Figure 9 shows a close-up of one of these datasets. It shows the detected events and an identified loading cycle. In this particular case, the visible sequence of events is $ubflbfubflb$, and in this sequence a loading cycle $flbfub$ has been identified. Figure 10 shows the full 3600 s of the same dataset. The light-gray segments indicate identified loading cycles, the dark-gray segments indicate cleaning cycles, and the white segments correspond to the parts that do not match any of the predefined cycles. The examination of this and the other datasets shows that the accuracy is in general very good. There are however some exceptions.

The first type is cases where the operator deliberately tries to drive in a peculiar way. The other type is at occasions, especially when handling shot
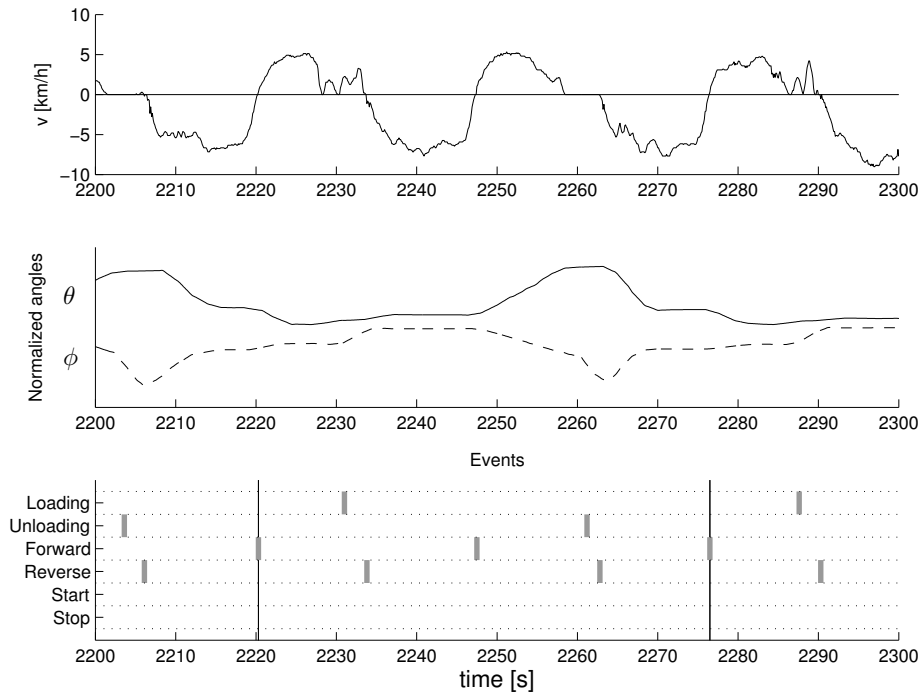
Figure 9: A data sequence with detected events and a detected loading cycle. The beginning and end of the loading cycle are marked with vertical lines in the lowest plot.
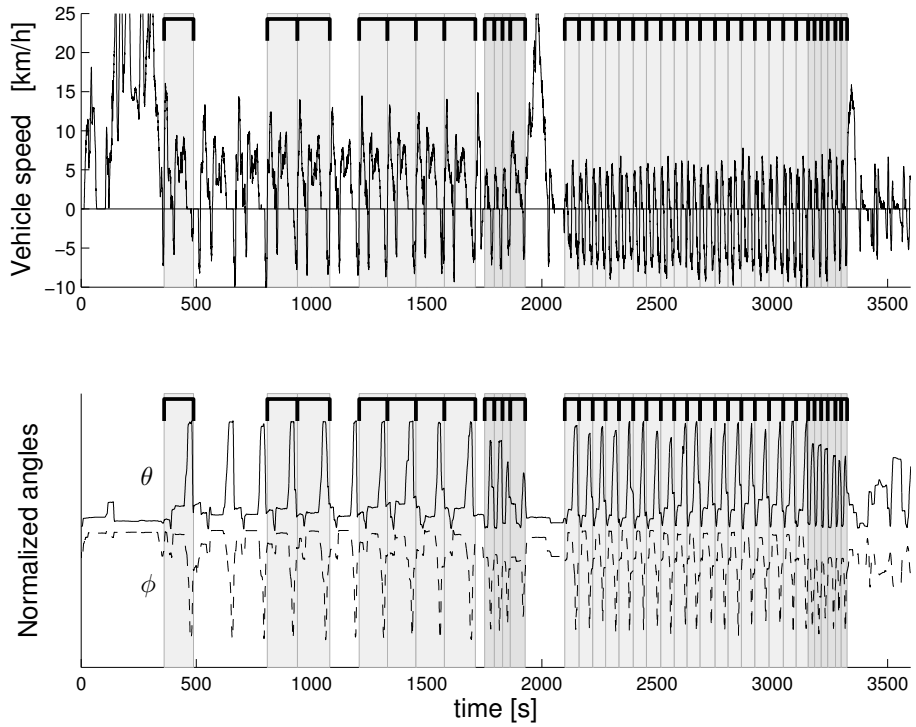
Figure 10: A cycle-partitioned dataset. White = no cycle, light gray = loading cycle, dark gray = cleaning cycle

Table 1: The number of loading cycles the algorithm identifies for different drivers with different missions. The values in parenthesis represent the number of cycles in each case.

Material	Operator	Short loading cycles	Long loading cycles	Cleaning cycles	Ratio detected
gravel	experienced	14 (15)	0 (0)	1 (0)	93%
	intermediate	15 (15)	0 (0)	0 (0)	100%
	beginner	11 (12)	0 (0)	1 (0)	92%
short rock	experienced	17 (18)	0 (0)	1 (0)	94%
	intermediate	11 (11)	0 (0)	6 (6)	100%
	beginner	10 (10)	0 (0)	0 (0)	100%
gravel	experienced	0 (0)	9 (13)	4 (0)	69%
	intermediate	0 (0)	15 (15)	0 (0)	100%
	beginner	0 (0)	5 (6)	1 (0)	83%
gravel	–	18 (18)	7 (10)	10 (10)	92%
		96 (99)	**36 (44)**	**24 (16)**	**93%**

rock, when the driver shakes the bucket at loading. It would be easy to adjust the loading cycle automata in Figure 5 to accept this behavior. Therefore, the main issue in these cases is to decide whether or not the cycle specifications are supposed to include the observed behavior as well. Without an adjustment of the algorithm, the results are still valuable, since most of the operation is partitioned into cycles resulting in an accurate overview of the usage. The algorithm can therefore help directing attention to data regions with unusual operation.

5.1 ROBUSTNESS OF CYCLE IDENTIFICATION ALGORITHM

Nine datasets have been collected to evaluate the performance and robustness of the cycle identification algorithm to different drivers and driving missions. A summary of the analysis of these datasets is shown in Table 1. The loader is operated by three different drivers with different experiences; one is experienced, one is intermediate, and one is a beginner. Each driver performs the following three driving missions; one including short loading cycles handling gravel, one including short loading cycles handling shot rock, and one including long loading cycles handling gravel. The drivers were instructed to drive the loader as they would during a normal working day including cleaning of the working site. In addition to these cases, data is collected from a mission combining long and short loading cycles and cleaning cycles, all handling gravel. The numbers of cycles detected by the algorithm are presented in the table, along with the actual numbers of cycles that the drivers have completed in parenthesis. The last row in the table summaries all missions in the evaluation.

The dataset on the next last line in the table is also presented in Figure 10,

and in this dataset all cleaning and short loading cycles are detected, but three of the long loading cycles are not detected. These cycles can be seen in Figure 10 starting at 500 seconds, 650 seconds, and 1100 seconds. The reason for not being classified as loading cycles is that after the second forward event in each cycle, see Figure 5, a dormant d and an activation event a are generated. The generated sequence of events will then neither match the automata given in Figures 5 nor the one in 6. In the first nine datasets presented in Table 1, the eight missed loading cycles have been wrongly classified as cleaning cycles. In seven of these cases a loading event is not generated, and in one case the transition from backward to forward motion is not detected since the loader is operating at a slope and starts to reverse with a forward gear selected, see Section 3.2 for details. In all, a total of 93% of the 159 cycles in the evaluation datasets are correctly detected and classified. This corroborates that the algorithm is robust to different drivers and missions.

5.2   Parameter estimation

As described in Section 4.3, a parameter r that separates short and long loading cycles is computed, and an estimation of the bucket load is performed. A histogram of the measure r that separate short and long loading cycles, as defined in (7), for the dataset presented in Figure 10 and the last line in Table 1, is found in Figure 11. It can be seen that there is a clear distinction between the values from short loading cycles ($r < 0$ m), and long loading cycles ($r > 60$ m), which indicate that this classification parameter can be used to separate the two cycle types.

The weight estimator described in Section 4.3 gives an acceptable accuracy, even though the main objective was to investigate whether the event and cycle identification would aid the weight estimation. Figure 12 shows a comparison between the estimated and actual load weight normalized with the maximum load weight m_{max} of the loader. As stated in Section 2.2, the hydraulic pressure in the lift cylinder, p_θ, is not measured in production wheel loaders, but can be estimated from the pump pressure, p_{Ls}, when the driver lifts the bucket. In finding the time interval when p_{Ls} can be used as an approximation for p_θ, it is advantageous to use the results from the event and cycle identification algorithm. The load estimation is based on the averaged pressure from (11) and an affine relation between the bucket load and the pressure using (8). Knowledge of the machine geometry can be used to improve the accuracy of the function $f(p_\theta)$ in (8), and thereby increase the accuracy in the load estimation. Still, using the machine geometry would not reduce the importance of finding a good estimation of the pressure p_θ, and it is shown that the event and cycle identification algorithm gives valuable information to achieve this.

Classification parameter to separate short and long loading cycles
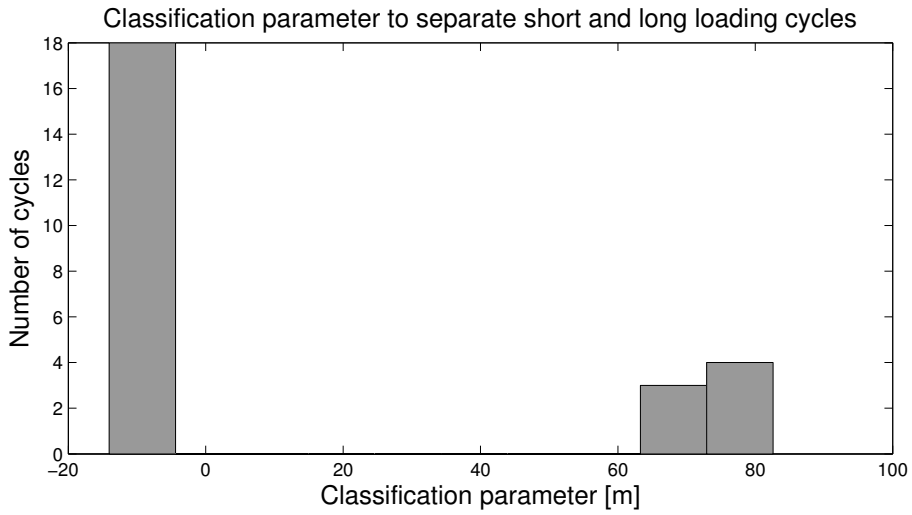
Figure 11: Histogram of r, as defined in (7), for the dataset presented in Figure 10.

Load weight estimation
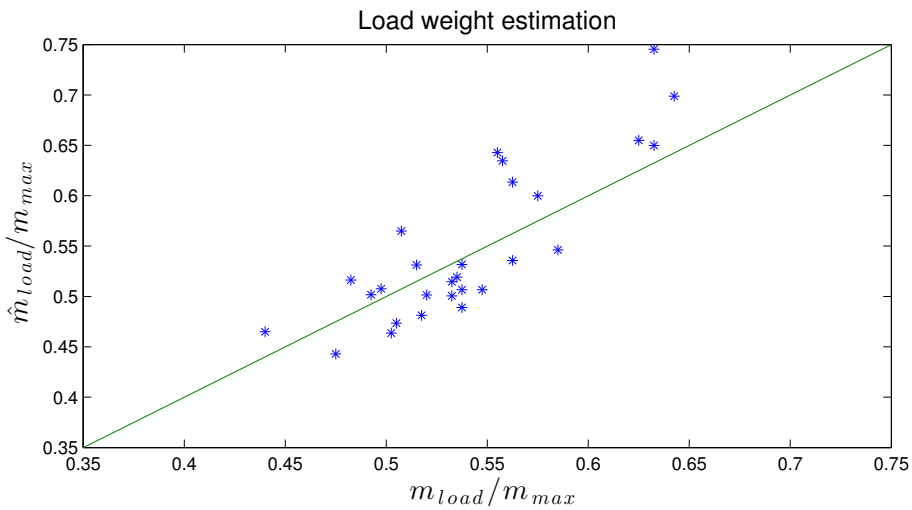
Figure 12: This figure shows the bucket load estimation, normalized with the maximum load of the wheel loader. The estimated normalized masses are given on the vertical axis and the sensor values on the horizontal axis.

5.3   Summing up

Based on the cycle identification and the parameter estimation it is possible to summarize how the wheel loader is used for a long period of operation. In Figure 11 this is done by a histogram of the classification parameter stating whether the loading cycle is short or long, and in Figure 13 the time spent in each cycle type is shown. Both these two figures are based on the dataset presented in Figure 10. In the pie-chart there is a significant part of the time that is unspecified. The reason for this can be seen in Figure 10. The driver does not drive according to any of the modeled cycles in the beginning, at around 2000 seconds, and at the end of the driving mission. These parts are correctly classified as unspecified operation and represents more than half of the time spent in unspecified operations. Further, as stated earlier, there are three long loading cycles that are not classified in this dataset. Even though a significant part of the time is stated to be unspecified, 92% of the cycles in the dataset are correctly classified according to Table 1. This illustrates that in realistic operation, the proposed algorithm is successful in detecting and identifying the pre-defined cycles. Based on the table it is shown that the cycle identification algorithm is robust, since 148 of the 159 cycles in the evaluation datasets collected from different drivers and driving missions are correctly classified.

Other values of interest to summarize over long time operation relates to fuel consumption and productivity, see Table 2 for an example. These values are based on the load weight estimation, that is shown to benefit in accuracy by using the event and cycle algorithm, and thereby avoid the use of additional sensors.

Table 2: The load handled by the loader per time unit and the load handled normalized with fuel consumption for the three drivers and the nine first datasets used in Table 1. The results are for the total of the three driving missions for each driver in the previous table.

Driver	**Weight/time [ton/hr]**	**Weight/fuel [ton/l]**
experienced	326	15.3
intermediate	269	14.3
beginner	138	10.2

6   Conclusions

A framework for characterizing wheel loader operation has been developed. Two types of cycles, loading cycles and cleaning cycles, have been considered, but the framework is generic and it is possible to also include models for other cycles. It
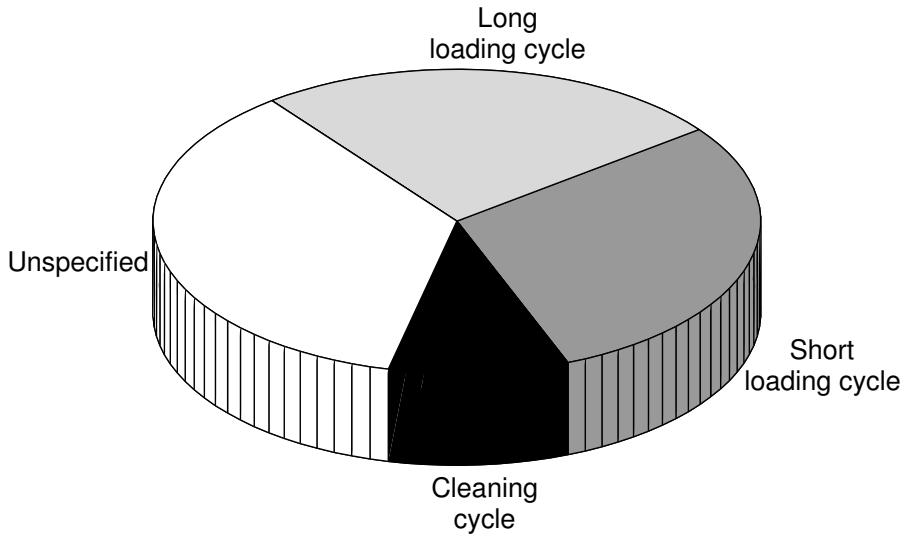
Figure 13: An example of a usage summary.

has been shown that the used cycle identification approach is robust to different drivers, material handled, and the working site layout. Ten datasets were used in the evaluation, in which four different drivers perform sequences of different loading and cleaning cycles. In total the ten datasets contain 159 cycles, out of which the algorithm correctly detects and identifies 148 cycles (93%). This is a high detection rate, especially considering the low theoretical complexity of the algorithm and the diversity of the operation.

It is shown that a proposed classification parameter to separate short and long loading cycles works well, since there is a clear distinction in the values of the parameter in the two types of cycles. Further, it has been shown that the use of the cycle and event detection algorithm is beneficial in the estimation of the bucket load.

References

P. Antoniou, J. Holub, C.S. Iliopoulos, B. Melichar, and Peterlongo P. Finding common motifs with gaps using finite automata. *Implementation and Application of Automata*, pages 69 –77, 2006.

G. Das, R. Fleischer, L. Gasieniec, D. Gunopulos, and J. Kärkkäinen. Episode matching. In *Combinatorial Pattern Matching*, volume 1264, pages 12–27. Springer Berlin / Heidelberg, 1997.

J. Engstrom and T. Victor. Real-time recognition of large-scale driving patterns. In *Proceedings of 2001 IEEE Intelligent Transportation Systems*, pages 1018 –1023, Oakland, CA., USA, 2001.

R. Filla. Study of a method for assessing operability of working machines in physical and virtual testing. *International Journal of Vehicle Systems Modelling and Testing*, 7(3):209–234, 2012.

J. Han, H. Cheng, D. Xin, and X. Yan. Frequent pattern mining: current status and future directions. *Data Mining and Knowledge Discovery*, 15(1): 55–86, 2007.

S. Jeon, S. Jo, Y. Park, and J. Lee. Multi-mode driving control of a parallel hybrid electric vehicle using driving pattern recognition. *Journal of Dynamic Systems, Measurement, and Control*, 124(1):141–149, 2002.

L. Johannesson. *Predictive Control of Hybrid Electric Vehicles on Prescribed Routes*. PhD thesis, Chalmers University of Technology, Sweden, 2009.

D. Kelley. *Automata and Formal Languages*. Prentice Hall, 1998.

C-C. Lin, S. Jeon, and J.M. Peng, H.and Lee. Driving pattern recognition for control of hybrid electric trucks. *Vehicle System Dynamics*, 42(1-2):41–58, 2004.

L. Ljung. *System Identification - Theory For the User*. Prentice Hall, 2nd edition, 1999.

H. Mannila, H. Toivonen, and I.A. Verkamo. Discovery of frequent episodes in event sequences. *Data Mining and Knowlegde Discovery*, 1:259–289, 1997.

C. Manzie, H. Watson, and S. Halgamuge. Fuel economy improvements for urban driving: Hybrid vs. intelligent vehicles. *Transportation Research Part C: Emerging Technologies*, 15(1):1 – 16, 2007. ISSN 0968-090X. doi:10.1016/j.trc.2006.11.003.

D. Mitrovic. Reliable method for driving events recognition. *IEEE Transactions on Intelligent Transportation Systems*, 6(2):198–205, 2005.

G. Navarro. A guided tour to approximate string matching. *ACM Computing Surveys*, 33:31–88, 2001.

K. Ohlsson-Öhman. Identifying operator usage of wheel loaders utilizing pattern recognition techniques. Master's thesis, Linköping University, SE-581 83 Linköping, 2012.

S. Park, A. A. Malikopoulos, M. Kokkolaras, and D. Jung. Thermal management system modelling and component sizing for heavy duty series hybrid electric vehicles. *International Journal of Heavy Vehicle Systems*, 18(3):272–287, 2011.

A. Rehnberg and L. Drugge. Ride comfort simulation of a wheel loader with suspended axles. *International Journal of Vehicle Systems Modelling and Testing*, 3(3):168–188, 2008.